Universität Rostock Traditio et Innovatio

Synthesis and Characterization of Zinc Phosphides

Master Thesis

to acquire the academic degree

Master of Science (M.Sc.)

at the Faculty of Mathematics and Natural Sciences

of the University of Rostock

submitted by Kirill Faust, born on 18.11.1992 in Osinniki, Russia

Rostock, 05.09.2016

This thesis was prepared during the period from April 2016 to September 2016 in the group of Prof. Dr. Axel Schulz, holder of the chair for Inorganic Chemistry at the Department of Chemistry of the University of Rostock.

1. Reviewer: Prof. Dr. Axel Schulz

2. Reviewer: Dr. Jonas Bresien

Statutory Declaration

I hereby testify that the thesis at hand has been written entirely by myself and that I have used no sources or aids other than those named. All passages taken from a source, whether verbatim or in substance, have been indicated as such.

Rostock, 05.09.2016

Kirill Faust

Erklärung

Ich versichere hiermit an Eides statt, dass ich die vorliegende Arbeit selbstständig angefertigt und ohne fremde Hilfe verfasst habe. Dazu habe ich keine außer den von mir angegebenen Hilfsmitteln und Quellen verwendet und die den benutzten Werken inhaltlich und wörtlich entnommenen Stellen habe ich als solche kenntlich gemacht.

Rostock, 05.09.2016

Kirill Faust

Acknowledgements

I am very grateful to **Professor Dr. Axel Schulz** for accepting me into his group, for providing me with an interesting subject of research, for the extensive scientific freedom, and for the trust put in me. Furthermore, I thank him for his outstanding lectures, which sparked my interest in inorganic chemistry.

Special thanks are also due to **Dr. Jonas Bresien** for the excellent supervision, for giving me the opportunity to contribute to his research and for introducing me into all kinds of work techniques and analytical methods. I am very grateful for his help with interpreting analytical data and for solving X-ray crystal structures, and furthermore, for the trust put in me, for the shown patience, for informative conversations, and for useful advice. I would also like to thank him for the second review of my Master thesis.

Furthermore, I would like to thank many more people: **Dr. Alexander Villinger** for assistance with the solution of X-ray crystal structures, **Richy Hauptmann** for doing some previous research on zinc phosphides, **René Labbow**, **Max Thomas**, **Sören Arlt, Alrik Stoffers**, **Tim Suhrbier,** and **Kerstin Bohn** for the great working atmosphere and the mutual assistance in the laboratory, and of course all the other members of the Schulz group for the acceptance, good collaboration, and for interesting group seminars.

I am greatly indebted to the analytical department of the Chemistry Department and the *Leibniz-Institut für Katalyse* for the acquisition of analytical data. Among those I would like to thank **Isabel Schicht** for her assistance with X-ray measurements, **Dr. Dirk Michalik**, **Heike Borgwaldt** and **Alice Voß** for the acquisition of NMR spectra, **Astrid Lehmann** for CHN analyses, as well as **Dr. Christine Fischer** and **Sigrun Roßmeisl** for the acquisition of mass spectra.

Last but not least I wish to thank **my friends and family** for loving care and all kinds of support during the whole duration of my studies and, of course, **Marlen Sommer**, for the love and support I needed to accomplish this work.

Thanks you very much!

Summary

In this work, the syntheses and characteristics of terphenyl substituted zinc phosphides as, for example, $[TerPH(ZnEt)]_2$, $[TerP(ZnEt)_2]_2$ or TerPH(ZnCl) were studied in the solid state as well as in solution.

Furthermore, in the case of $[TerPH(ZnEt)]_2$ and $[TerP(ZnEt)_2]_2$, the applicability in the preparation of cyclic polyphosphorus frameworks was investigated in the attempt to find a reaction pathway that would selectively give rise to 1,3-dichloro-*cyclo*-tetraphosphanes $[ClP(\mu\text{-PTer})]_2$ starting from P1 building blocks. However, for both phosphides, only product mixtures were obtained regardless of the reaction conditions.

In the case of $[TerP(ZnEt)_2]_2$, reactions with DMSO or dichloromethane were carried out, however, the isolation of the reaction products could not be facilitated.

Zusammenfassung

In dieser Arbeit wurden die Synthesen und Eigenschaften von Terphenyl-substituierten Zinkphosphiden wie z.B. $[TerPH(ZnEt)]_2$, $[TerP(ZnEt)_2]_2$ oder TerPH(ZnCl) im Festkörper als auch in Lösung untersucht.

Darüber hinaus wurde, im Falle von $[TerPH(ZnEt)]_2$ und $[TerP(ZnEt)_2]_2$, die Anwendbarkeit in der Darstellung zyklischer Polyphosphor-Gerüste untersucht, mit dem Ziel, einen Reaktionsweg zu finden, der selektiv zur Darstellung von 1,3-Dichlor-*cyclo*-tetraphosphanen $[ClP(\mu\text{-PTer})]_2$ ausgehend von P1-Bausteinen führen würde. In beiden Fällen wurden jedoch nur eine Vielzahl von Produkten erhalten, unabhängig davon, wie die Reaktion durchgeführt wurde.

Im Falle des $[TerP(ZnEt)_2]_2$ wurden weiterhin Reaktionen mit DMSO und Dichlormethan durchgeführt, allerdings konnten auch nach zahlreichen Versuchen keine Reaktionsprodukte isoliert werden.

Table of contents

Abbreviations

approx.	approximately
arom.	aromatic
ATR	attenuated total reflexion
avg.	average
Bu	butyl
calc.	calculated
cf.	compare (lat. *conferre*)
CI	chemical ionisation
conc.	concentration
cov.	covalent
Cp	cyclopentadienyl
δ	chemical shift
d	doublet
DFT	density functional theory
Dipp	2,6-diisopropylphenyl
dmap	4-dimethylaminopyridine
dmb	2,3-dimethyl-1,3-butadiene
DMSO	dimethylsulfoxide
DSC	differential scanning calorimetry
equiv.	equivalent
Et	ethyl
et al.	and others (lat. *et alii/aliae*)
exp.	experimental
GIAO	gauge-independent atomic orbital
IR	infrared spectroscopy
i	*iso, ipso*
J	coupling constant
m	multiplet (NMR), *medium* (IR)
m	*meta*
μ-	bridging group (in formulae)
Me	methyl
Mes	mesityl (2,4,6-trimethylphenyl)
Mes*	supermesityl (2,4,6-tri-*tert*-butylphenyl)
M	molar (= mol/L)
Mp.	melting point
MS	mass spectrometry
m/z	mass to charge
n	*normal*
$\tilde{\nu}$	wavenumber
NBO	natural bond analysis
NMR	nuclear magnetic resonance
o	*ortho*
p	*para*
Ph	phenyl
PhF	fluorobenzene
Pn	pnictogen
ppm	parts per million
Pr	propyl
q	quartet
R^F	hexafluoroisopropyl ($CH(CF_3)_2$)
ref.	reference
Rel.	relative
r.t.	room temperature
s	singlet (NMR), *strong* (IR)
t	triplet
t	*tert-*, *tertiary*
Ter	terphenyl (2,6-dimesitylphenyl)
THF	tetrahydrofuran
TMEDA	tetramethylethylenediamine
vdW	van der Waals
VT	variable temperature
w	*weak* (IR)

Units of measure

The system of measurement employed in this thesis is that of the International System of Units (SI). Deviating measuring units and their transformations into SI units are shown below.

Parameter	Unit	Description	Transformation
frequency	MHz	megahertz	1 MHz = 1 × 10^{6} s^{-1}
	Hz	hertz	1 Hz = 1 s^{-1}
length	cm	centimeter	1 cm = 1 × 10^{-2} m
	mm	millimeter	1 mm = 1 × 10^{-3} m
	nm	nanometer	1 nm = 1 × 10^{-9} m
	Å	Ångström	1 Å = 1 × 10^{-10} m
power	mW	milliwatt	1 mW = 1 × 10^{-3} kg m^{2} s^{-1}
mass	g	gram	1 g = 1 × 10^{-3} kg
	mg	milligramm	1 mg = 1 × 10^{-6} kg
amount of substance	mmol	millimol	1 mmol = 1 × 10^{-3} mol
temperature	°C	degrees celsius	T/K = T/°C – 273.15
volume	mL	millilitre	1 mL = 1 cm^{3} = 1 × 10^{-6} m^{3}
heat	kJ	kilojoule	1 kJ = 1 × 10^{3} m^{2} kg s^{-2}
wavenumber	cm^{-1}	reciprocal centimeter	1 cm^{-1} = 100 m^{-1}
time	d	day	1 d = 8.64 × 10^{4} s
	h	hour	1 h = 3.6 × 10^{3} s
	min	minute	1 min = 60 s

1 Aim and Motivation

Ring systems composed of group 15 elements (pnictogens, Pn) have been of major interest to inorganic chemists for over a century.[1,2] Our group is especially interested in the synthesis of small pnictogen or interpnictogen ring systems bearing easily abstractable halide substituents such as the well established *cyclo*-1,3-diphospha-2,4-diazanes [XP(μ-NR)]$_2$ (R = C or Si based substituent, X = (pseudo)halogen)[3] or their phosphorus congeners [XP(μ-PR)]$_2$, two examples of which were recently reported (**2** and **4**, Scheme 1).[4,5] While 1,3-dichloro-*cyclo*-tetraphosphane **2** can easily be obtained via a base-assisted P–P coupling reaction starting from Mes*PH$_2$ (**1**, Mes* = 2,4,6-tri-*tert*-butylphenyl) and PCl$_3$, the analogous approach starting from TerPH$_2$ (**3**, Ter = 2,6-bis-(2,4,6-trimethyl-phenyl)phenyl) did not give rise to 1,3-dichloro-*cyclo*-tetraphosphane **4**.[4] However, it was obtained following a rather complicated multi-step synthetic route that involved a metathesis reaction of heavier interpnictogen ring systems with PCl$_3$ (Scheme 1).

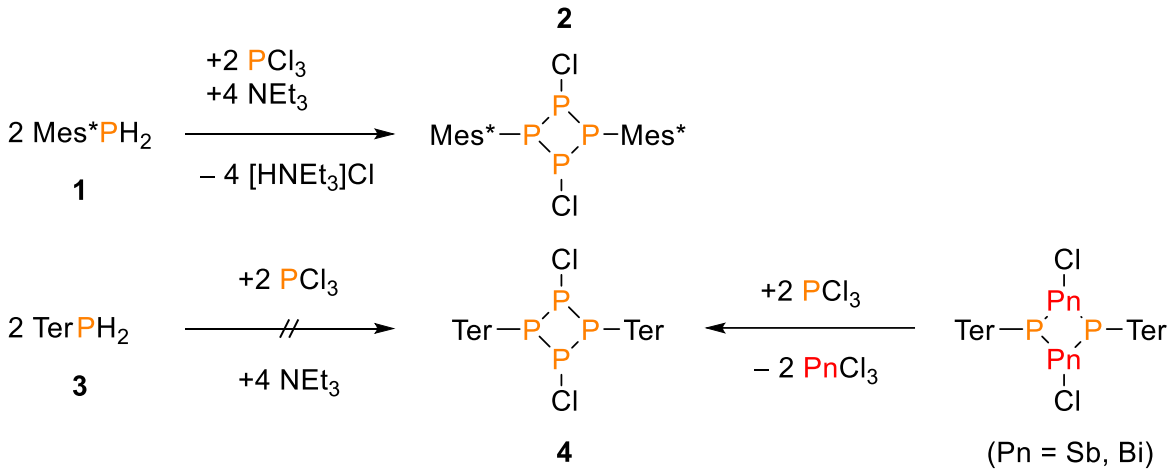

Scheme 1: Synthetic approaches to 1,3-dichloro-*cyclo*-tetraphosphanes **2** and **4**.[4,5]

Therefore, it was desirable to find a more facile synthetic route to 1,3-dichloro-*cyclo*-tetraphosphane **4** in order to investigate its reactivity and to determine whether it is as versatile a reagent as *cyclo*-tetraphosphane **2**.[6] For that purpose and in analogy to known tin amides, which were used as soft amination reagents to synthesize *cyclo*-1,3-distiba- and *cyclo*-1,3-dibisma-2,4-diazanes (cf. Chapter 2.2),[7,8] it was desirable to investigate phosphide reagents that can be utilized in nucleophilic substitution reactions at electrophilic

pnictogen centers. In addition to tin phosphides, which are currently under investigation in our group, zinc phosphides also appeared to be appropriate precursors for such purposes.

Hence, the aim of this project was to synthesize novel Ter-substituted zinc phosphides and to research their applicability in the preparation of compound **4**. The synthesized compounds were to be fully characterized by means of NMR and vibrational spectroscopy, X-ray crystal structure determination, mass spectrometry, and other analytical methods. Furthermore, the data thus obtained were to be evaluated by means of computational studies.

2 Introduction

2.1 *Cyclo*-Tetraphosphanes of the type [XP(*μ*-PR)]$_2$

Cyclo-tetraphosphanes of the type [PR]$_4$ were first discovered in 1956 by Kuchen and Buchwald who reinvestigated the reaction of phenyldichlorophosphane $PhPCl_2$ with the parent phenylphosphane which gave rise to a 1,2,3,4-tetraphenyl-*cyclo*-tetraphosphane (**5,** Scheme 2). The same reaction had already been performed and reported by Michaelis and Köhler in 1877, however, since they had only obtained analytical data from elemental analyses, they were convinced that they had prepared a 1,2-diphenyl-diphosphene (**6**).[1] Not until Kuchen and Buchwald determined the molecular mass of this reaction's product, the actual structure was found to be a formal dimer of the previously postulated diphosphene.[9]

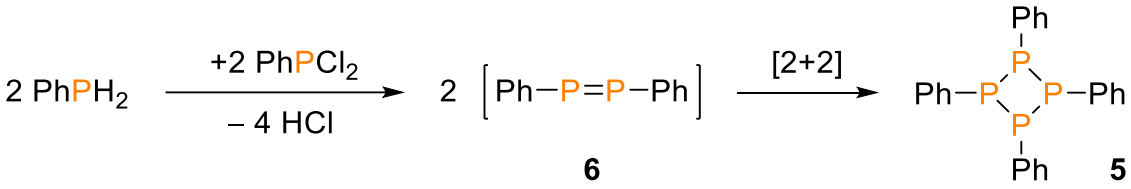

Scheme 2: Synthesis of 1,2,3,4-tetraphenyl-*cyclo*-tetraphosphane (**5**).[1,9]

Since their first discovery, several more *cyclo*-tetraphosphanes have been prepared.[3] However, one class of *cyclo*-tetraphosphanes, namely those with more easily abstractable halide substituents, are by far not as well established and researched as their lighter congeners, the 1,3-dihalo-*cyclo*-1,3-diphospha-2,4-diazanes of the type [XP(*μ*-NR)]$_2$ (R = C or Si based substituent, X = (pseudo)halogen).[3]

In fact, *cyclo*-tetraphosphanes of the type [XP(*μ*-PR)]$_2$ were unknown to the scientific literature up until 2002, when the first example was prepared by Karaghiosoff and co-workers. They reported on the reaction of NaSi(*t*-Bu)$_3$ with PCl_3 which gave rise to the 1,3-dichloro-*cyclo*-tetraphosphane [ClP(*μ*-PSi(*t*-Bu)$_3$)]$_2$ (**7**) among other products. However, **7** could not be isolated and was therefore only characterized by ^{31}P NMR spectroscopy.[10] The first group to prepare, successfully isolate, and to fully characterize one such compound was that of Lerner in 2009. Their synthetic approach (Scheme 3) started

from white phosphorus (P_4), which they treated with NaSi(*t*-Bu)$_3$ to form the acyclic tetraphosphenediide $Na_2[(t\text{-Bu})_3SiPPPPSi(t\text{-Bu})_3]$ (**8**). The 1,3-diiodo-*cyclo*-tetraphosphane $[IP(\mu\text{-PSi}(t\text{-Bu})_3)]_2$ (**9**, Scheme 3) was then obtained by treating **8** with two equivalents of gold iodide.

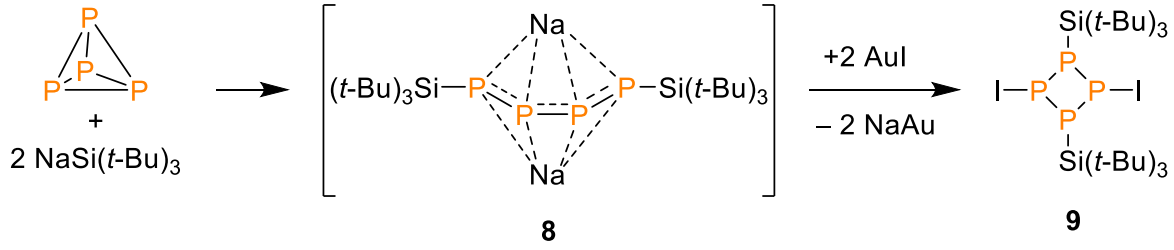

Scheme 3: Synthesis of **9** starting from white phosphorus.

Furthermore, Schulz *et al*. reported the most comprehensive knowledge on 1,3-dichloro-*cyclo*-tetraphosphanes over the course of the last few years by introducing two novel compounds and by investigating their reactivity more deeply for the first time.

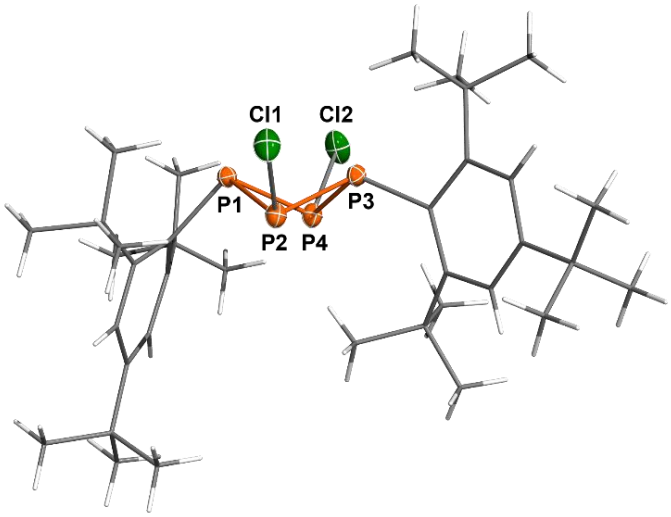

Figure 1: Molecular structure of **2** in the crystal ($P2_1/c$). Thermal ellipsoids drawn at the 50 % probability level and −100 °C. Carbon and hydrogen atoms rendered as wireframe for clarity. Selected bond lengths (Å), angles (°) and dihedral angles (°): P1–P2 2.2731(5), P1–P4 2.2596(5), P1–C1 1.869(1), P2–P3 2.1905(5), P2–Cl1 2.0967(5), P3–P4 2.2026(5), P3–C19 1.844(1), P4–Cl2 2.1061(6); C1–P1–P2 99.23(4), C1–P1–P4 101.96(4), P1–P2–P3 80.54(2), P1–P2–Cl1 106.45(2), P3–P2–Cl1 97.97(2), P2–P3–P4 84.65(2), P2–P3–C19 108.97(5), P4–P3–C19 122.05(5), P3–P4–P1 80.58(2), P3–P4–Cl2 97.32(2), P1–P4–Cl2 104.47(2); P1–P2–P4–P3 119.45(3).[4]

The first 1,3-dichloro-*cyclo*-tetraphosphane to be fully characterized was obtained by treatment of sterically hindered Mes*PH_2 (**1**, Mes* = 2,4,6-tri-*tert*-butylphenyl) with PCl_3 in the presence of basic NEt_3 which gave $[ClP(\mu\text{-PMes*})]_2$ (**2**) in up to 50 % yield

(Scheme 1).[4] **2** was crystallized from saturated fluorobenzene (PhF) solutions in three polymorphous modifications as a PhF solvate **2**·PhF in the monoclinic space group $P2_1/n$ and solvate-free in the monoclinic space group $P2_1/c$ and the triclinic space group $P\bar{1}$. The P–Cl bonds were within the range of typical P–Cl single bonds whereas the P–P bond lengths ranged from 2.1905(5) Å for the P2–P3 bond to 2.2731(5) Å for the P1–P2 bond ($P2_1/c$, cf. Σr_{cov}(P–Cl) = 2.10 Å, Σr_{cov}(P–P) = 2.22 Å).[11] This was attributed to the different arrangement of the Mes* substituents in the solid state, which was also the reason why the chlorine atoms were slightly bent towards P1 (Figure 1). **2** exhibited a butterfly conformation with differing fold angles for the central P_4 unit depending on the modification. They ranged from 120° ($P2_1/c$), over 139° ($P\bar{1}$) to 143° ($P2_1/n$). The differences were likely caused by packing effects in the crystal.[4]

1,3-Dichloro-*cyclo*-tetraphosphane **2** was the compound for which the reactivity of such systems was investigated for the first time. For example, the treatment of **2** with Lewis base 4-(*N*,*N*-dimethylamino)-pyridine (dmap) afforded the isolation of the first [3.1.0.0^{2,4}]-tricyclic hexaphosphane Mes*P_6Mes* (**10**) via a monocyclic *cyclo*-triphosphane intermediate (Scheme 4).[12]

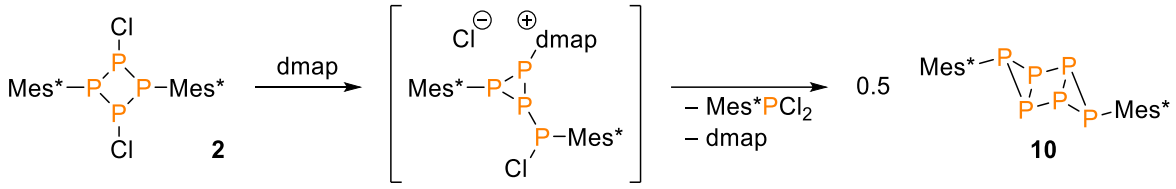

Scheme 4: Synthesis of the tricyclic hexaphosphane **10**.[12]

On the other hand, treating **2** with Lewis acid $GaCl_3$ afforded the low-temperature isolation of bicyclic phosphinophosphonium salt [Mes*$_2$$P_4$Cl][$GaCl_4$] (**11**[$GaCl_4$]) which represents the first example of a bicyclic tetraphosphane that comprises a cationic phosphonium center. **11**[$GaCl_4$] was formed as a mixture of two isomers of which only isomer **11a**[$GaCl_4$] with both Mes* substituents in *exo*-position was successfully crystallized and fully characterized (Scheme 5). Furthermore, the intermediate formation of a transient *cyclo*-tetraphosphenium cation (**12**$^+$) was observed by ^{31}P NMR spectroscopy. Its quantitative intermediate formation at low temperatures was eventually proved by addition of dimethylbutadiene (dmb) as a trapping reagent, which led to quantitative formation of tetraphosphabicyclo[4.2.0]octenium

salt **13**[$GaCl_4$] (Scheme 5), which can be regarded as the [4+2] cycloaddition product of transient **12**$^+$ and dmb.[13]

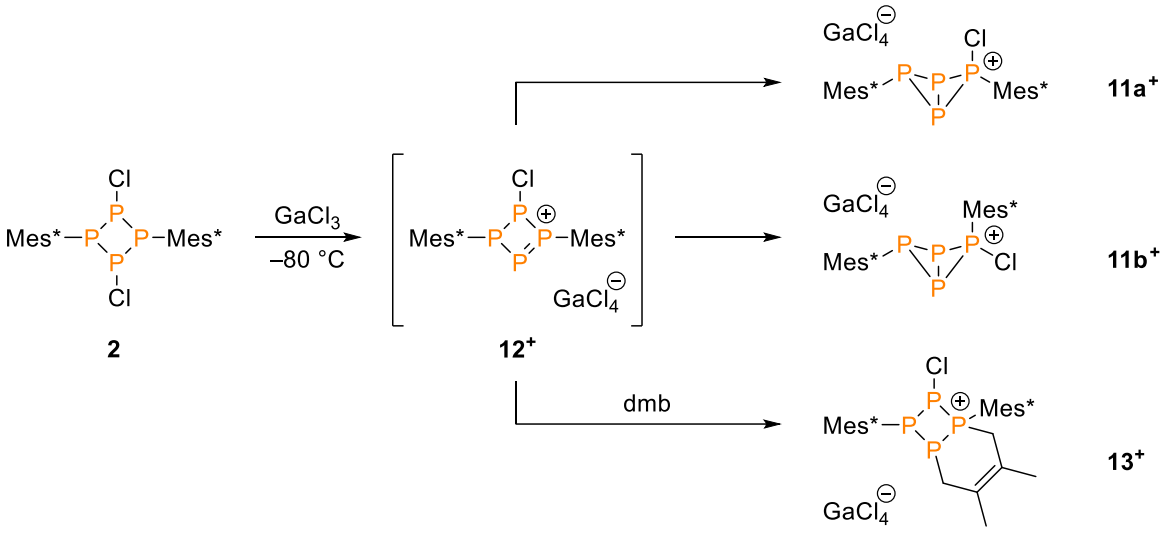

Scheme 5: Treatment of **2** with $GaCl_3$ gave rise to transient **12**[$GaCl_4$]. Longer reaction times led to the formation of **11**[$GaCl_4$] while trapping with dmb yielded **13**[$GaCl_4$].[13]

In an attempt to stabilize the transient *cyclo*-tetraphosphenium cation **12**$^+$, the reactivity of **2** towards silver salts of the weakly coordinating anion $[Al(OR^F)_4]^-$ (R^F = $CH(CF_3)_2$)[14] was explored. However, instead of precipitating AgCl while stabilizing transient **12**$^+$ with the weakly coordinating anion, this reaction gave rise to the dinuclear silver complex **14**$[Al(OR^F)_4]_2$ (Scheme 6).[15]

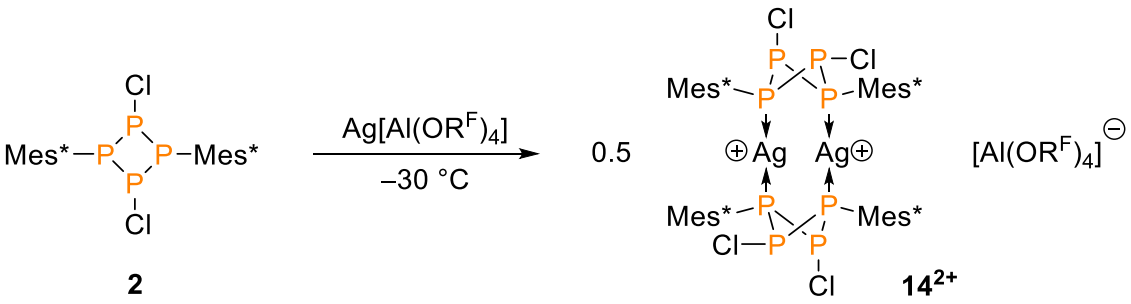

Scheme 6: Reaction of **2** with $Ag[Al(OR^F)_4]$ yielded the dinuclear silver complex **14**$[Al(OR^F)_4]_2$.[15]

Finally, synthetic routes to selectively obtain *exo-exo*-bicyclo[1.1.0]tetraphosphane **15a** and *endo-exo*-bicyclo[1.1.0]tetraphosphane **15b** starting from **2** were reported. Isomer **15a** was previously prepared in very low yields and characterized by Fluck *et al*. in 1985,[16] whereas the isomer **15b** was not isolated until almost thirty years later.[17] **15a** and **15b**, which usually formed as mixtures of both isomers, were prepared separately starting from **2** by either

reduction with elemental magnesium or treatment with tetramethylimidazolylidene (Scheme 7). While the former reaction gave pure **15a** in high yields, the latter led to carbene promoted degradation of **2**. However, the product mixture of the degradation reaction contained both isomers of **15** in a convenient isomeric ratio (**15a** : **15b**) of 1 : 12, which facilitated comparatively easy isolation of **15b**.[17]

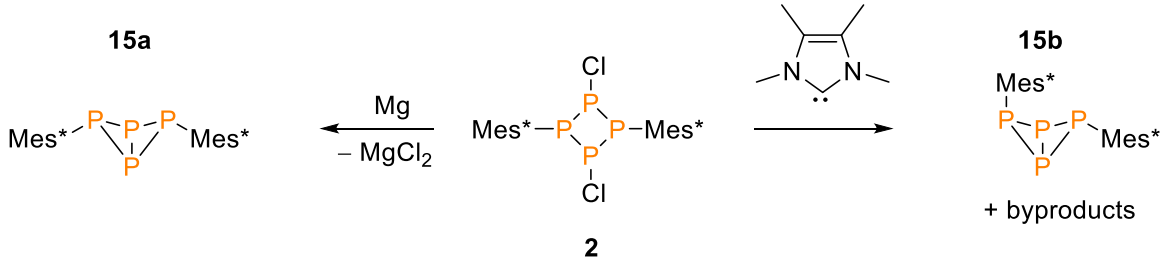

Scheme 7: Synthetic routes to selectively obtain **15a** or **15b** from **2**.[17]

To further extend the knowledge on such systems, synthetic approaches for 1,3-dichloro-*cyclo*-tetraphosphanes bearing other sterically demanding groups, namely the terphenyl moiety (Ter = 2,6-bis-(2,4,6-trimethylphenyl)phenyl) were investigated. However, the synthesis of $[ClP(\mu\text{-PTer})]_2$ (**4**) proved to be more complicated than that of its Mes*-substituted derivative. The analogous preparative route of treating the parent $TerPH_2$ (**3**) with PCl_3 in the presence of base did not yield the *cyclo*-tetraphosphane **4**, but instead a *cyclo*-triphosphane with an exocyclic phosphanyl moiety (**16**, Scheme 8). However, upon heating a solution of **16** in THF to 75 °C over an extended period of time, it was found to slowly isomerize into two configurational isomers of the desired 1,3-dichloro-*cyclo*-tetraphosphane **4** among other byproducts, as observed by means of ^{31}P NMR spectroscopy.

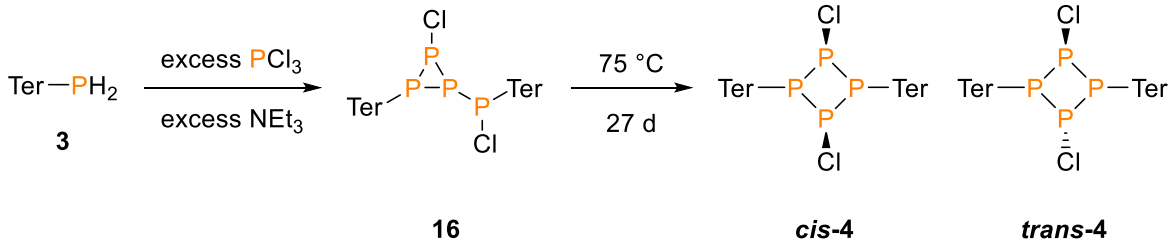

Scheme 8: Synthesis of **16** and its slow isomerization into ***cis*-4** and ***trans*-4**.[4]

Both isomers were found to differ in the spatial arrangement of the chloride substituents. ***Cis*-4** had both chloride substituents in equatorial positions, whereas ***trans*-4** had one chloride in equatorial and the second in axial position (Scheme 8). In the end, even though **16** was indeed found to isomerize into **4**, the long reaction time of about a month rendered

this approach unfeasible for synthetic use. Furthermore, isolation of any products thus obtained was not facilitated.[4]

Only recently, however, the Schulz group reported on another synthetic approach that afforded the successful isolation of ***cis*-4** (Figure 2). A metathesis reaction starting from 1,3-dichloro-*cyclo*-1,3-dipnicta-2,4-diphosphanes [ClPn(μ-PTer)]$_2$ (**17a**, Pn = Sb; **17b**, Pn = Bi) with PCl_3, for which especially the precipitation of $BiCl_3$ was a major driving force, gave a product mixture with both isomers of **4** being the major products among other compounds observed by ^{31}P NMR spectroscopy (Scheme 9).[5]

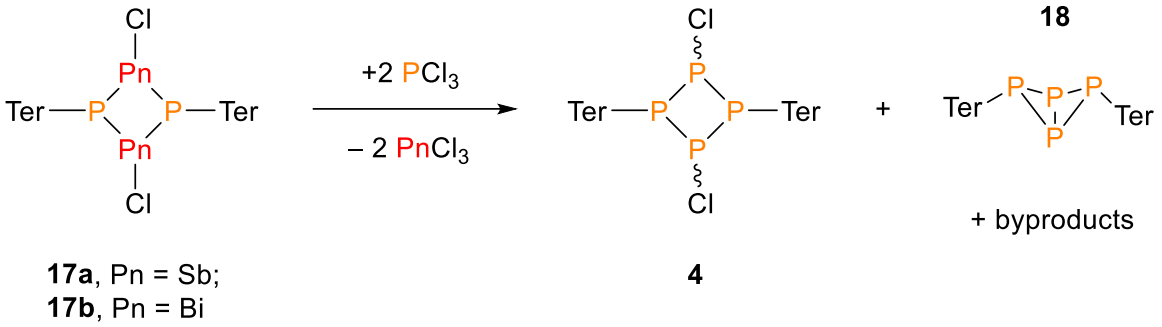

Scheme 9: Metathesis route to ***cis*-4** and ***trans*-4** that afforded the isolation of ***cis*-4**.[5]

The main drawback of this synthetic route was the concomitant formation of [1.1.0]bicyclic tetraphosphane **18** for which only the resonances of the *exo*-*exo*-bicyclo[1.1.0]-tetraphosphane were observed by ^{31}P NMR spectroscopy. Prolonged reaction times seemed to benefit the formation of **18** rather than that of **4**. Even though the primarily observed combined yield for both isomers of **4** was very high according to ^{31}P NMR spectroscopy, isolation of the target compounds proved difficult due to the presence of byproducts. However, it was possible to isolate pure crystals of ***cis*-4** in 21 % yield for full characterization, rendering this metathesis route the first feasible synthetic approach to **4**.[5]

Colorless crystals of ***cis*-4** were obtained from saturated solutions in dichloromethane. ***Cis*-4** crystallized in the monoclinic space group $P2_1/c$ with four molecules per unit cell. The P−Cl bond lengths were very similar with an average value of 2.076 Å, which is shortened compared to typical P−Cl single bonds. The P−C bond lengths with an average of 1.853 Å are within the range of P−C single bonds whereas the P−P bonds lengths averaged to 2.231 Å, which is marginally longer than the sum of covalent radii for P−P single bonds (cf. Σr_{cov}(P–C) = 1.84 Å, Σr_{cov}(P–Cl) = 2.10 Å, Σr_{cov}(P–P) = 2.22 Å).[11] All P−P−P angles

within the P_4 ring are very similar and range from 83.92(4)° for P2−P3−P4 to 84.53(4)° for P1−P2−P3. For the abovementioned crystal structure of **2** ($P2_1/c$, Figure 1), especially the latter value was smaller by almost 4° while the P2−P3−P4 angle was within the same range.

The observed fold angle of the P_4 butterfly of **4** in the crystal with −129.50(5)° was only a little smaller than the average fold angle of all three crystal modifications observed for **2**. In contrast to all crystal modifications observed for **2**, though, the chloride substituents in **4** are arranged more or less in the center of the P_4 unit whereas they were significantly bent towards P1 in **2** in the solid state.

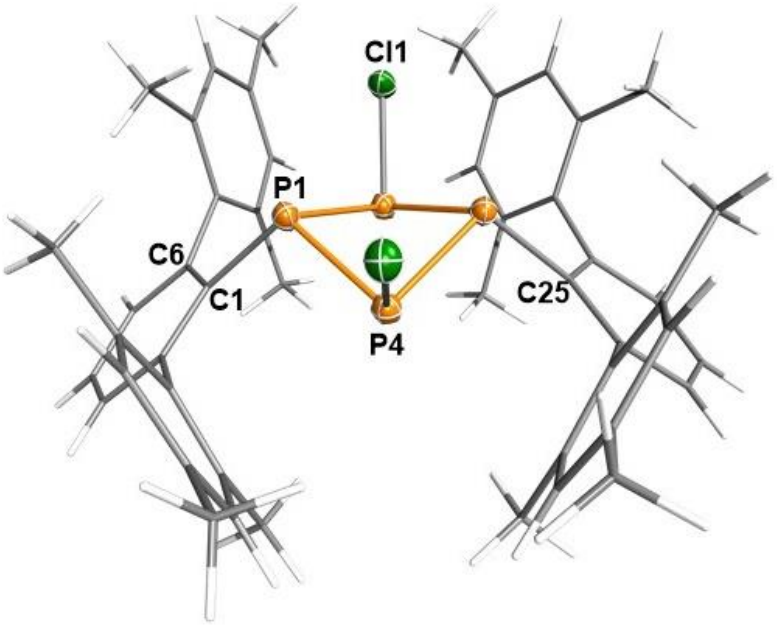

Figure 2: Molecular structure of ***cis*-4** in the crystal ($P2_1/c$). Thermal ellipsoids drawn at the 50 % probability level and −150 °C. Carbon and hydrogen atoms rendered as wireframe for clarity. Selected bond lengths (Å), angles (°) and dihedral angles (°): Cl1−P2 2.072(1), Cl2−P4 2.079(1), P1−C1 1.852(3), P1−P2 2.227(1), P1−P4 2.230(1), P2−P3 2.231(1), P3−C25 1.854(3), P3−P4 2.236(1); P1−P2−P3 84.53(4), P2−P1−P4 84.15(4); P1−P2−P4−P3 −129.50(5).[5]

It is quite obvious that, although a successful preparative route for 1,3-dichloro-*cyclo*-tetraphosphane **4** was found, it is much more complicated than the rather straightforward synthesis of **2**. Moreover, the fact that **4** was always formed as a mixture of two configurational isomers, isolation of pure compounds was impaired and was only achieved for ***cis*-4**. In order to investigate the reactivity of **4** in the same manner as the reactivity of **2** was researched, another, more facile synthetic approach must be established.

2.2 Metathesis reactions of tin amides of the type [Sn(μ-NR)]$_2$

Generally applied, base-assisted P−P coupling reactions with the parent phosphane TerPH$_2$ (**3**) and PCl$_3$ did not readily yield the target compound **4**. Metathesis reactions, however, were successfully applied to prepare **4**, the only drawback being the impaired isolation of pure compounds which could be attributed to the presence of byproducts. Therefore, optimization of the metathesis reaction appeared to be the best way to synthesize 1,3-dichloro-*cyclo*-tetraphosphanes **4**. One possible optimization, for example, could be the employment of different starting materials.

In 2010, Power and co-workers reported on the preparation of a series of dimeric metal(II) imido complexes of the type [M(μ-NTer)]$_2$ (**19a**, M = Ge; **19b**, M = Sn; **19c**, M = Pb).[7] They were obtained by treating the parent primary terphenylamine TerNH$_2$ with the respective metal amides M{N(SiMe$_3$)$_2$}$_2$ (M = Ge, Sn, Pb) which, in each case, afforded deeply colored crystals of dimeric *cyclo*-1,3-dimetalla-2,4-diazanes [M(μ-NTer)]$_2$ with concomitant elimination of volatile HN(SiMe$_3$)$_2$ (Scheme 10).[7] All three metal imides **19** comprised central, non-planar four-membered M$_2$N$_2$ cores that were bent along their M−M axes with dihedral angles ranging from 172° for **19a** to approx. 148° for **19b** and **19c**.

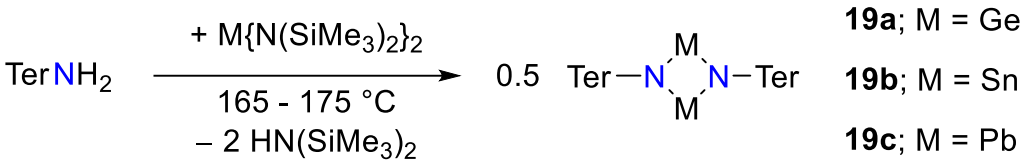

Scheme 10: Syntheses of **19a**, **19b**, and **19c** by treatment of TerNH$_2$ with M{N(SiMe$_3$)$_2$}$_2$.[7]

The *cyclo*-1,3-distanna-2,4-diazane [Sn(μ-NTer)]$_2$ (**19b**) was then successfully applied by the Schulz group in a metathesis reaction as a soft amination reagent to synthesize 1,3-dichloro-*cyclo*-1,3-dipnicta-2,4-diazanes [ClPn(μ-NTer)]$_2$ (**20a**, Pn = Sb; **20b**, Pn = Bi) under concomitant elimination of SnCl$_2$ (Scheme 11). This procedure, for the first time, allowed the preparation of pure **20a** and **20b** in large quantities and good yields. Moreover, unlike other synthetic approaches, this procedure afforded **20a** and **20b** cleanly with almost no observable side reactions.[8]

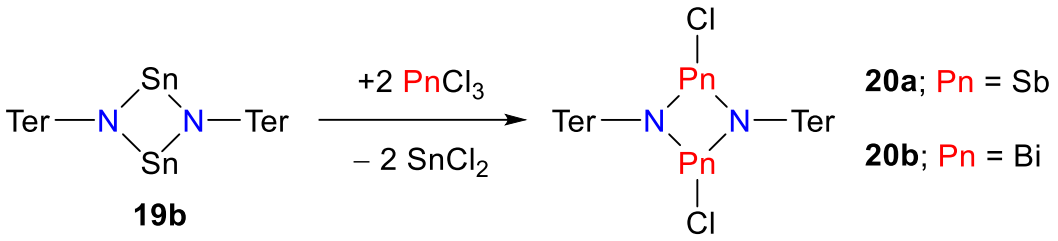

Scheme 11: Synthesis of **20a** and **20b** via a metathesis route.[8]

Inspired by these results, we decided that it could be worthwhile to investigate terphenyl-phosphides other than **17a** and **17b** (Scheme 9) as starting materials for the preparation of Ter-substituted *cyclo*-tetraphosphane **4**. For that purpose, tin phosphides are currently under investigation, while the latest results on Ter-substituted zinc phosphides are the subject of this work.

2.3 Sterically encumbered zinc phosphides and phosphadiides

At the beginning of this project, a comprehensive review of the scientific literature on zinc phosphides was conducted. It was thus found that, in the literature, there are few examples of zinc phosphides that were obtained from primary phosphanes.

In 1996, Westerhausen *et al.* reported on the reaction of tris(trimethylsilyl)methylzinc chloride with *in situ* generated, lithiated primary phosphane (*i*-Pr)$_3$SiP(H)Li, which gave rise to the first example of a monomeric phosphadiide of zinc, the bis-[tris-(trimethylsilyl)-methylzinc]-triisopropyl-silylphosphadiide (**21**, Scheme 12) with a three-coordinate phosphorus atom.[18] Moreover, to the best of our knowledge, **21** is the only example of a sterically encumbered phosphadiide of zinc that was synthesized from a primary phosphane to date.

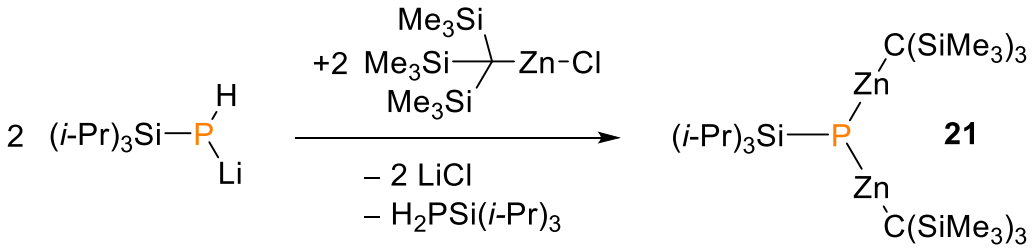

Scheme 12: Synthesis of monomeric zinc phosphadiide **21** from a lithiated primary phosphane.[18]

21 was characterized in solution and in the solid state and was thus found to exist as a monomeric zinc phosphadiide in solution as well as in the crystal. This was attributed to the high steric demand of the substituents at the zinc atoms.

In case of smaller substituents at the zinc atom, dimers, trimers and tetramers were observed more often. For example, in 2003, Wright and co-workers reported on the reaction of dimethylzinc with two equivalents of *t*-BuPH$_2$ and subsequent treatment with Sb(NMe$_2$)$_2$, which gave rise to trimeric zinc phosphide [MeZn(μ-PH(*t*-Bu))·NHMe$_2$]$_3$ (**22**, Scheme 13). **22** comprised a six-membered P−Zn ring with four-coordinate phosphorus and zinc atoms and was fully characterized in solution and the solid state.[19]

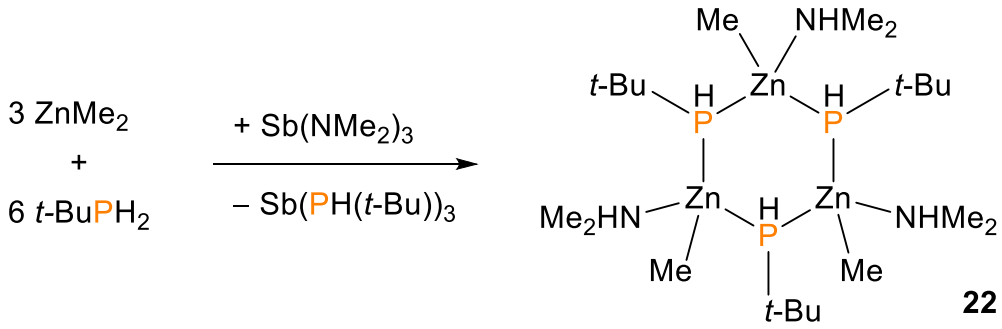

Scheme 13: Synthesis of trimeric zinc phosphide **22** from *t*-BuPH$_2$ and ZnMe$_2$.[19]

In 2005, Westerhausen and co-workers reported on further zinc phosphides which they obtained via treatment of (*t*-Bu)$_3$SiPH$_2$ with ZnMe$_2$ or ZnEt$_2$, respectively (**23** & **24**, Scheme 14). Both compounds formed dimeric species in solution, thus comprising four-membered P−Zn rings with four-coordinate phosphorus atoms. However, **23** was also characterized by X-ray single crystal diffractometry and was thus found to exist as tetrameric, cubane-type [(*t*-Bu)$_3$SiPH(ZnMe)]$_4$ in the solid state (Figure 3).[20,21]

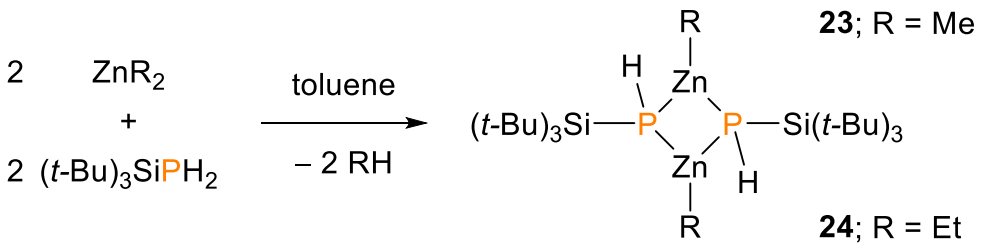

Scheme 14: Synthesis of **23** and **24** from (*t*-Bu)$_3$SiPH$_2$ and ZnMe$_2$ or ZnEt$_2$, respectively.[20,21]

23 crystallized as a toluene solvate (**23**·2Tol) in the tetragonal space group *I*4̄2*m* with two molecules per unit cell. The P−Si and Zn−C bond lengths were found to be within the

respective range of typical single bonds, however, the P−Zn bonds were considerably elongated compared to the sum of the covalent radii (cf. Σr_{cov}(P–Zn) = 2.29 Å, Σr_{cov}(P–Si) = 2.27 Å, Σr_{cov}(Zn–C) = 1.93 Å).[11] All angles within the central P_4Zn_4 cube were close to 90 °, although the Zn–P–Zn angles were found to be slightly larger than the P–Zn–P angles.

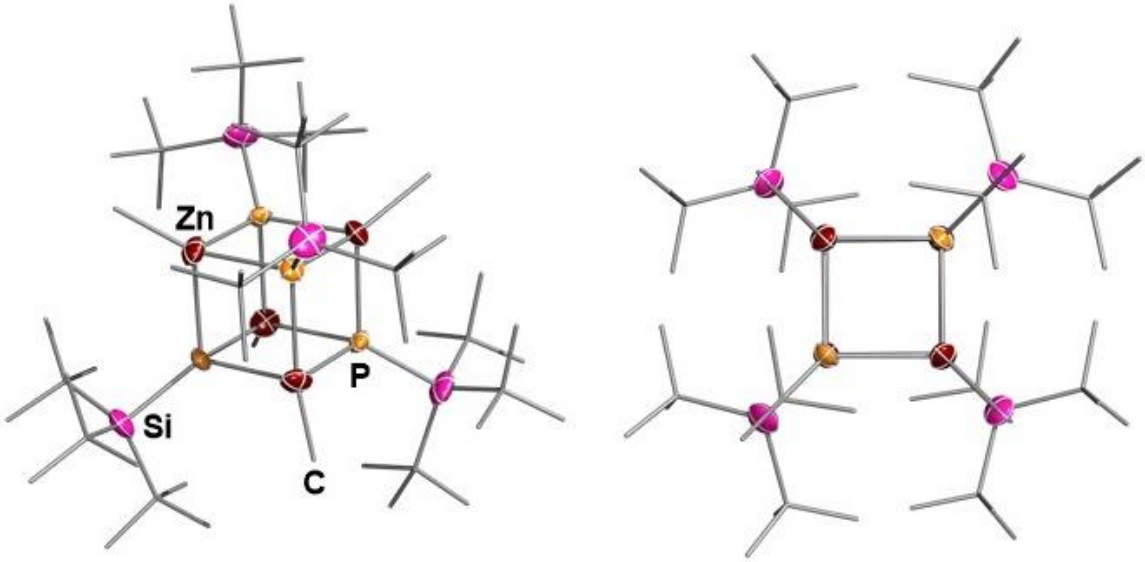

Figure 3: Molecular structure of **23** in the crystal (*I*42*m*) seen from the side (left) and from above (right). Thermal ellipsoids drawn at the 50 % probability level and −73 °C. Carbon atoms rendered as wireframe, hydrogen atoms and solvent molecules omitted for clarity. Averaged selected bond lengths (Å) and angles (°): P−Zn 2.485, P−Si 2.202, Zn−C 1.978; Zn−P−Zn 91.27, P−Zn−P 88.72.[20]

The abovementioned zinc phosphides **23** and **24** were obtained following the synthetic route depicted in Scheme 14. However, applying 1.5 equivalents of $ZnEt_2$ on $(t\text{-Bu})_3SiPH_2$ gave rise to zinc phosphadiide $(EtZn)_4Zn_2(PSi(t\text{-Bu})_3)_4$ (**25**, Figure 4). **25** was a binary cage compound that comprised two four-membered Zn_2P_2 rings with three-coordinate zinc atoms, which were interconnected via two P−Zn−P bridges with two-coordinate zinc atoms.[22]

25 crystallized from toluene in the form of yellow platelets in the orthorhombic space group *Pbca* with four molecules per unit cell. The P−Zn bonds lengths within the four-membered rings averaged to 2.420 Å whereas the bonds between phosphorus and the two-coordinate zinc atoms were found to be much shorter with an average length of 2.244 Å, which is shorter than the sum of the covalent radii for P−Zn single bonds (cf. Σr_{cov}(P–Zn) = 2.29 Å).[11] The coordination environment at the two-coordinate zinc atoms (Zn2) was bent with P−Zn2−P angles of 163.28°. The coordination environment at the three-coordinate zinc atoms was trigonal pyramidal while the coordination environment at the four-coordinate

phosphorus atoms resembled a distorted tetrahedron. The four-membered P_2Zn_2 ring comprised almost rectangular P−Zn−P angles (avg. 91.33°), slightly acute Zn−P−Zn angles (avg. 86.77°), and was found to be puckered with a fold angle of 159.57(2)°.[22]

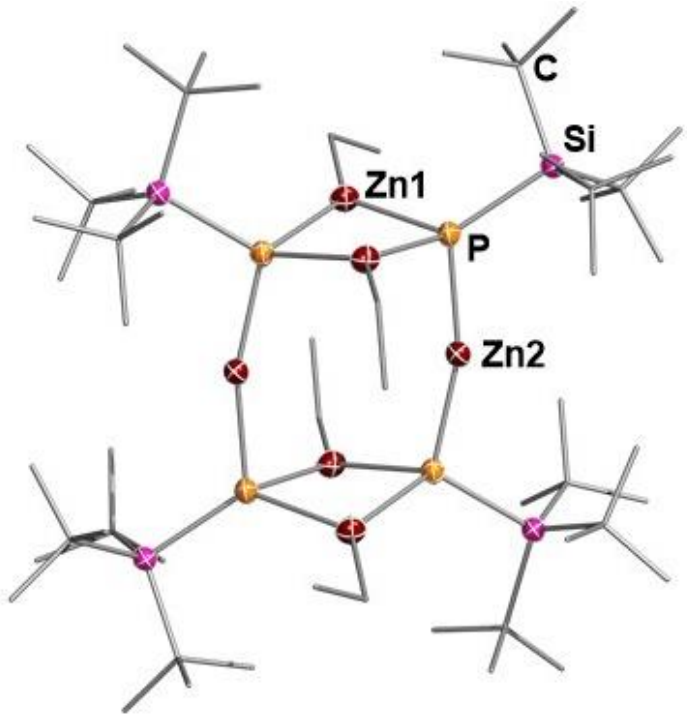

Figure 4: Molecular structure of **25** in the crystal (*Pbca*). Thermal ellipsoids drawn at the 50 % probability level and −100 °C. Carbon atoms rendered as wireframe, hydrogen atoms and solvent molecules omitted for clarity. Averaged selected bond lengths (Å), angles (°) and dihedral angles (°): P−Si 2.276, P−Zn1 2.420, P−Zn2 2.244, Zn−C 1.981; P−Zn1−P 91.33, P−Zn2−P 163.28, Zn−P−Zn 86.77; P−Zn1−Zn1−P 159.57.[22]

Finally, one last zinc phosphide is worthy of note. In 2014, Driess *et al.* reported on the reactivity of what they called a half-parent phosphasilene (**26**, Scheme 15) towards small molecules. Treatment of **26** with dimethylzinc in the presence of *N,N,N',N'*-tetramethyl-ethylenediamine (TMEDA), for instance, afforded the 1,2-addition product **27** which was isolated and fully characterized. Although **27** was not generated starting from a primary phosphane, it is, however, the only known example of a monomeric zinc monophosphide with a three-coordinate phosphorus atom (Figure 5).[23]

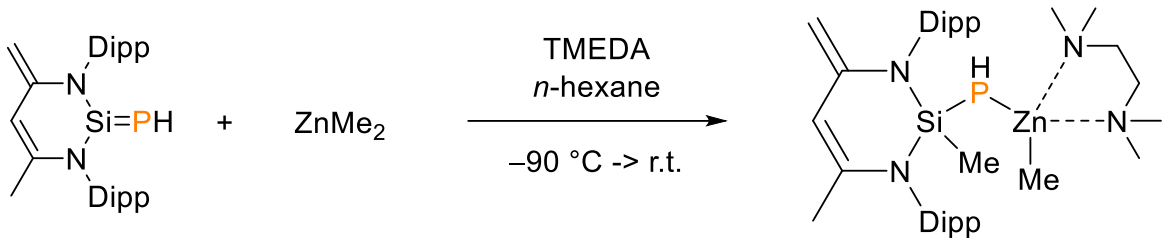

26 **27**

Scheme 15: Synthesis of monomeric zinc phosphide **27**.[23]

27 crystallized in the triclinic space group $P\bar{1}$ with two molecules per unit cell. The P1–Si1 bond (2.2022(1) Å) was found shorter than the sum of the covalent radii whereas the P1−Zn1 bond (2.3670(2) Å) as well as the Zn1–C31 bond (1.9902(1) Å) were found to be slightly longer than expected for average single bonds (cf. Σr_{cov}(P–Zn) = 2.29 Å, Σr_{cov}(P–Si) = 2.27 Å, Σr_{cov}(Zn–C) = 1.93 Å).[11] The coordination environment at Zn1 is that of a considerably distorted tetrahedron with a large P1–Zn1–C31 angle of 137.1(2)° and a very small N3–Zn1–N4 angle of 81.8(1)°.

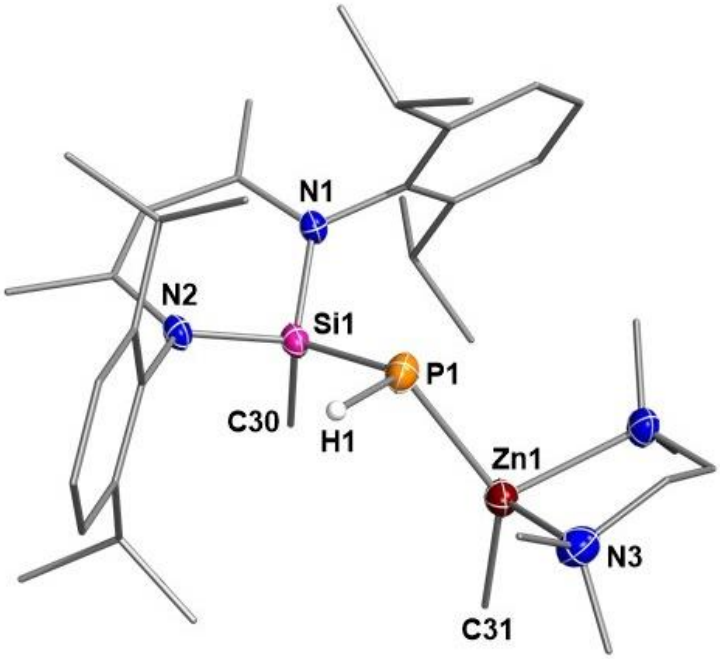

Figure 5: Molecular structure of **27** in the crystal ($P\bar{1}$).Thermal ellipsoids drawn at the 50 % probability level and −123 °C. Carbon atoms rendered as wireframe, hydrogen atoms are omitted for clarity except for that at P1. Selected bond lengths (Å) and angles (°): Si1−P1 2.2022(1), Zn1−C31 1.9902(1), P1−Zn1 2.3670(2), Si1−P1−Zn1 106.66(6), P1−Zn1−C31 137.1(2), N3−Zn1−N4 81.8(1), H1−P1−Zn1 112(2).[23]

3 Results and Discussion

3.1 Preparation of starting materials

3.1.1 Preparation of $TerPH_2$ (3)

The preparation of terphenylphosphane ($TerPH_2$, **3**, Ter = 2,6-bis-(2,4,6-trimethylphenyl)-phenyl) was carried out in two steps following a modified synthetic route taken from the literature (Scheme 16).[4] In the first step, mesityl bromide (MesBr, Mes = 2,4,6-trimethylphenyl) was treated with elemental magnesium in THF to afford the Grignard reagent MesMgBr. In the meantime, 1,3-dichlorobenzene was lithiated with *n*-butyllithium at −80 °C, whereupon the Grignard reagent was added dropwise at −80 °C. Subsequently, the mixture was treated with PCl_3 at −80 °C, which gave rise to a mixture of the three terphenyldihalophosphanes $TerPCl_2$ (**28a**), $TerPBr_2$ (**28b**), and TerPBrCl (**28c**) in approximately 50 % yield. This product distribution is most likely the result of performing this experiment as a one-pot procedure, which allows for halogen exchange at the phosphorus atom. However, since all three products can easily be reduced with $LiAlH_4$ to give the desired $TerPH_2$ (**3**), further separation and purification was not necessary.

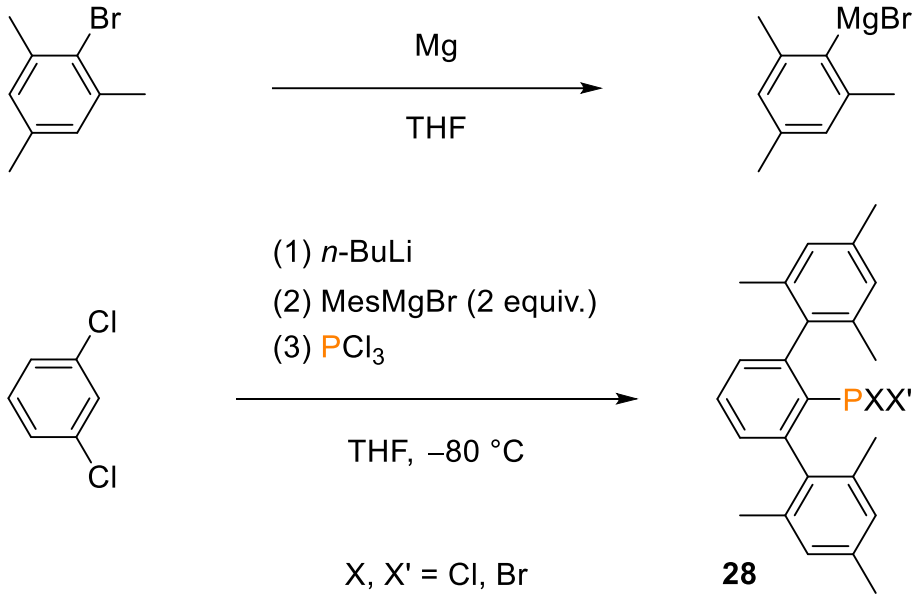

Scheme 16: One-pot synthesis of TerPXX‘ **28** (X, X‘ = Cl, Br).

It is noteworthy that the product distribution seems to vary for each particular experiment, however, some commonalities were observed. Firstly, the mixed-halogenated phosphane TerPBrCl (**28c**) appears to be the major product being formed to the extent of about 40-50 %. Secondly, the terphenyldibromophosphane **28b** was found to be the minor product in most cases, being formed to the extent of about 20 %.[4]

Additionally, two further byproducts were observed by ^{31}P NMR spectroscopy, each displaying a singlet resonance at 85.6 ppm and 75.0 ppm, respectively. They could not be separated from the dihalophosphane mixture but it was possible to identify them as Mes_2PCl and Mes_2PBr by comparison with literature data.[24,25] Their formation is most likely due to the slightly excessive use of the Grignard reagent MesMgBr (cf. Chapter 5.3.1), however, further purification of the dihalophosphane mixture was not attempted since the byproducts were formed to a very small extent.

In a second step, the mixture of dihalophosphanes was reduced with $LiAlH_4$ in boiling diethyl ether to give $TerPH_2$ (**3**) in about 65 % yield (Scheme 17).

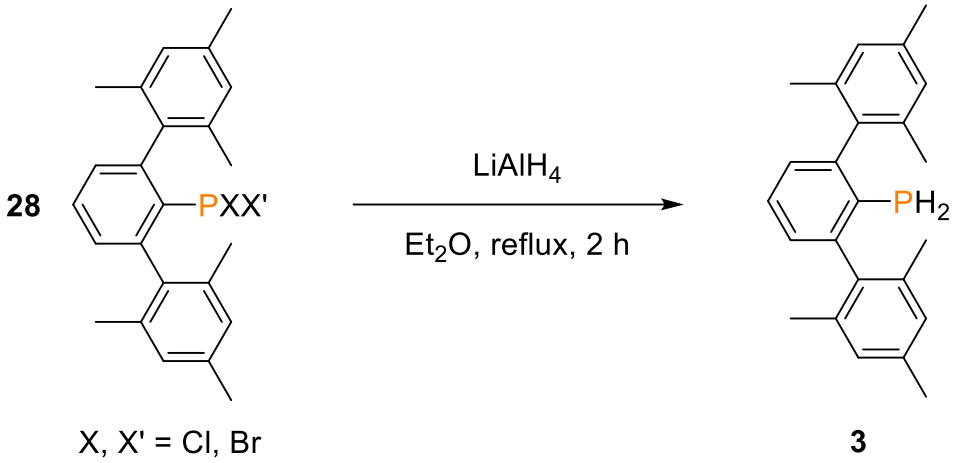

Scheme 17: Synthesis of $TerPH_2$ (**3**) from TerPXX‘ (X, X‘ = Cl, Br).

As expected, a byproduct displaying a singlet resonance at −93.8 ppm was observed in the ^{31}P NMR spectrum of the product mixture, which was attributable to the formation of Mes_2PH. The observed chemical shift was in good agreement with literature data.[26] However, Mes_2PH was easily removed by recrystallization from benzene, which afforded analytically pure $TerPH_2$, which was used in further experiments.

3.1.2 Preparation of TerP(H)Li·3THF (29)

The first preparation of a lithium terphenylphosphide was reported by Urnezius and Protasiewicz in 1996. It can easily be obtained starting from $TerPH_2$ by simple lithiation with *n*-BuLi in coordinating solvents such as diethyl ether.[27] Since 1996, lithium terphenylphosphides were applied to synthesize a number of transition metal complexes.[28–31] Especially the zirconium complexes **30** and **31**, which were reported by Protasiewicz and co-workers, were of interest to us since they had both been obtained by chloride abstraction reactions starting from Cp_2ZrCl_2 with one or two equivalents of $TerP(H)Li{\cdot}Et_2O$, respectively (Scheme 18).[28]

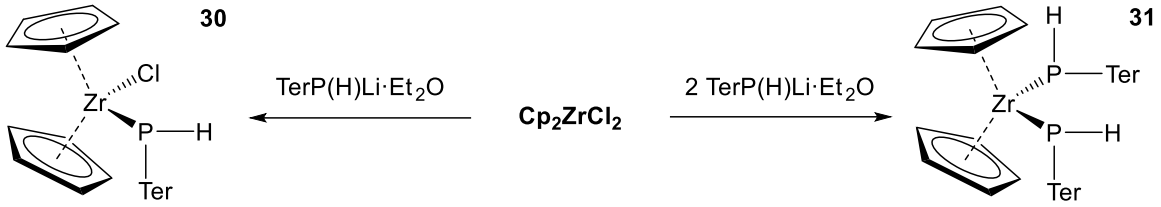

Scheme 18: Synthesis of zirconocene-terphenylphosphido complexes **30** and **31**.[28]

If such a chloride abstraction reaction could be facilitated for commercially available $ZnCl_2$ with lithiated terphenylphosphides, this could possibly give rise to interesting zinc phosphides as well.

For that purpose, TerP(H)Li·3THF (**29**) was synthesized according to a modified literature procedure.[27] $TerPH_2$ (**3**) was treated with *n*-BuLi in diethyl ether at −80 °C, giving a yellow solution (Scheme 19). The solvent was removed *in vacuo* and the yellow residue was dissolved in THF, from which analytically pure, yellow, block-shaped crystals of **29** were grown that were of sufficient quality for X-ray crystal structure determination (Figure 6).[32]

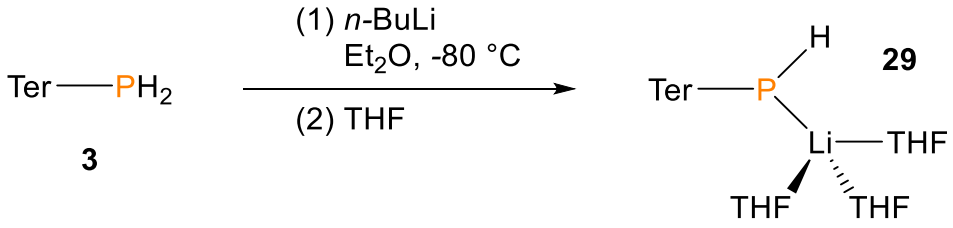

Scheme 19: Synthesis of TerP(H)Li·3THF (**29**).

29 crystallized in the monoclinic space group $P2_1/n$ with four molecules per unit cell. The P−C bond length is 1.8061(2) Å, which is shortened compared to the sum of covalent radii for P−C single bonds (cf. Σr_{cov}(P–C) = 1.86 Å).[11] The distance between the phosphorus and lithium atom is 2.5358(4) Å and thus only slightly longer than the sum of covalent radii but considerably shorter than the sum of van der Waals radii, which suggests strong interactions between phosphorus and lithium (cf. Σr_{cov}(P–Li) = 2.44 Å, Σr_{vdW}(P–Li) = 3.61 Å).[11,33] The average Li–O distance is approximately 2.01 Å, which is very close to the sum of covalent radii for Li–O single bonds (cf. Σr_{cov}(Li–O) = 1.96 Å).[11]

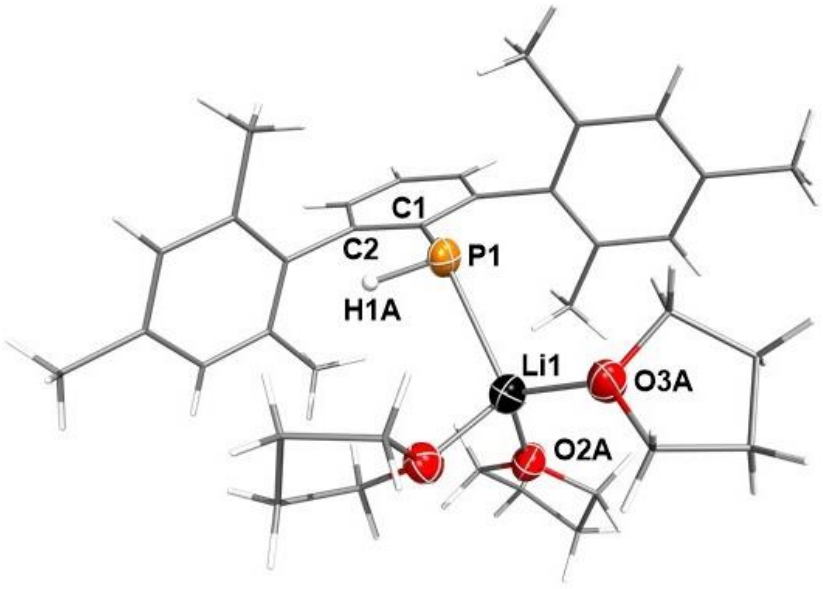

Figure 6: Molecular structure of **29** in the crystal ($P2_1/n$). Thermal ellipsoids drawn at the 50 % probability level and −100 °C. Carbon and hydrogen atoms rendered as wireframe for clarity. Selected bond lengths (Å), angles (°) and dihedral angles (°): P1−C1 1.8061(2), P1−Li1 2.536(4), Li1−O1A 1.931(9), Li1−O2A 1.938(6), Li1−O3A 1.946(8); C1−P1−Li1 125.43(2), C1–P1–H1A 98.03(1), Li1–P1–H1A 92.41(1); Li1−P1−C1−C2 99.8(2), Li1−P1−C1−C6 −82.30(2), H1A−P1−C1−C2 0.99(1).

The proton at P1 is almost in plane with the central phenyl ring of the terphenyl substituent with the torsion angle between H1A, P1, C1 and C2 being approx. 1°. The C1–P1–H1A and Li1–P1–H1A angles are 98.03(1)° and 92.41(1)°, respectively. The C1–P1–Li1 angle, on the other hand, is considerably larger (125.43(2)°). In the literature, there is only one other example of a lithium terphenylphosphide for which crystallographic data had been obtained. However, in contrast to **29**, [TerP(H)Li·Pyr]$_2$ (**32**, Figure 7, left) crystallized as a dimer, exhibited a trigonal planar coordination environment at lithium, and had a considerably larger Li–P–H angle of 114.836(3)°. The other angles at the phosphorus atom are in good

agreement with those of **29**. On the other hand, Mes*P(H)Li·3Pyr (**33**, Figure 7, right, Mes* = 2,4,6-tri-*tert*-butylphenyl) exhibited a completely analogous crystal structure with bond lengths and angles that compare very well with those observed for **29**, except for the C1−P1−Li1 angle, which was found to be considerably smaller (105.8(2)°).[34]

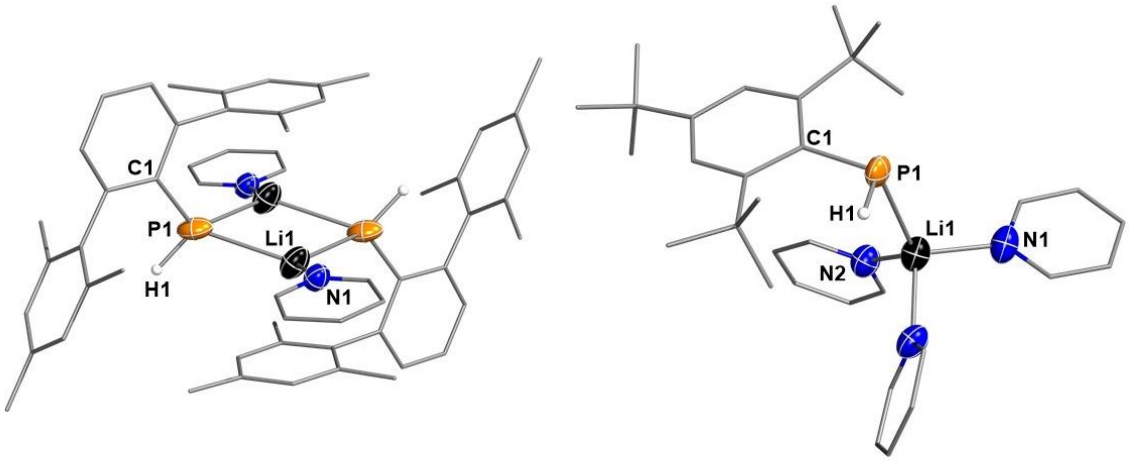

Figure 7: Left: Molecular structure of **32** in the crystal ($P\bar{1}$). Right: Molecular structure of **33** in the crystal ($P2_1/c$). Thermal ellipsoids drawn at the 50 % probability level and −75 °C. Carbon atoms rendered as wireframe, hydrogen atoms at substituents and solvent molecules are omitted for clarity. Selected bond lengths (Å) and angles (°) of **32**: P1−C1 1.8293(6), P1−Li1 2.6737(2); C1−P1−Li1 122.969(4), C1–P1–H1A 100.854(3), Li1–P1–H1A 114.836(3). Selected bond lengths (Å) and angles (°) of **33**: P1−C1 1.840(3), P1−Li1 2.609(7); C1−P1−Li1 105.8(2), C1–P1–H1A 102.442(3), Li1–P1–H1A 90.333(3).

In the ^{31}P NMR spectrum, **29** displays a singlet resonance at −138.3 ppm in CD_2Cl_2. It is shifted highfield by approximately 10 ppm compared to the parent phosphane, while the diethyl ether solvate was reported to resonate as a broad singlet at −145 ppm in deuterated benzene.[28]

The Raman spectrum of **29** could not be evaluated yet. Two vibrational modes at 2288 cm^{-1} and 2352 cm^{-1}, which is in the typical region of P−H stretching modes, were observed, although only one vibrational is to be expected. Calculations at the PBE1PBE/6-31G(d,p) level of theory support this expectation. The measured crystal most likely suffered from decomposition.

Unfortunately, due to time limitations, no experiments were conducted in order to investigate the reactivity of **29** towards $ZnCl_2$, yet. They are, however, subject of ongoing research.

3.2 Preparation and Characterization of zinc phosphides

3.2.1 Preparation of [TerPH(ZnEt)]$_2$ (34)

In our first experiments, we were interested in treating TerPH$_2$ (**3**) with commercially available dialkylzinc reagents in procedures similar to those employed by Westerhausen and co-workers (Scheme 14).[20,21]

For that purpose, equimolar amounts of ZnEt$_2$ (1 M in hexanes) were added to a solution of TerPH$_2$ (**3**) in THF at ambient temperature. At first, no reaction was observed until the degassed solution was heated to 80 °C and stirred for a period of 16 hours (Scheme 20). During that time, the solution took on a yellow hue. The reaction solution was concentrated to incipient crystallization, whereupon colorless, block-shaped crystals grew over the course of a few days at ambient temperature. The isolated crystals were suitable for X-ray crystal structure determination and were additionally characterized by elemental analysis, NMR and Raman spectroscopy as well as mass spectrometry. The isolated compound was thus found to be [TerPH(ZnEt)]$_2$ (**34**), an ethylzinc phosphide that exists as a dimer in solution *and* in the solid state (Figure 8), which is in contrast to the methylzinc phosphide **23** (Figure 3), which was reported to form a tetrameric cubane-type structure in the solid state.[20]

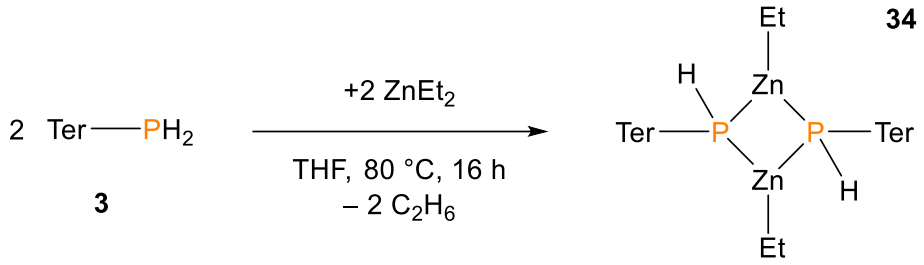

Scheme 20: Synthesis of dimeric [TerPH(ZnEt)]$_2$ (**34**) from TerPH$_2$ (**3**) and ZnEt$_2$.

34 crystallized in the form of colorless blocks in the triclinic space group $P\bar{1}$ with two molecules per unit cell. It comprises a planar four-membered P−Zn ring system with average P−Zn bond lengths of 2.440 Å, which is longer than the sum of the covalent radii for P−Zn single bonds but shorter than the P−Zn bonds observed for tetrameric **23** in the solid state (cf. Σr_{cov}(P–Zn) = 2.29 Å).[11] The P−C bonds (1.826(2) Å) are marginally shorter while the Zn−C bonds (1.977(2) Å) are marginally longer than the sum of covalent radii for P−C and Zn−C single bonds, respectively (cf. Σr_{cov}(P–C) = 1.84 Å, Σr_{cov}(Zn–C) = 1.93 Å),[11] a trend

that was also observed for **23** in the crystal. Compared to **23**, the P–Zn–P angles in **34** are only slightly more acute (87.87(2)°) while the Zn–P–Zn angles are more obtuse (92.13(2)°). The P1–Zn1–C25 angle is 135.07(7)° and compares very well with the P1–Zn1–C31 angle of 137.1(2)° that was observed for **27** in the crystal.[23] The terphenyl substituent and the hydrogen atom H1 are arranged above and below the plane that is spanned by the central four-membered P_2Zn_2 unit, respectively, with a C1–P1–H1 angle of 99(1)°, the coordination environment at the four-coordinate phosphorus atom is therefore that of a distorted tetrahedron. The coordination environment at the three-coordinate zinc atoms, on the other hand, is almost trigonal planar with small P–Zn–P angles of 87.87(2)° and considerably larger P–Zn1–C25 angles of average 135.74°. Furthermore, the ethyl substituent is bent out of planarity by approximately 6° (Zn1'–Zn1–C25).

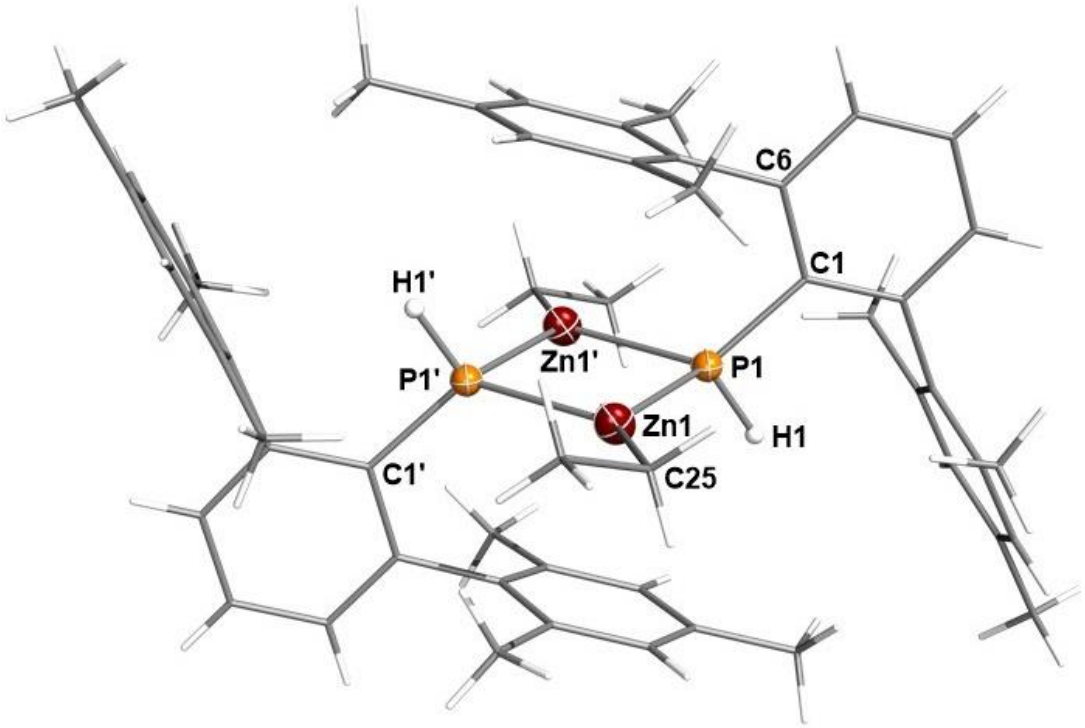

Figure 8: Molecular structure of **34** in the crystal ($P\bar{1}$). Thermal ellipsoids drawn at the 50 % probability level and −100 °C. Carbon and hydrogen atoms rendered as wireframe for clarity, except for the hydrogens at P1 and P1'. The second molecule in the unit cell is not shown. Selected bond lengths (Å), angles (°) and dihedral angles (°): P1−C1 1.826(2), P1−Zn1 2.4367(5), P1−Zn1' 2.4428(5), Zn1−C25 1.977(2); C1−P1−Zn1 118.45(6), Zn1−P1−Zn1' 92.13(2), P1−Zn1−P1' 87.87(2), P1−Zn1−C25 135.07(7), Zn1−P1−H1 111(1), C1−P1−H1 99(1); P1−Zn1−Zn1'−P1' 180.00(3), Zn1'−P1−C1−C6 49.8(2), H1−P1−Zn1−Zn1' −117(1).

All these values are in very good agreement with geometric values obtained from the optimized structure of **34** in the gas phase. The structure was optimized at the PBE1PBE/6-31G(d,p) and the PBE1PBE/aug-cc-pVDZ/ECP10MDF level of theory (cf. Chapter 5.4.1). For comparison, selected values are summarized in Table 1.

Table 1: Comparison of selected experimental and calculated structural parameters of **34** (PBE1PBE/6-31G(d,p) and PBE1PBE/aug-cc-pVDZ/ECP10MDF level of theory). Bond lengths in Å, angles and dihedral angles in °.

Parameter	**Experimental**	***Calculated***	
		6-31G(d,p)	***aug-cc-pVDZ***
P1−C1	1.826(2)	*1.823*	*1.837*
P1−Zn1	2.4367(5)	*2.418*	*2.450*
P1−Zn1’	2.4428(5)	*2.431*	*2.451*
Zn1−C25	1.977(2)	*1.962*	*1.976*
C1−P1−Zn1	118.45(6)	*119.3*	*120.7*
Zn1−P1−Zn1’	92.13(2)	*92.8*	*93.4*
P1−Zn1−P1’	87.87(2)	*87.3*	*86.6*
P1−Zn1−C25	135.07(7)	*134.3*	*134.9*
Zn1−P1−H1	111(1)	*107.8*	*107.9*
C1−P1−H1	99(1)	*101.4*	*100.8*
P1−Zn1−Zn1’−P1’	180.00(3)	*−179.3*	*180.0*

In addition to X-ray crystal structure determination, **34** was fully characterized by ^{1}H-, ^{13}C-, and ^{31}P NMR spectroscopy, Raman spectroscopy, elemental analysis, mass spectrometry, and differential scanning calorimetry.

The isolated compound **34** passed elemental analysis. In the mass spectrum (CI positive), no signal for the intact molecule was observed, however, a signal at m/z = 851 was assigned to the molecule lacking one ethyl group.

In the ^{31}P{^{1}H} NMR spectrum, **34** displays a significantly broadened singlet at −166.2 ppm in THF-d_8, which hints at dynamic processes in solution. This observation could be explained with different states of oligomerization in solution. Due to the high steric demand of the terphenyl substituent, a tetrameric arrangement of the molecule forming [TerPH(ZnEt)]$_4$ seemed unlikely. However, it appeared worthwhile to investigate an equilibrium between monomeric [TerPH(ZnEt)] and dimeric [TerPH(ZnEt)]$_2$, which was

performed by means of computational studies for a model dimerization reaction according to Scheme 21 in the gas phase.

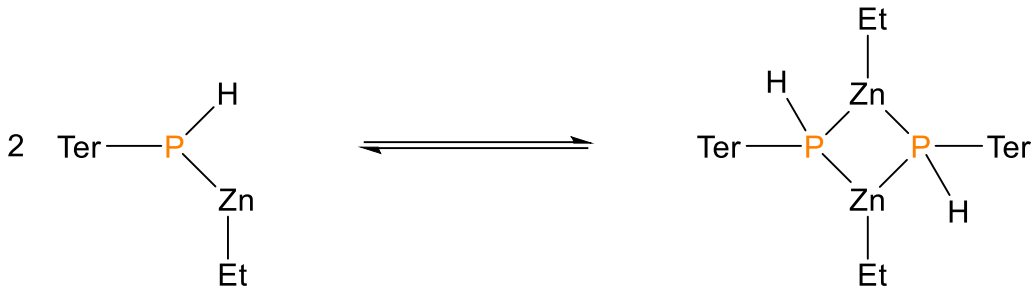

Scheme 21: Model monomer-dimer equilibrium of [TerPH(ZnEt)].

According to calculations at the PBE1PBE/6-31G(d,p) level of theory, the Gibbs energy for the dimerization reaction amounts to −35.5 kJ/mol ($\Delta_R G^{298}$) whereas, at the PBE1PBE/ aug-cc-pVDZ/ECP10MDF level of theory, it amounts to just −0.5 kJ/mol. This data is consistent with the fact that, in the solid state, the dimeric species $[TerPH(ZnEt)]_2$ (**34**) was observed. However, taking into consideration that the actual Gibbs energy for the dimerization could be somewhere in between both abovementioned values, the broadening of the ^{31}P NMR resonance could, indeed, be attributed to a dynamic monomer-dimer equilibrium in solution.

The ^{1}H NMR spectrum of **34** in THF-d_8 exhibits eight signal groups that were assigned to the respective hydrogen atoms in **34**. Five signal groups at 2.03 ppm (s), 2.25 ppm (s), 6.77 ppm (d), 6.86 ppm (s), and 7.05 ppm (t) were assigned to the terphenyl substituents. Two resonances at 0.02 ppm (q) and 1.04 ppm (t) can be attributed to the ethyl groups that are attached to the zinc atoms. The proton at phosphorus resonates at 3.02 ppm with a $^{1}J(^{1}H,^{31}P)$ coupling constant of 209 Hz, which is comparable to the coupling constant observed for $TerPH_2$ (211 Hz). Furthermore, all resonances in the ^{13}C NMR spectrum were assigned to the respective carbon atoms of the terphenyl substituent with the exception of the *ipso*-C, which was not observed.

In the Raman spectrum, **34** is characterized by a distinctive vibrational band at 2359 cm^{-1} which can be assigned to overlapping symmetric as well as antisymmetric P−H stretching modes. Other vibrational modes were assigned by comparison of the experimental Raman spectrum with calculated frequencies for the optimized structure in the gas phase (Figure 9).

The vibrational bands at 1612 cm^{-1} and 1579 cm^{-1} were assigned to in-phase aromatic ring vibrations of the mesityl groups and the central phenyl ring of the terphenyl substituent, respectively, while the shoulder at 1566 cm^{-1} was assigned to out-of-phase aromatic ring vibrations. The vibrational band at 1393 cm^{-1} appears to be a combined mode of C−H scissoring of the methylene (−CH_2−) at the zinc atoms, in-plane C−H vibrations of the aromatic rings, and an in-plane deformation vibration of the central phenyl ring of the terphenyl substituent. The intensive band at 1306 cm^{-1} was assigned to combined in-plane aromatic ring vibrations of the whole terphenyl substituent while the band at 1046 cm^{-1} can be attributed to aromatic ring deformation vibrations of the central phenyl rings.

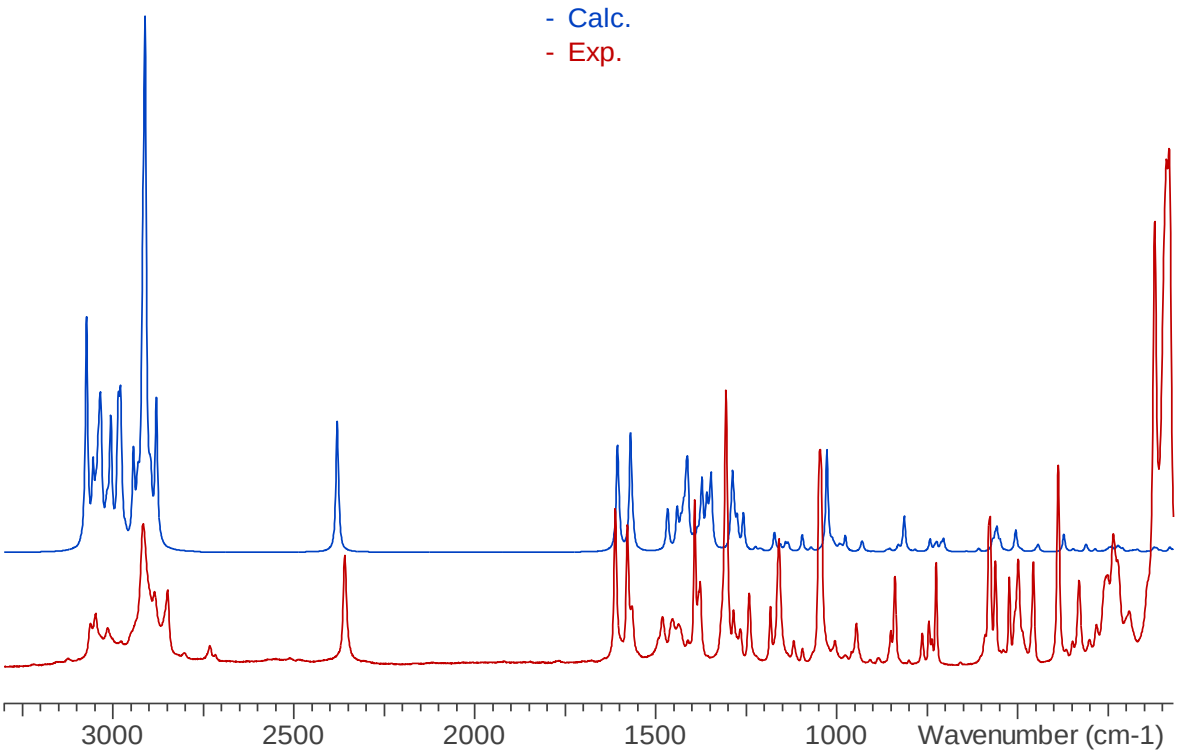

Figure 9: Experimental and calculated Raman spectrum of [TerPH(ZnEt)]$_2$ (**34**) (PBE1PBE/ 6-31G(d,p) level of theory). The calculated relative intensities are not accurate due to the relatively small 6-31G(d,p) basis set,[35] however, the calculated frequencies were corrected by multiplication with the factor 0.9512[36] and are in good agreement with experimental data.

Two different bands at 745 cm^{-1} and 578 cm^{-1} are in good agreement with the frequencies calculated for P−H wagging modes parallel to the P−C bond and perpendicular to the P−C bond, respectively. Vibrational bands that are exclusively caused by modes of the four-membered P_2Zn_2 ring were not observed, however, a few vibrational bands were identified that are caused by combined vibrations that include P_2Zn_2 ring vibrations (Table 2).

Table 2: Vibrational modes in the Raman spectrum of **34** that include the P_2Zn_2 ring.

Vibration mode	Frequency [cm^{-1}]
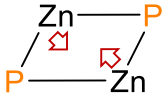	122
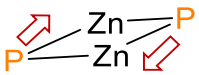	388
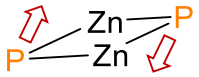	457

Eventually, **34** was also characterized by differential scanning calorimetry. The outcome of the reaction of $TerPH_2$ (**3**) and $ZnEt_2$ was not surprising since the corresponding reaction with $(t\text{-Bu})_3SiPH_2$ had already afforded the analogous zinc phosphide **23** (Scheme 14, Figure 3).[20] However, it was interesting to observe that the remaining, formally negatively charged ethyl substituent at the zinc atom was apparently not basic enough to deprotonate the phosphide a second time, although the reaction was carried out at 80 °C instead of 0 °C and although the extrusion of ethane can be considered a driving force. Therefore, it seemed worthwhile to investigate compound **34** further by means of differential scanning calorimetry and thermogravimetry in order to see if a second deprotonation under concomitant extrusion of ethane was possible at temperatures above 80 °C.

Unfortunately, no loss of mass which could be correlated with the extrusion of one equivalent of ethane was observed. Instead, the sample began to lose mass due to decomposition above 195 °C. DSC analyses showed that at 195 °C an endothermic melting process was initialized which changed directly into an exothermic decomposition process followed by continuous loss of mass with increasing temperature. Apparently, a second intramolecular deprotonation of the phosphide cannot be achieved even at higher temperatures.

3.2.2 Preparation of $[TerP(ZnEt)_2]_2$ (35)

The reaction of $TerPH_2$ (**3**) with equimolar amounts of diethylzinc gave rise to dimeric ethylzinc terphenylphosphide $[TerPH(ZnEt)]_2$ (**34**). Thermogravimetric analysis showed that a second, intramolecular deprotonation of the phosphide under concomitant extrusion of ethane cannot be achieved even at higher temperatures. In an attempt to remove that second hydrogen atom, another experiment was conducted.

For that purpose, a solution of $TerPH_2$ in THF was prepared to which two equivalents of $ZnEt_2$ (1 M in hexanes) were added at ambient temperature. The degassed solution was then heated to 80 °C overnight, during which the solution took on a yellow hue. After approx. 16 hours of reaction time, a ^{31}P NMR spectrum of the reaction mixture was acquired which indicated that, in addition to **34**, a new species had formed. This reaction was optimized by treating **3** with an excessive amount of three equivalents of $ZnEt_2$ and heating the thoroughly degassed solution to 100 °C for a period of two hours during which a white precipitate formed under a yellowish supernatant. This procedure was followed by additional 16 hours of reaction time at 80 °C (Scheme 22). This way, quantitative conversion was achieved according to ^{31}P NMR spectroscopy. THF was added to the mixture until the precipitate dissolved in warm THF, whereupon the solution was allowed to slowly cool to ambient temperature. This afforded a copious amount of colorless, block-shaped crystals that were suitable for X-ray crystal structure determination and were additionally characterized by elemental analysis, NMR and Raman spectroscopy as well as mass spectrometry. The isolated compound was thus found to be $[TerP(ZnEt)_2]_2$ (**35**), a doubly ethylzinc-substituted phosphadiide which exists as a dimer in the solid state (Figure 10) and presumably undergoes a monomer-dimer equilibrium in solution.

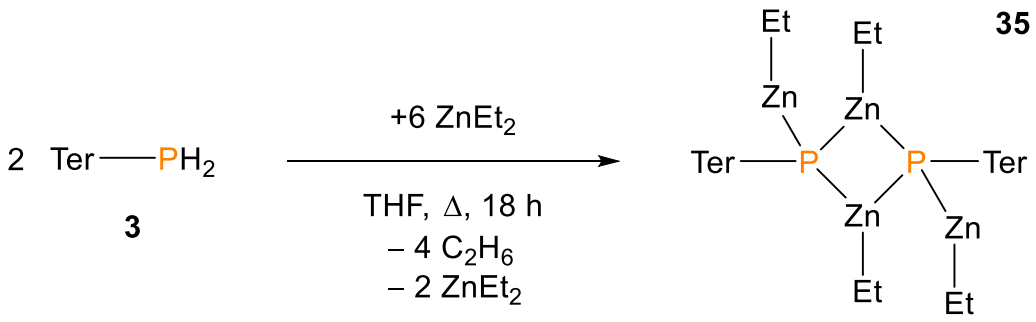

Scheme 22: Synthesis of dimeric $[TerP(ZnEt)_2]_2$ (**35**) from $TerPH_2$ (**3**) and excessive $ZnEt_2$.

This is in contrast to phosphadiide $[(i\text{-Pr})_3SiP(ZnC(SiMe_3))_2]$ (**21**, Scheme 12) which was reported to exist as a monomeric species in solution and in the solid state due to the sterically demanding substituents at the zinc atoms. Ethyl groups at the zinc atoms, however, appear to be small enough substituents to allow for dimerization.

35 crystallized in the form of colorless blocks in the triclinic space group $P\bar{1}$ with one molecule per unit cell. It comprises a planar four-membered P−Zn ring system with average P−Zn bond lengths of 2.431 Å, which is longer than the sum of the covalent radii for P−Zn single bonds but shorter than the P−Zn bonds observed for tetrameric **23** or dimeric **34** in the solid state (cf. Σr_{cov}(P–Zn) = 2.29 Å).[11] Additionally, instead of hydrogens, both phosphorus atoms bear exocyclic ethylzinc substituents with considerably shorter P−Zn bonds of 2.2758(6) Å. This is even shorter than the sum of covalent radii for P−Zn single bonds, which is attributable to the small coordination number at the exocyclic zinc atoms and to high electrostatic attraction.

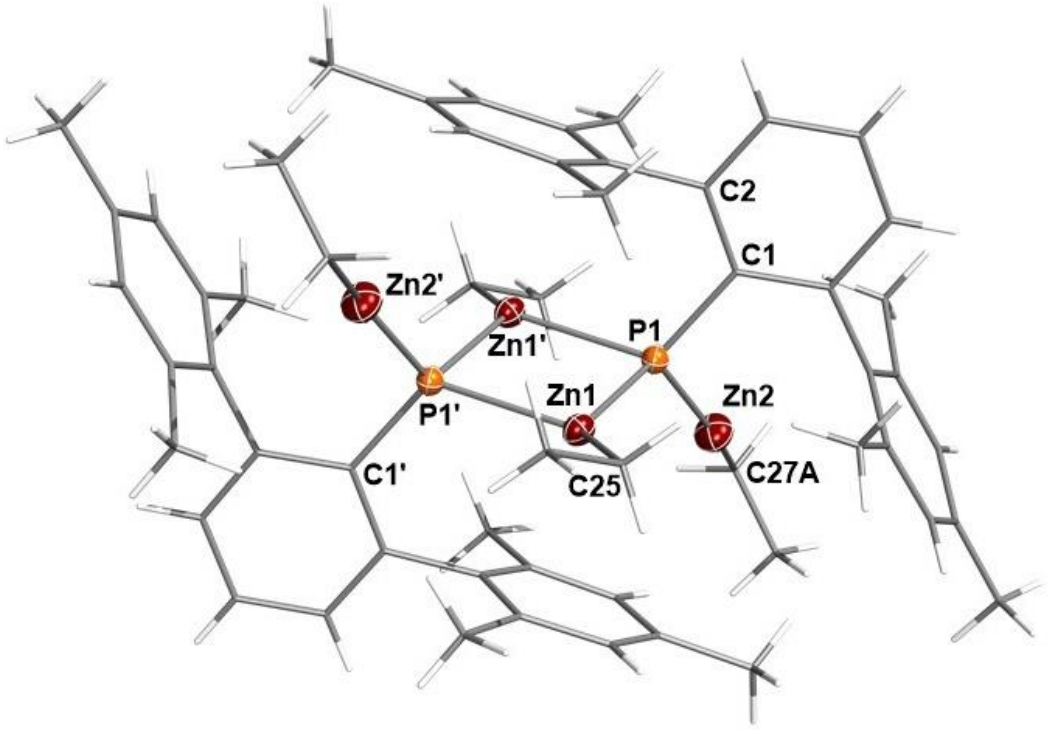

Figure 10: Molecular structure of **35** in the crystal ($P\bar{1}$). Thermal ellipsoids drawn at the 50 % probability level and −100 °C. Carbon and hydrogen atoms rendered as wireframe for clarity. Selected bond lengths (Å), angles (°) and dihedral angles (°): P1−C1 1.841(2), P1−Zn1 2.4298(6), P1−Zn1' 2.4323(6), P1−Zn2 2.2758(6), Zn1−C25 1.990(2), Zn2−C27A 1.985(6); C1−P1−Zn1 117.78(7), C1−P1−Zn1' 112.94(7), C1−P1−Zn2 107.55(7), Zn1−P1−Zn1' 86.77(2), P1−Zn1−P1' 93.23(2), P1−Zn1−C25 131.80(7), P1−Zn2−C27A 160.7(2), Zn1−P1−Zn2 124.82(2); P1−Zn1−Zn1'−P1' 180.00(3).

The P−C bonds (1.841(2) Å) are within the range of typical P–C single bond lengths (cf. Σr_{cov}(P−C) = 1.84 Å).[11] The Zn−C bonds with an average length of 1.988 Å are both longer than the sum of the covalent radii for single bonds (cf. Σr_{cov}(Zn–C) = 1.93 Å).[11]

Interestingly, in contrast to **23** or **34** in the solid state, in **35** the P–Zn–P angles within the central four-membered P−Zn ring system are obtuse (93.23(2)°), while the Zn–P–Zn angles are acute (86.77(2)°). The P1–Zn1–C25 angle is 131.80(7)°, which is smaller than the respective angle observed for **34**. The terphenyl substituent is arranged almost perpendicularly to the central P_2Zn_2 ring with C1–P1–P1'–Zn1' being 93.91(9)°, while the dihedral angle Zn2–P1–P1'–Zn1' is more acute (–74.63(3)°). The C1–P1–Zn2 angle in **35** (107.55(7)°) is larger than the C1–P1–H1 angle in **34** (99(1)°). The coordination environment at the four-coordinate phosphorus atom is that of a distorted tetrahedron. The coordination environment at the three-coordinate zinc atoms within the central four-membered P_2Zn_2 ring is best described as distorted trigonal pyramidal with a small P1–Zn1–P1' angle (93.23(2)°) and larger average P–Zn1–C25 angles of 130.64°. The Zn1'–Zn1–C25 angle (161.45(7)°) is considerably smaller than the respective angle in the solid state structure of **34** (173.98(7)°). Moreover, **35** comprises two-coordinate zinc atoms with a bent coordination environment as depicted by the obtuse P1–Zn2–C27A angle of 160.7(2)°.

All these values are in very good agreement with geometric values obtained from the optimized structure of **35** in the gas phase. The structure was optimized at the PBE1PBE/6-31G(d,p) and the PBE1PBE/aug-cc-pVDZ/ECP10MDF level of theory (cf. Chapter 5.4.1). For comparison, selected values are summarized in Table 3.

Table 3: Comparison of selected experimental and calculated structural parameters of **35** (PBE1PBE/6-31G(d,p) and PBE1PBE/aug-cc-pVDZ/ECP10MDF level of theory). Bond lengths in Å, angles and dihedral angles in °.

Parameter	**Experimental**	***Calculated***	
		6-31G(d,p)	***aug-cc-pVDZ***
P1−C1	1.841(2)	*1.827*	*1.852*
P1−Zn1	2.4298(6)	*2.414*	*2.453*
P1−Zn1'	2.4323(6)	*2.401*	*2.438*
P1−Zn2	2.2758(6)	*2.246*	*2.272*
Zn1−C25	1.990(2)	*1.977*	*1.991*
Zn2−C27A	1.985(6)	*1.952*	*1.961*

Table 3: Continuation.

Parameter	**Experimental**	***Calculated***	
		6-31G(d,p)	***aug-cc-pVDZ***
C1−P1−Zn1	117.78(7)	*111.4*	*113.9*
C1−P1−Zn1'	112.94(7)	*116.8*	*119.1*
C1−P1−Zn2	107.55(7)	*106.2*	*107.2*
Zn1−P1−Zn1'	86.77(2)	*86.9*	*86.7*
P1−Zn1−P1'	93.23(2)	*93.1*	*93.4*
P1−Zn1−C25	131.80(7)	*129.7*	*130.3*
P1−Zn2−C27A	160.7(2)	*155.6*	*163.0*
Zn1−P1−Zn2	124.82(2)	*122.8*	*124.5*
P1−Zn1−Zn1'−P1'	180.00(3)	*180.0*	*180.0*

In addition to X-ray crystal structure determination, **35** was also fully characterized by ^{1}H-, ^{13}C-, and ^{31}P NMR spectroscopy, Raman spectroscopy, elemental analysis and mass spectrometry. Furthermore, ^{31}P{^{1}H} NMR spectroscopic investigations at variable temperatures as well as computational studies were carried out in order to gain insight into the compound's behavior in solution.

The isolated compound **35** passed elemental analysis. In the mass spectrum (CI positive), no signal for the intact molecule was observed, however, fragments with mass-to-charge values of 1037 and 942 were assigned to the intact molecule missing one ethyl group or one ethyl and one ethylzinc group, respectively.

In the ^{31}P{^{1}H} NMR spectrum, **35** displays a significantly broadened singlet at −161.7 ppm in THF-d_8, which hints at dynamic processes in solution. Additionally, a sharp singlet at −142.5 ppm was observed in the ^{31}P{^{1}H} NMR spectrum (Figure 11). This resonance cannot be attributed to either the starting material $TerPH_2$ (**3**), nor to the dimeric zinc phosphide $[TerPH(ZnEt)]_2$ (**34**). Since the second resonance can possibly be attributed to a monomeric $[TerP(ZnEt)_2]$, the most reasonable explanation for the broadening of the resonance at −161.7 ppm seemed to be intramolecular movement and changes of conformation. In contrast to **34**, however, for which monomeric [TerPH(ZnEt)] might have been too short-lived to be observed in the ^{31}P NMR spectrum, **35** might be more stable as a monomer and could therefore possibly be observed by means of NMR spectroscopy. Therefore, it appeared worthwhile to investigate the solution behavior of **35** more thoroughly.

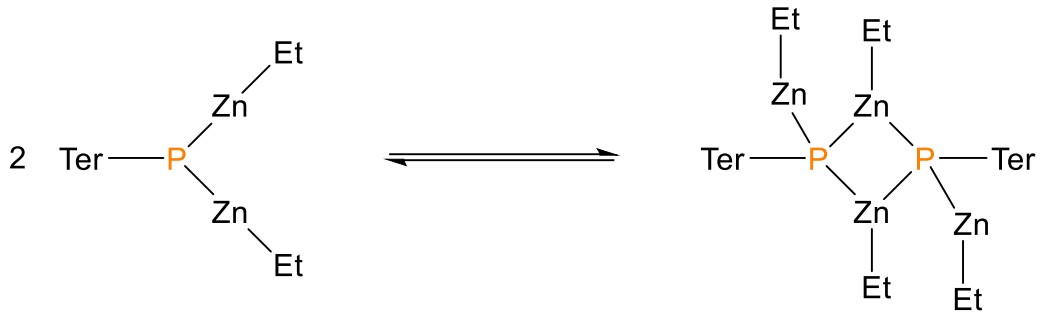

Scheme 23: Model monomer-dimer equilibrium of [TerP(ZnEt)$_2$].

According to calculations at the PBE1PBE/6-31G(d,p) level of theory, the Gibbs energy for the dimerization reaction (Scheme 23) amounts to −24.0 kJ/mol ($\Delta_R G^{298}$) which suggests that the dimer is energetically favored. This is consistent with the observation of dimeric [TerP(ZnEt)$_2$]$_2$ (**35**) in the solid state. However, at the PBE1PBE/aug-cc-pVDZ/ECP10MDF level of theory, the Gibbs energy amounts to +17.3 kJ/mol, which suggests that the monomeric species is actually lower in energy. Taking into consideration that the actual Gibbs energy for the dimerization could be somewhere in between both abovementioned values, a dynamic monomer-dimer equilibrium in solution could, indeed, be possible. Moreover, the monomer could be stable enough to actually be observed by means of NMR spectroscopy.

For comparison, the sterically encumbered zinc phosphadiide **21**, which was found to be monomeric in solution as well as in the solid state, was characterized by a singlet resonance at −297.1 ppm in deuterated benzene, which is shifted considerably further to the highfield compared with our observed resonances. However, calculations of the ^{31}P NMR chemical shifts of monomeric [TerP(ZnEt)$_2$] and dimeric [TerP(ZnEt)$_2$]$_2$ at the PBE1PBE/ aug-cc-pVDZ/ECP10MDF level of theory (cf. Chapter 5.4.1) showed that the resonances should be expected in the observed region (cf. Table 4).

Table 4: Experimental and calculated ^{31}P NMR chemical shifts of presumably monomeric [TerP(ZnEt)$_2$] and dimeric [TerP(ZnEt)$_2$]$_2$ at the PBE1PBE/aug-cc-pVDZ/ECP10MDF level of theory.

Resonating species	**$\delta_{exp.}$ [ppm]**	***$\delta_{calc.}$ [ppm]***	
		6-31G(d,p)	***aug-cc-pVDZ***
[TerP(ZnEt)$_2$]	−142.5	−208.1	−165.3
[TerP(ZnEt)$_2$]$_2$	−161.7	−213.6	−158.2

It is apparent that the calculated NMR chemical shifts at the PBE1PBE/aug-cc-pVDZ/ECP10MDF level of theory (cf. Chapter 5.4.1) are in good agreement with the experimentally observed values for what we assume to be the monomer and dimer.

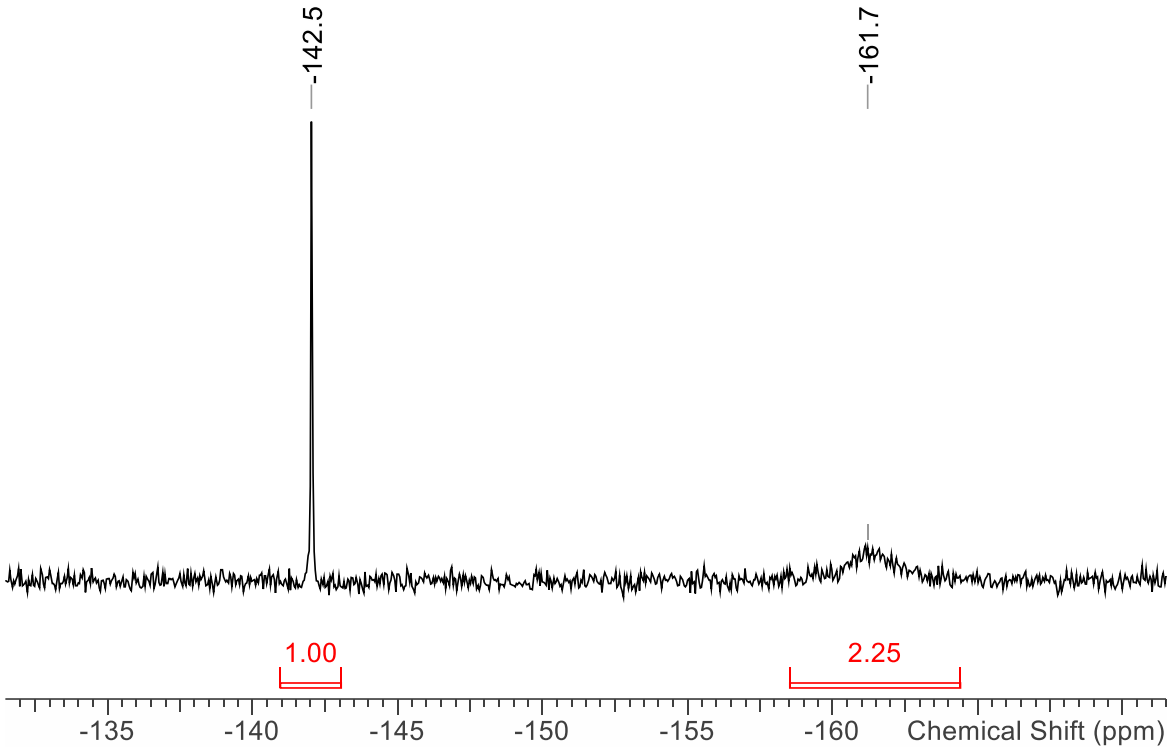

Figure 11: $^{31}P\{^{1}H\}$ NMR spectrum of crystalline **35** in THF-d_8 at 25 °C.

Another interesting observation within the ^{31}P NMR spectra was made by integration of the two resonances. It became apparent that the ratio of the integrals was not constant even though the spectra were acquired for crystals that originated from the same batch. Keeping in mind that the resonance at −161.7 ppm was assigned to two phosphorus atoms, the observed integral ratios (monomer : dimer) ranged from 1 : 1 to approx. 1 : 1.5 (Figure 11), which can most likely be attributed to a shifted equilibrium due to deviations in sample concentration and temperature. In order to further investigate the equilibrium and possibly determine the Gibbs energy for the dimerization reaction empirically, a variable temperature NMR experiment was conducted.

For that purpose, 13 mg of triphenylphosphane (PPh_3) and 12 mg of crystalline **35** were weighed into a J. Young NMR tube. PPh_3 was supposed to function as an internal standard. Thereupon, at the Schlenk line, 771 mg (≅ 0.78 mL) of deuterated THF were degassed, condensed onto the sample, and ultrasonicated until a clear solution was obtained.

$^{31}P\{^{1}H\}$ NMR spectra were obtained at a 500 MHz spectrometer at the following temperatures and in the following order: −60 °C, −40 °C, −20 °C, 0 °C, 20 °C, 40 °C, −20 °C, −60 °C, and −80 °C (Figure 12).

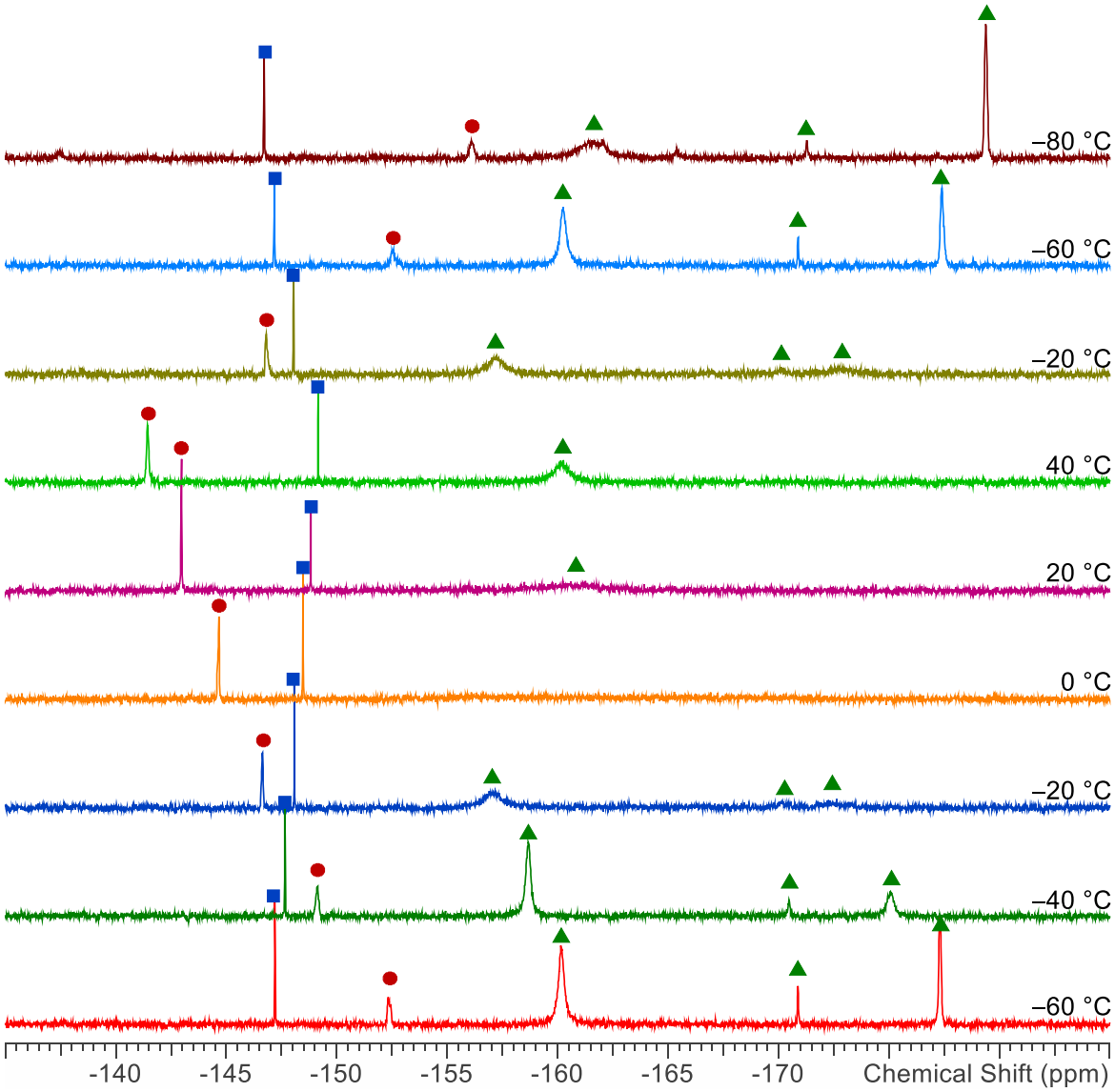

Figure 12: $^{31}P\{^{1}H\}$ NMR spectra of crystalline **35** in THF-d_8 at temperatures from −80 °C to 40 °C. Related resonances are colored accordingly (blue = $TerPH_2$ (**3**), red = monomeric $[TerP(ZnEt)_2]$, green = dimeric $[TerP(ZnEt)_2]_2$). Spectra measured on a 500 MHz spectrometer.

In order to calculate the concentrations of both species of interest, the integral of the internal standard (PPh_3, resonance not shown in Figure 12) was set to 100. The relative integral ratios and the concentration of PPh_3 within the sample were used to determine the respective concentration of monomer and dimer at all temperatures. $TerPH_2$ (**3**, blue box, Figure 12) was an impurity within the sample. Its concentration was found to stay constant.

The chemical shift of the resonance of monomeric [TerP(ZnEt)$_2$] (red circle, Figure 12) displays a considerable temperature dependence such that it is observed at −156.1 ppm at −80 °C and at −141.4 ppm at 40 °C. Interestingly, the signal appeared to broaden with increasing temperature. According to the integrals, the concentration of monomeric [TerP(ZnEt)$_2$] is lowest at low temperatures and highest at higher temperatures (Table 5), which is consistent with the observations so far.

The dimeric [TerP(ZnEt)$_2$]$_2$ displays an interesting temperature dependence within the scanned temperature interval. At 40 °C, a broad singlet was observed that broadens even more with decreasing temperature. At about 0 °C the resonance was not observed due to coalescence. Below 0 °C, the signal splits into three broadened resonances at −157.0 ppm, −170.2 ppm and −172.5 ppm, all of which become sharper and experience a slight shift into higher field as the temperature decreases further. This observation is reversible and can most likely be attributed to restricted rotations and movement of the substituents at lower temperatures. At higher temperatures, however, the substituents can move and rotate more freely which apparently causes the resonances to coincide. This is also supported by the fact that the chemical shift of the single resonance at higher temperatures is approx. equal to the averaged chemical shift of the three resonances that can be observed at lower temperatures. They were therefore attributed to the dimer (green triangle, Figure 12).

Table 5: Relative integrals and calculated concentrations of monomeric [TerP(ZnEt)$_2$] (**M**) and dimeric [TerP(ZnEt)$_2$]$_2$ (**D**) within the sample at variable temperatures. The relative integral values for the dimer are halved to account for two phosphorus atoms causing the respective resonances. K represents the calculated equilibrium constant at each respective temperature.

Temp. [°C]	**Rel. Integral (M)**	**Conc. (M)** [mmol/L]	**Rel. Integral (D)**	**Conc. (D)** [mmol/L]	**K** [L/mmol]
−60	1.89	1.20	11.43	7.24	5.05
−40	2.42	1.53	9.93	6.29	2.68
−20	3.02	1.91	7.69	4.87	1.33
0	5.08	3.22	–	–	–
+20	6.66	4.32	8.75	5.54	0.31
+40	7.30	4.62	9.38	5.94	0.28
−20	3.09	1.96	8.08	5.11	1.34
−60	1.99	1.26	10.93	6.92	4.36
−80	1.56	0.99	9.97	6.31	6.47

With the calculated values for the concentrations of monomer and dimer, the equilibrium constants for the dimerization reaction depicted in Scheme 23 at each respective temperature were calculated using Equation 1 under the following approximation that the activity is equal to the concentration.

$$K = \frac{a(\text{Dimer})}{[a(\text{Monomer})]^2} \approx \frac{c(\text{Dimer})}{[c(\text{Monomer})]^2} \quad \textbf{(1)}$$

The equilibrium constants are summarized in Table 5. In order to calculate the Gibbs energy for the dimerization reaction, the logarithmized equilibrium constants were plotted against the reciprocal temperature (Equation 2 and 3).

$$\Delta_R G° = -RT \cdot \ln K \quad \textbf{(2)}$$

$$\frac{1}{T} = -\frac{R}{\Delta_R G°} \cdot \ln K \quad \textbf{(3)}$$

Using the gradient of the straight line that was obtained by means of linear regression, the Gibbs energy was calculated to be −14.1(5) kJ/mol. This is in relatively good agreement with the computationally obtained value of −24.0 kJ/mol at the PBE1PBE/6-31G(d,p) level of theory and with our experimental observations. This indicates that dimeric $[TerP(ZnEt)_2]_2$ (**35**) is energetically favored and therefore crystallizes as such. Moreover, the data agrees with the assumption of a monomer-dimer equilibrium in solution.

The ^{1}H NMR spectrum of **35** in THF-d_8 exhibits seven signal groups that were assigned to the respective hydrogen atoms in **35**. Five signal groups at 1.99 ppm (s), 2.33 ppm (s), 6.73 ppm (d), 6.99 ppm (s), and 7.04 ppm (t) were assigned to the terphenyl substituents. Two resonances at −0.03 ppm (q) and 1.02 ppm (t) can be attributed to the ethyl groups that are attached to the zinc atoms. It was not possible to distinguish between ethyl groups that are bound to endocyclic or exocyclic zinc atoms, however, the quartet resonance at −0.03 ppm was found to be slightly broadened compared to other resonances. Furthermore, in accord with the observations made by means of ^{31}P NMR spectroscopy, the ^{1}H NMR spectrum displayed five more signal groups that can be assigned to the terphenyl substituent of the, presumably, monomeric zinc phosphadiide $[TerP(ZnEt)_2]$. Additional resonances for the monomer were also observed by means of ^{13}C NMR spectroscopy, which is why not all of the resonances were unambiguously assigned to the respective carbon atoms.

The Raman spectrum of crystalline **35** was evaluated by comparison with calculated frequencies of the optimized structure in the gas phase at the PBE1PBE/6-31G(d,p) level of theory (Figure 13). **35** is characterized by in-phase aromatic ring vibrations of the mesityl groups and the central phenyl rings of the terphenyl substituent at 1613 cm^{-1} and 1576 cm^{-1}, respectively. The out-of-phase ring vibrations were observed at 1566 cm^{-1}. Intensive bands at 1385 cm^{-1} and 1286 cm^{-1} were assigned to C−H scissoring of the methylene (−CH_2−) at the zinc atoms and in-phase, in-plane ring deformation vibrations, respectively. The vibrational bands at 1176 cm^{-1}, 1166 cm^{-1}, and 1151 cm^{-1} are attributable to C−H wagging of the ethyl groups at exocyclic zinc atoms, the ethyl groups at endocyclic zinc atoms, and to aromatic, in-plane C−H bending. An in-phase ring deformation vibration of the central phenyl ring was observed at 1040 cm^{-1} and the C−C stretching of the ethyl groups at exocyclic zinc atoms was assigned to a vibrational band at 1007 cm^{-1}. Another intensive band at 494 cm^{-1} was attributed to out-of-plane ring deformation vibrations, while its less intensive shoulder at 506 cm^{-1} was identified as a Zn−C stretching mode of the exocyclic ethylzinc moiety.

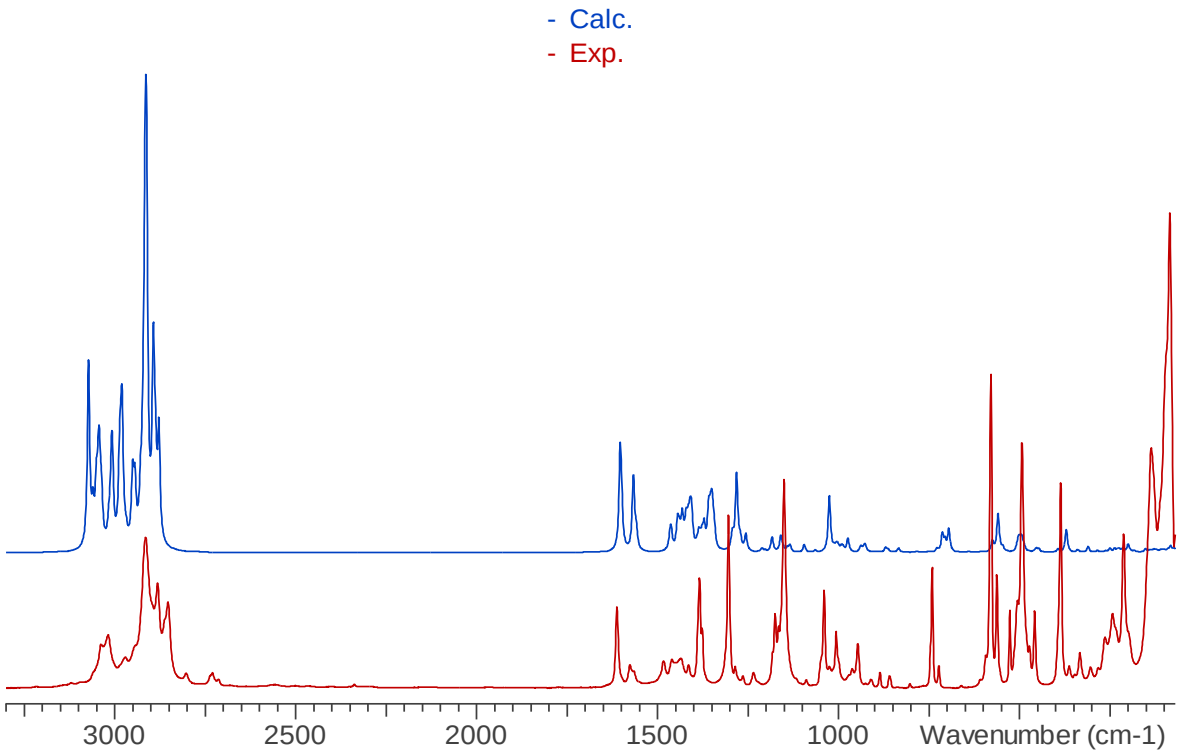

Figure 13: Experimental and calculated Raman spectrum of $[TerP(ZnEt)_2]_2$ (**35**) (PBE1PBE/6-31G(d,p) level of theory). The calculated relative intensities are not accurate due to the relatively small 6-31G(d,p) basis set,[35] however, the calculated frequencies were corrected by multiplication with the factor 0.9512[36] and are in good agreement with experimental data.

In addition, a rather intensive vibration at 387 cm^{-1} was identified as a combined vibration that included the terphenyl substituents as well as both phosphorus atoms as depicted in Table 6 for the latter.

Table 6: Vibrational mode in the Raman spectrum of **35** that include the P_2Zn_2 ring.

Vibration mode	Frequency [cm^{-1}]
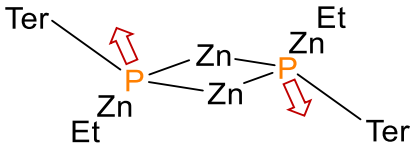	387

Finally, in our attempts to characterize $[TerP(ZnEt)_2]_2$ (**35**) and to gain insight into its presumed monomer-dimer equilibrium in solution, we also tried investigating the effects of different solvents on said equilibrium. Several usual solvents like *n*-pentane, *n*-hexane, benzene, toluene, diethyl ether, dimethoxy ethane, and acetonitrile were tested but, unfortunately, **35** proved to be practically insoluble in anything but tetrahydrofuran. DMSO was tested as well, however, **35** was found to react with DMSO. After heating **35** in DMSO to 70 °C for a day, an almost brown mixture was obtained that contained a brown precipitate under a similarly colored supernatant which, after filtration, afforded a clear orange-red filtrate. A ^{31}P NMR spectrum showed that a plethora of different, phosphorus-containing products had formed of which none could be isolated. In addition, dichloromethane (CH_2Cl_2) was similarly tested as solvent, although, in this case, **35** was expected to react with the chlorinated solvent under elimination of $ZnCl_2$. Due to poor solubility at ambient temperature, the mixture of **35** in dichloromethane was heated to 60 °C overnight under autogenous pressure, whereupon a clear solution was obtained. A ^{31}P NMR spectrum of this solution showed that **35** had, indeed, reacted with the solvent to form various unidentified products of which none could be isolated even after several attempts. Eventually we were not able to find any suitable solvents to further investigate the solution behavior of $[TerP(ZnEt)_2]_2$ (**35**). However, up until now, addition of coordinating solvents like acetonitrile or less polar solvents like diethyl ether to already dissolved samples of **35** in THF has not been investigated yet.

3.2.3 Preparation of TerPH(ZnCl)·2THF (36)

The treatment of $TerPH_2$ (**3**) with equimolar amounts of diethylzinc gave rise to the dimeric phosphide $[TerPH(ZnEt)]_2$ which comprises a remaining ethyl substituent at the zinc atom. Although the basicity of that remaining ethyl group was apparently not high enough to further deprotonate the phosphide and eliminate another equivalent of ethane, it was found to be reactive enough to undergo side reactions upon treatment with PCl_3 (cf. Chapter 3.3). Therefore, and since it proved to be too difficult to remove the second ethyl substituent at the zinc atom entirely, we were interested in synthesizing zinc phosphide reagents with less reactive substituents at the zinc atom. On our search for suitable substitutions for $ZnEt_2$ in the literature, we came across the ethylzinc chloride (EtZnCl) reagent, which appeared to be a perfect candidate for such investigations. EtZnCl could easily be prepared by treating the organometallic reagent $ZnEt_2$ with equimolar amounts of $ZnCl_2$ (Scheme 24) and it still comprised a formally negatively charged, basic ethyl substituent at the zinc atom as well as a much less reactive chloride substituent. Furthermore, EtZnCl was reported to be a solid that is stable under inert conditions and soluble even in unpolar solvents which would make it a reagent that is much easier to handle than solutions of $ZnEt_2$.[37,38]

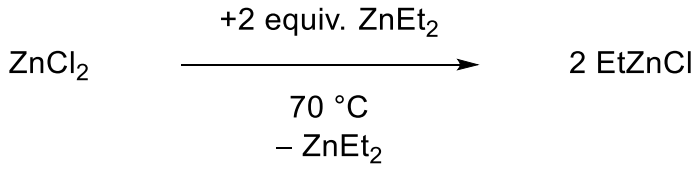

Scheme 24: Preparative route to EtZnCl.

We decided to generate EtZnCl *in situ* in THF and add the reaction solution directly to a solution of $TerPH_2$ (**3**) in THF afterwards. In analogy to the synthesis of $[TerPH(ZnEt)]_2$ (**34**), we expected the reaction to proceed as depicted in Scheme 25.

For that purpose, $ZnCl_2$ was suspended in THF, whereupon equimolar amounts of $ZnEt_2$ (1 M in hexanes) were added. The mixture was degassed and heated to 60 °C while being treated with ultrasound, until a clear solution was obtained. The still hot solution was then transferred into another flask containing a solution of **3** in THF and a stir bar, whereupon the mixture was degassed, placed into a preheated oil bath (75 °C), and stirred overnight.

Eventually, colorless, block-shaped crystals of **36** were isolated from the concentrated reaction solution that were of sufficient quality for X-ray crystal structure determination and were additionally characterized by NMR and Raman spectroscopy.

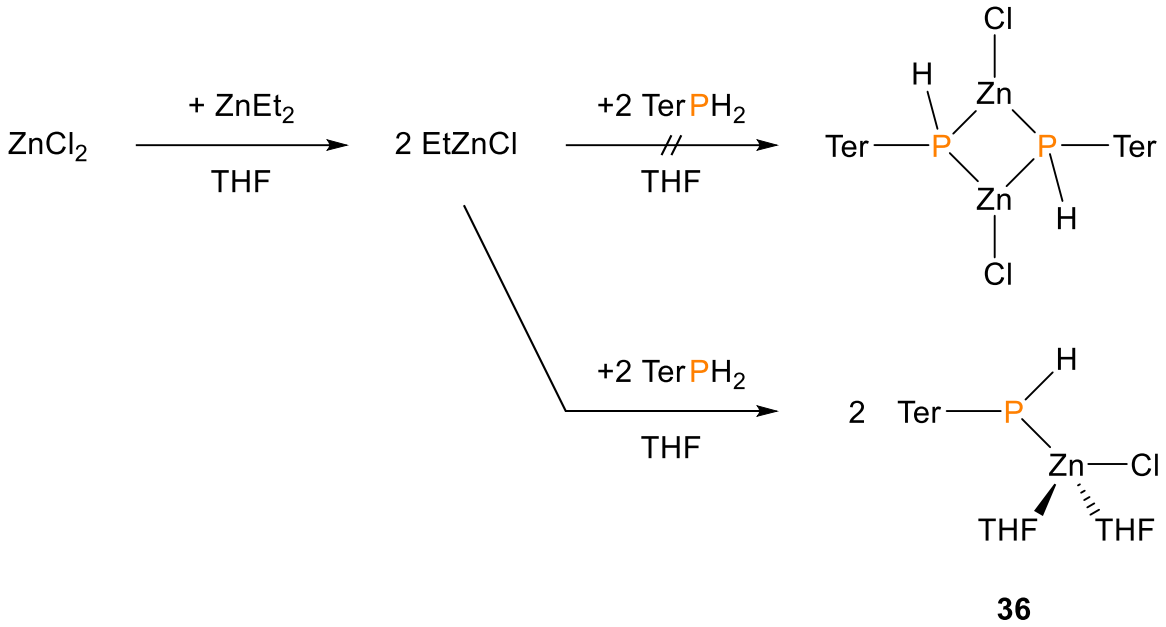

36

Scheme 25: Synthetic approach for the reaction of EtZnCl with $TerPH_2$ (**3**) that yielded the monomeric phosphide TerPH(ZnCl)·2THF (**36**) instead of the initially predicted, dimeric $[TerPH(ZnCl)]_2$.

36 crystallized in the monoclinic space group $P2_1/n$ with four molecules per unit cell (Figure 14). Its crystal structure comprises a chlorozinc substituent at the phosphorus atom with two THF ligands at the zinc atom. It is worthy of note that, to the best of our knowledge, a bonding situation for chlorozinc phosphides as observed in the molecular structure of **36** is unprecedented.

The P1−C1 bond length with 1.836(2) Å is in good agreement with the sum of covalent radii for P−C single bonds. The P1−Zn1 bond with 2.3092(7) Å is only marginally longer than the sum of the covalent radii for P−Zn single bonds, which is also the case for the Zn1−Cl1 bond length with 2.2057(7) Å (cf. Σr_{cov}(P–C) = 1.84 Å, Σr_{cov}(P–Zn) = 2.29 Å, Σr_{cov}(Zn–Cl) = 2.17 Å).[11] The Zn1−O bonds with an average length of 2.084 Å, however, are considerably longer than the sum of the covalent radii for Zn−O single bonds, thus indicating a weak interaction with the tetrahydrofuran ligands (cf. Σr_{cov}(Zn–O) = 1.81 Å).[11]

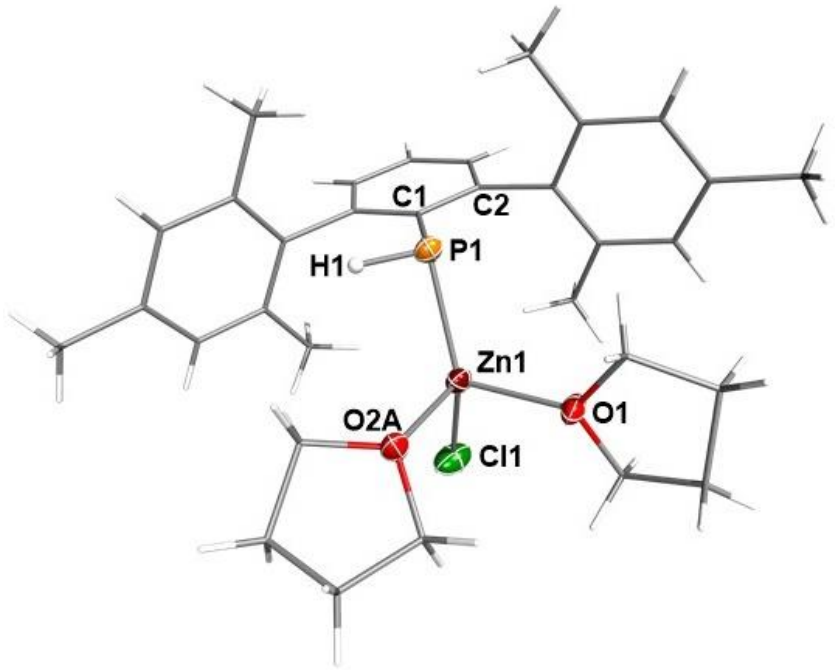

Figure 14: Molecular structure of **36** in the crystal ($P2_1/n$). Thermal ellipsoids drawn at the 50 % probability level and −150 °C. Carbon and hydrogen atoms rendered as wireframe for clarity. Selected bond lengths (Å), angles (°) and dihedral angles (°): P1−C1 1.836(2), P1−Zn1 2.3092(7), Zn1−Cl1 2.2057(7), Zn1−O1 2.0705(2), Zn1−O2A 2.097(2); C1−P1−Zn1 105.87(7), Cl1−Zn1−P1 143.10(3), C1−P1−H1 100.0(2), Zn1−P1−H1 92.2(2), O1−Zn1−O2A 92.3(3); H1−P1−C1−C6 −1.647(2), Zn1−P1−C1−C2 −90.44(2).

The coordination environment of the four-coordinate zinc atom is that of a considerably distorted tetrahedron with a large P1–Zn1–Cl1 angle of 143.10(3)° and, on the other hand, a distinctly smaller O1–Zn1–O2A angle of 92.3(3)° which can be attributed to the high steric demand of the terphenyl substituent. At the phosphorus atom, the C1–P1–H1 angle and the H1–P1–Zn1 angle with 100.0(2)° and 92.2(2)°, respectively, are very similar to those observed in the crystal structure of TerP(H)Li·3THF (**29**, Figure 6). The C1–P1−Zn1 angle with 105.87(7)°, however, is much smaller than the C1–P1–Li1 angle observed in **29** (125.43(2)°). This can be attributed to the fact that, although the P1–Zn1 bond is shorter than the P1–Li1 bond in **29** (2.536(4) Å), the comparatively smaller chloride substituent induces less steric strain than a third THF ligand. In accordance with the crystal structure of **29**, the P1–H1 bond in **36** is slightly bent out of the plane of the central phenyl ring of the terphenyl substituent by –1.647(2)° (H1–P1–C1–C6) while the P1–Zn1 bond is arranged nearly perpendicularly with a Zn1–P1–C1–C2 dihedral angle of –90.44(2)°.

The structural parameters of **36** in the crystal are in very good agreement with those that were obtained from the optimized structure in the gas phase at the PBE1PBE/6-31G(d,p) level of theory (Table 7).

Table 7: Comparison of selected experimental and calculated structural parameters of **36** (PBE1PBE/6-31G(d,p) level of theory). Bond lengths in Å, angles and dihedral angles in °.

Parameter	**Experimental**	***Calculated***
C1−P1	1.836(2)	*1.838*
P1−Zn1	2.3092(7)	*2.303*
Zn1−Cl1	2.2057(7)	*2.224*
Zn1−O1	2.0705(2)	*2.073*
Zn1−O2A	2.097(2)	*2.098*
C1−P1−Zn1	105.87(7)	*108.953*
P1−Zn1−Cl1	143.10(3)	*139.493*
O1−Zn1−O2A	92.3(3)	*90.441*
C1−P1−H1	100.0(2)	*97.059*
Zn1−P1−H1	92.2(2)	*96.835*
H1−P1−C1−C6	−1.647(2)	*−2.136*
Zn1−P1−C1−C2	−90.44(2)	*−87.382*

TerPH(ZnCl)·2THF (**36**) was characterized by ^{1}H-, ^{13}C-, and ^{31}P NMR spectroscopy in deuterated tetrahydrofuran (THF-d_8). It is characterized by a broad singlet at −182.9 ppm in its ^{31}P{^{1}H} NMR spectrum, which splits into a broad doublet with a coupling constant of approx. 198 Hz when coupling with hydrogen is enabled. The coupling constant is only slightly smaller than that observed for the parent phosphane **3** with 211 Hz. The broadening of the ^{31}P NMR resonance hints at dynamic processes in solution, the nature of which was not investigated yet. The ^{1}H NMR spectrum exhibits five signal groups that were assigned to the respective protons of the terphenyl substituent by integration and comparison with the ^{1}H NMR spectrum of the parent phosphane **3**. The proton at the phosphorus atom, however, could not be assigned yet. Furthermore, all resonances in the ^{13}C NMR spectrum could be assigned to the respective carbon atoms of the terphenyl substituent with the exception of the *ipso*-C, which was not observed. The resonances of the THF ligands could not be distinguished from those of the non-deuterated THF molecules that were present within the deuterated solvent.

In addition to the abovementioned analytical methods, **36** was characterized by Raman spectroscopy. Its Raman spectrum exhibits a distinctive vibrational mode at 2316 cm^{-1}, which can be assigned to P−H stretching. Other vibrational modes were assigned by comparison of the experimental Raman spectrum with calculated frequencies for the optimized structure in the gas phase (Figure 15).

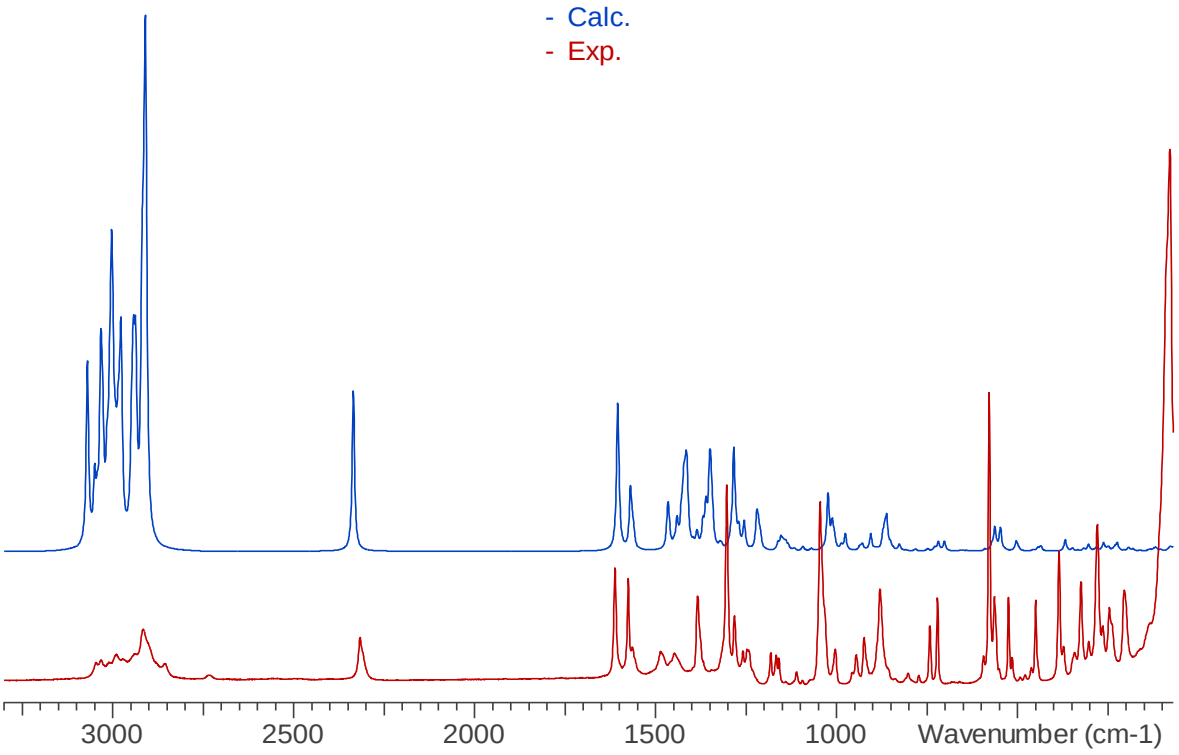

Figure 15: Experimental and calculated Raman spectrum of TerPH(ZnCl)·2THF (**36**) (PBE1PBE/6-31G(d,p) level of theory). The calculated relative intensities are not accurate due to the relatively small 6-31G(d,p) basis set,[35] however, the calculated frequencies were corrected by multiplication with the factor 0.9512[36] and are in good agreement with experimental data.

The vibrational bands at 1613 cm^{-1} and 1576 cm^{-1} were assigned to in-phase aromatic ring vibrations of the mesityl groups and of the central phenyl ring, respectively. The bands at 1304 cm^{-1} and 1046 cm^{-1} were assigned to in-plane ring vibrations of the terphenyl substituent and out-of-phase C−O−C stretching of the THF ligands, respectively. The intensive vibration at 579 cm^{-1} is caused by a combined vibration of P−H wagging and out-of-plane deformation of the mesityl groups.

It is worthy of note that the isolated crystals were not entirely pure. The ^{31}P NMR spectrum showed that they contained small residual amounts of the starting material **3**, as well as two further, so far unidentified, phosphorus-containing species to a combined extent of approximately 5 %. Recrystallization of the isolated solid could not be attempted yet.

In contrast to the previously discussed phosphides [TerPH(ZnEt)]$_2$ (**34**) and [TerP(ZnEt)$_2$]$_2$ (**35**) that both comprise reactive ethylzinc moieties, the chlorozinc phosphide TerPH(ZnCl)·2THF (**36**) is different in that it comprises a presumably much less reactive Zn−Cl bond. Although the four-membered ring is not preformed as it is with the four-membered P−Zn ring systems in **34** and **35**, TerPH(ZnCl)·2THF (**36**) might still be a promising candidate for the treatment with PCl_3.

3.3 P–P coupling reactions of zinc phosphides with PCl_3

In order to investigate the applicability of our novel zinc phosphides for the synthesis of pnictogen or interpnictogen ring systems, model experiments were carried out for which the zinc phosphides were treated with PCl_3. However, due to time limitations, only $[TerPH(ZnEt)]_2$ (**34**) and $[TerP(ZnEt)_2]_2$ (**35**) were investigated in such manner for $TerPH(ZnCl)\cdot 2THF$ (**36**) was synthesized only towards the end of the project. In both cases, the target was to obtain either isomer of the 1,3-dichloro-*cyclo*-tetraphosphanes ***cis*-4** and ***trans*-4** (Scheme 26), which had both been observed before.[5]

3.3.1 Treating $[TerPH(ZnEt)]_2$ (34) with PCl_3 in the presence of NEt_3

Since the ethylzinc terphenylphosphide **34** is still carrying a hydrogen atom at the phosphorus center, a reaction with PCl_3 alone would unlikely give rise to the desired 1,3-dichloro-*cyclo*-tetraphosphanes ***cis*-4** or ***trans*-4**. A base-assisted reaction with PCl_3, however, might afford such cyclic tetraphosphanes. For that reason, a twentyfold excess of triethylamine (NEt_3) was added to a solution of **34** in THF. Thereupon, twenty equivalents of PCl_3 were added to the stirred solution at −80 °C (Scheme 26). A twentyfold excess of base and PCl_3 was used for reasons of practicality in order to test the general reactivity of **34**. Upon addition of PCl_3, the solution immediately took on a yellow color. After 18 hours of stirring at ambient temperature, the volatile components were removed *in vacuo* and the foamy, yellow residue was dissolved in benzene. A ^{31}P NMR spectrum of the solution at this stage of workup showed that a mixture of a plethora of products was formed (Figure 16), five of which were identified by their ^{31}P NMR resonances and by means of computational studies.

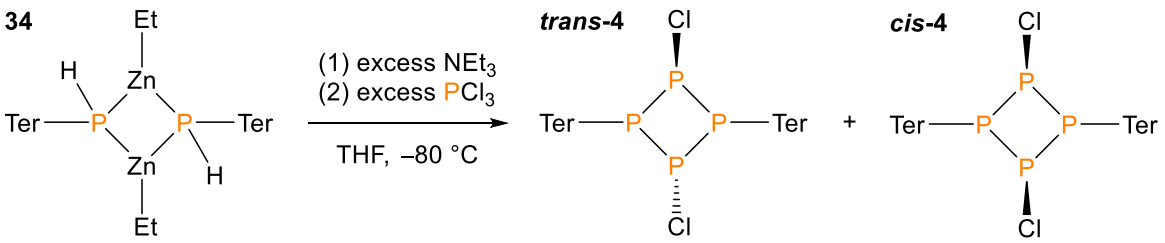

Scheme 26: Attempted synthesis of ***trans*-4** and ***cis*-4** starting from **34**.

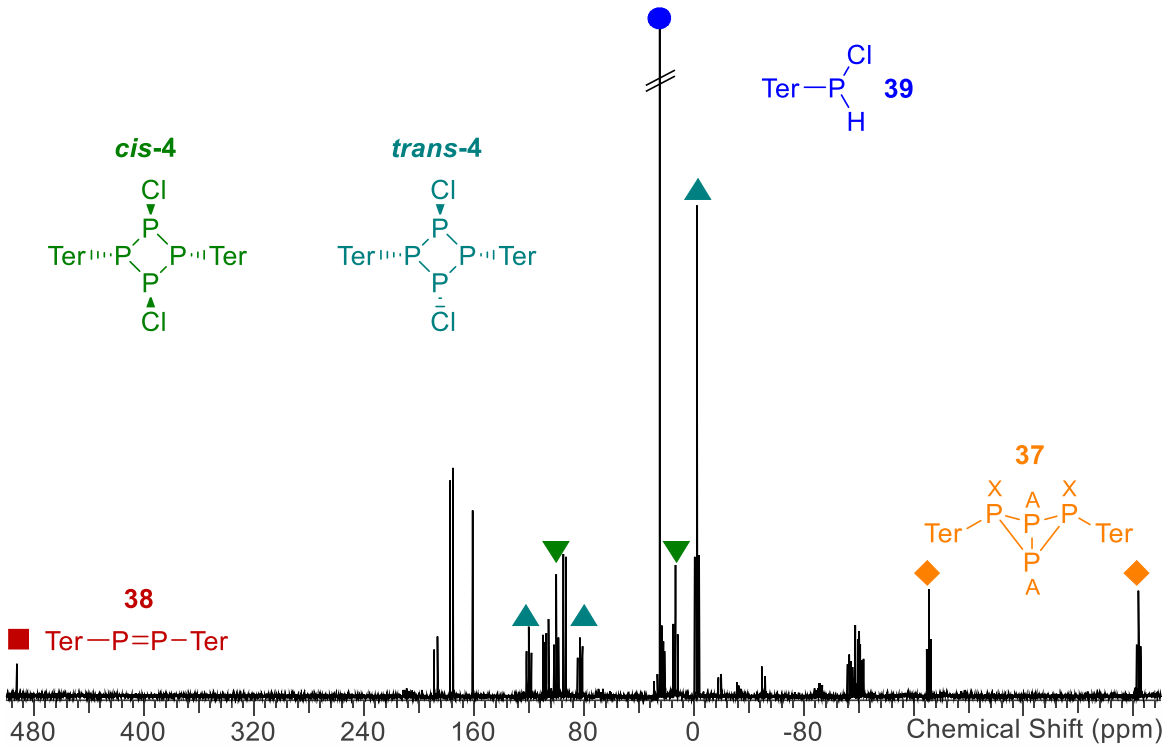

Figure 16: ^{31}P NMR spectrum of the reaction mixture after removal of all volatile components.

The disphosphene TerPPTer (**38**) exhibits a singlet resonance at 492.6 ppm and was identified by comparison with literature data.[27]

Unlike the *endo-exo*-bicyclo[1.1.0]-tetraphosphane TerP$_4$Ter which had been isolated and characterized,[39] the *exo-exo*-bicyclo[1.1.0]tetraphosphane (**37**) has merely been observed by ^{31}P NMR spectroscopy[5] but has never been isolated before. It was identified by comparison with reported NMR data for the *exo-exo*-isomer of Ar^{Dipp}P$_4$Ar^{Dipp} (Ar^{Dipp} = 2,6-bis-(2,6-diisopropylphenyl)phenyl)[40] and the assignment supported by calculated ^{31}P NMR data (Table 8).

Table 8: Experimental ^{31}P NMR chemical shifts and ^{31}P-^{31}P coupling constants of **37** in C_6D_6. Calculated values in parentheses (PBE1PBE/6-31G(d,p)).

X	***δ* [ppm]**	***J* [Hz]** P_A-X
P_A	−323.8 (−313.3)	–
P_X	−169.6 (−186.5)	−182.1 (−154.8)

Furthermore, the desired *cyclo*-tetraphosphanes ***cis*-4** and ***trans*-4** were observed in the ^{31}P NMR spectrum of the reaction mixture. All attempts to isolate ***cis*-4** or ***trans*-4** were unsuccessful. However, it was possible to identify them unambiguously by complete analysis of their ^{31}P NMR resonances and, in addition, assign the observed resonances to the respective phosphorus atoms with the help of calculated ^{31}P NMR data.

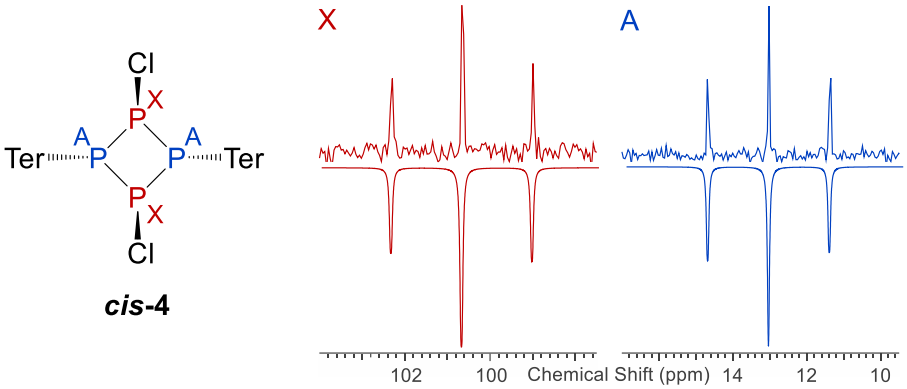

Figure 17: Experimental (upwards) and simulated (downwards) ^{31}P NMR resonances of ***cis*-4** in CD_2Cl_2.

The ^{31}P NMR spectrum of ***cis*-4** in CD_2Cl_2 exhibits two triplet resonances of an A_2X_2 spin system at 13.0 ppm and 100.6 ppm, of which the first resonance can be assigned to the terphenyl substituted phosphorus atoms (P_A, Figure 17) and the latter to the chloride substituted phosphorus atoms (P_X, Figure 17). The experimentally observed ^1J coupling constant is −201 Hz. ^{31}P NMR data that was calculated at the PBE1PBE/6-31G(d,p) level of theory matches well with the experimentally observed values (Table 9).

Table 9: Experimental ^{31}P NMR chemical shifts and ^{31}P-^{31}P coupling constants of ***cis*-4** in CD_2Cl_2. Calculated values in parentheses (PBE1PBE/6-31G(d,p)).

X	***δ* [ppm]**	***J* [Hz]** P_A-X
P_A	13.0 (−0.4)	–
P_X	100.6 (99.5)	−200.9 (−168.2)

***Trans*-4**, on the other hand, is characterized by an A_2MX spin system that comprises a triplet resonance at −3.3 ppm and two triplet-of-doublets resonances at 82.5 ppm and 118.8 ppm in CD_2Cl_2. This is caused by the inequivalency of the two chloride substituted phosphorus

atoms which could unambiguously be assigned to their respective resonances by comparison with calculated ^{31}P NMR data (Figure 18).

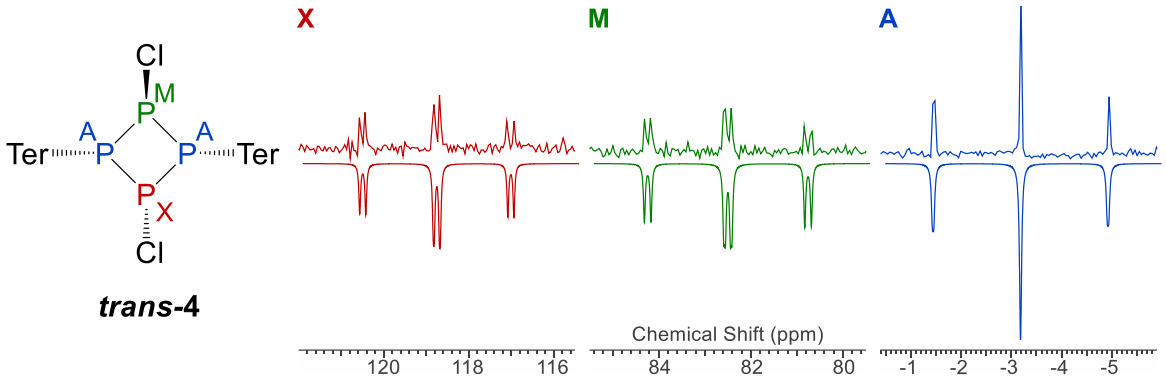

Figure 18: Experimental (upwards) and simulated (downwards) ^{31}P NMR signals of ***trans*-4** in CD_2Cl_2.

The Ter-substituted phosphorus atom P_A (Figure 18) exhibits the triplet resonance at −3.3 ppm. The resonance at 82.5 ppm can be assigned to the phosphorus atom P_M with its chloride substituent in equatorial position, while the most downfield shifted resonance at 118.8 ppm can be assigned to P_X with its chloride substituent in axial position. Interestingly, the ^1J coupling constants between P_A and P_M and P_A and P_X, respectively, are virtually equal with −213 Hz, thus causing the resonance at −3.3 ppm to appear as a triplet. While the observed ^1J coupling constants are, in both cases, larger than the calculated values (Table 10), the experimentally observed ^2J coupling constant between P_M and P_X, on the other hand, is rather small with merely 15.6 Hz, which is even smaller than the calculated value. However, the calculated ^{31}P chemical shifts for ***trans*-4** are in good agreement with experimental values (Table 10).

Table 10: Experimental ^{31}P NMR chemical shifts and ^{31}P-^{31}P coupling constants of ***trans*-4** in CD_2Cl_2. Calculated values in parentheses (PBE1PBE/6-31G(d,p)).

X	δ [ppm]	J [Hz]	
		P_A-X	P_M-X
P_A	−3.3 (−18.7)	–	–
P_M	82.5 (92.2)	−213.0 (−171.7)	–
P_X	118.8 (128.6)	−213.0 (−190.8)	−15.6 (−43.5)

It is worthy of note that the *cyclo*-tetraphosphane ***trans*-4** was apparently formed to a higher extent than *cyclo*-tetraphosphane ***cis*-4**. Comparing the integrals of their respective P_A resonances, it can be deduced that, in the product mixture, they were present in a ratio of roughly 2 : 1. This could be attributed to the fact that, according to calculated values for the enthalpy ΔH at the PBE1PBE/6-31G(d,p) level of theory, ***trans*-4** is thermodynamically lower in energy than ***cis*-4** by 0.64 kJ/mol. However, to the best of our knowledge, there are no other examples of 1,3-dichloro-*cyclo*-tetraphosphanes for which both the *trans*- and the *cis*-isomer were observed to be compared with.

Another signal that could be identified in the ^{31}P NMR spectrum of the product mixture was the singlet resonance at 24.5 ppm which can be assigned to TerP(H)Cl (**39**). After several attempts of isolating any product from the product mixture, colorless block-shaped crystals of **39** were grown in fluorobenzene (PhF) that were of sufficient quality for X-ray crystal structure determination. Although **39** has been known in the literature since 2000,[41] up until now there were no reports on crystallographic data for this compound (Figure 19).

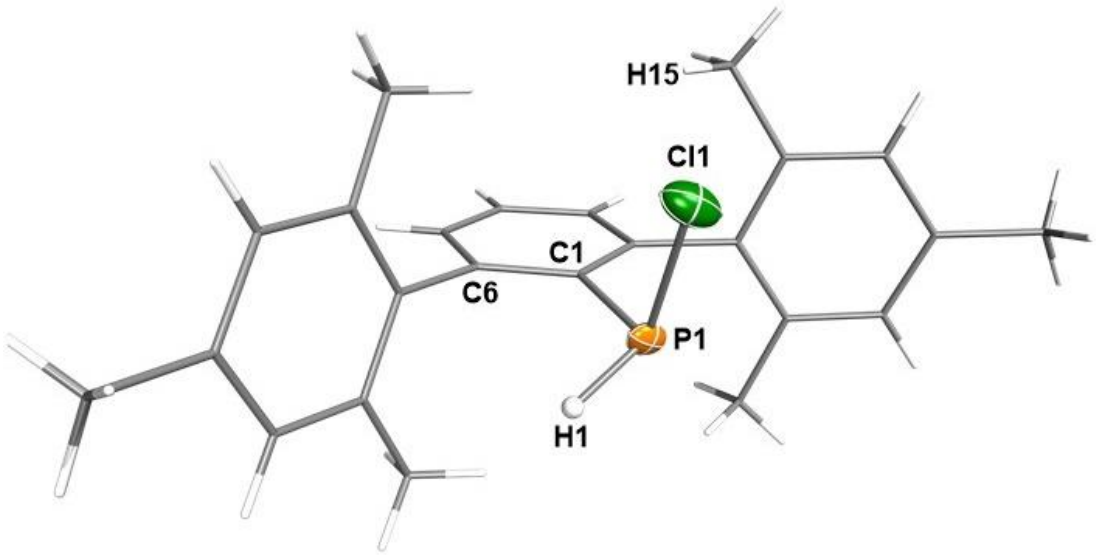

Figure 19: Molecular structure of **39** in the crystal (*Pc*). Thermal ellipsoids drawn at the 50 % probability level and −150 °C. Carbon and hydrogen atoms rendered as wireframe for clarity. Selected bond lengths (Å), angles (°) and dihedral angles (°): P1−C1 1.830(3), P1−Cl1 2.0732(2); H1−P1−Cl1 109.0(3), H1−P1−C1 106.0(3), Cl1−P1−C1 103.07(1), P1−C1−C2 118.3(2), P1−C1−C6 121.1(2); Cl1−P1−C1−C2 89.923(3), H1−P1−C1−C6 21.218(3).

39 crystallized in the monoclinic space group *Pc* with two molecules per unit cell. The P−C bond length is 1.830(3) Å, which is slightly shorter than the sum of the covalent radii for P−C single bonds as is the P−Cl bond with its 2.0732(2) Å (cf. Σr_{cov}(P–C) = 1.86 Å,

Σr_{cov}(P–Cl) = 2.10 Å).[11] Both bond lengths compare well with those observed for $TerPCl_2$ (**28a**).[42] Noteworthy is also the distance between Cl1 and H15A (Figure 19). In the crystal it is 2.9956(2) Å, which is slightly longer than the van der Waals radius (cf. Σr_{vdW}(Cl–H) = 2.85 Å).[33]

The bond angles at the phosphorus atom are close to tetrahedral angles with H1−P1−C1, H1−P1−Cl1, and Cl1−P1−C1 being 106.0(3)°, 109.0(3)°, and 103.07(1)°, respectively. The angles between P1−C1−C2 and P1−C1−C6 are 118.3(2)° and 121.1(2)°, respectively. This is in contrast to **28a**, in which the average angle at the phosphorus center is 101.9°. Furthermore, the phosphorus atom in **28a** is significantly bent towards C2 with a P1−C1−C2 angle of 109.87(2)°,[42] which is due to the larger steric demand of the chloride substituent compared to the hydrogen atom in **39**. In **39**, however, the steric repulsion between the terphenyl and the single chloride substituent is minimized as the chloride stands almost perpendicularly to the central phenyl ring of the terphenyl substituent with the dihedral angle between Cl1−P1−C1−C2 being 89.923(3)°.

In its $^{31}P\{^{1}H\}$ NMR spectrum, **39** is characterized by a singlet resonance at 24.5 ppm which splits into a doublet with a ^{31}P-^{1}H coupling constant of 205 Hz when coupling is enabled. Intriguingly, the ^{1}H NMR spectrum of **39** exhibits three separate resonances for the methyl groups of the therphenyl substituent at 2.00 ppm, 2.14 ppm, and 2.19 ppm, indicating inequivalency of the *o*-Me groups. In addition, it exhibits two separate resonances for the *meta*-protons of the mesityl groups at 6.85 ppm and 6.88 ppm. Such an effect was not observed for the parent phosphane $TerPH_2$ (**3**) nor the dichlorophosphane $TerPCl_2$ (**28a**).[42] However, according to computational studies at the PBE1PBE/6-31G(d,p) level of theory, the observation of separate NMR resonances for both the *meta*-hydrogens as well as the *ortho*-methyl groups of **39** is consistent with calculated NMR chemical shifts. The separate resonances can primarily be attributed to the fact that **39** comprises a chiral phosphorus center and secondly to hindered rotation of the mesityl groups.

In the Raman spectrum, **39** displays a characteristic P−H stretching mode at 2327 cm^{-1} which matches very well with the calculated, corrected value of 2324.3 cm^{-1}.[36]

3.3.2 Treating $[TerP(ZnEt)_2]_2$ (35) with PCl_3

The experiment of treating $[TerP(ZnEt)_2]_2$ (**35**) with equimolar amounts of PCl_3 was carried out twice with slightly modified reaction conditions. It was expected that, upon treatment with PCl_3, **35** would subsequently undergo nucleophilic substitution reactions, eventually eliminating $ZnCl_2$ to form the desired 1,3-dichloro-*cyclo*-tetraphosphanes ***cis*-4** and ***trans*-4** (Scheme 27).

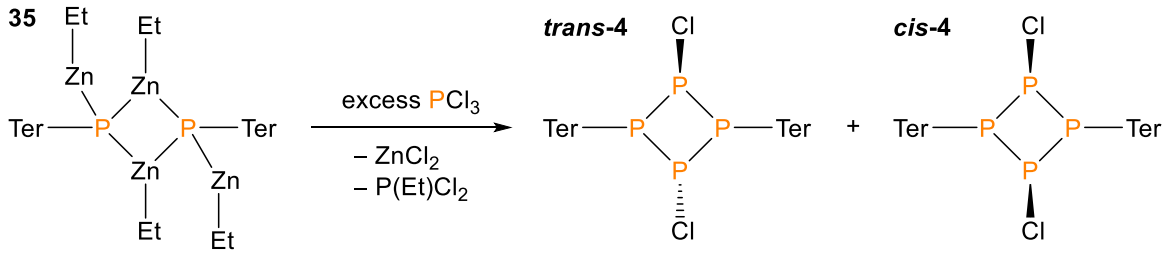

Scheme 27: Attempted synthesis of ***trans*-4** and ***cis*-4** starting from **35**.

Following *Method A* (cf. Chapter 5.3.6), 36 equivalents of neat PCl_3 were added directly to a solution of **35** in THF at −80 °C, whereupon the solution immediately took on a yellow color. After allowing the solution to warm to ambient temperature, the volatile components were removed *in vacuo*, the residue was extracted with benzene, and filtered through a glass sintered frit. From the concentrated filtrate, small colorless platelets as well as larger, colorless, block-shaped crystals were isolated. The former were found to be $ZnCl_2 \cdot THF$,[32] thus proving that indeed $ZnCl_2$ was eliminated during the reaction, whereas the latter were characterized by $^{31}P\{^1H\}$ NMR spectroscopy and X-ray diffractometry. They were thus found to be mixed crystals of 1,3-dichloro-*cyclo*-tetraphosphanes ***cis*-4** and ***trans*-4**, 1-chloro-3-ethyl-*cyclo*-tetraphosphane **40** and bicyclo[1.1.0]tetraphosphane **37**, although the latter was only observed in the $^{31}P\{^1H\}$ NMR spectrum (Figure 20) but not in the crystal.

The two triplet resonances at −324.4 ppm and −172.2 ppm can be assigned to the bicyclo[1.1.0]-tetraphosphane **37** which was formed to the extent of roughly 6.5 %. The signal groups at −3.3 ppm, 85.5 ppm and 118.8 ppm belong to ***trans*-4** (20.4 %), while the two triplet resonances at 13.0 ppm and 100.6 ppm were assigned to ***cis*-4** (10.8 %). The complete analyses of these three compounds' ^{31}P NMR spectra were discussed in Chapter 3.3.1. It is noteworthy that, according to the integral values of the respective P_A phosphorus centers of ***trans*-4** and ***cis*-4**, they were, again, formed in a ratio of roughly 2 : 1.

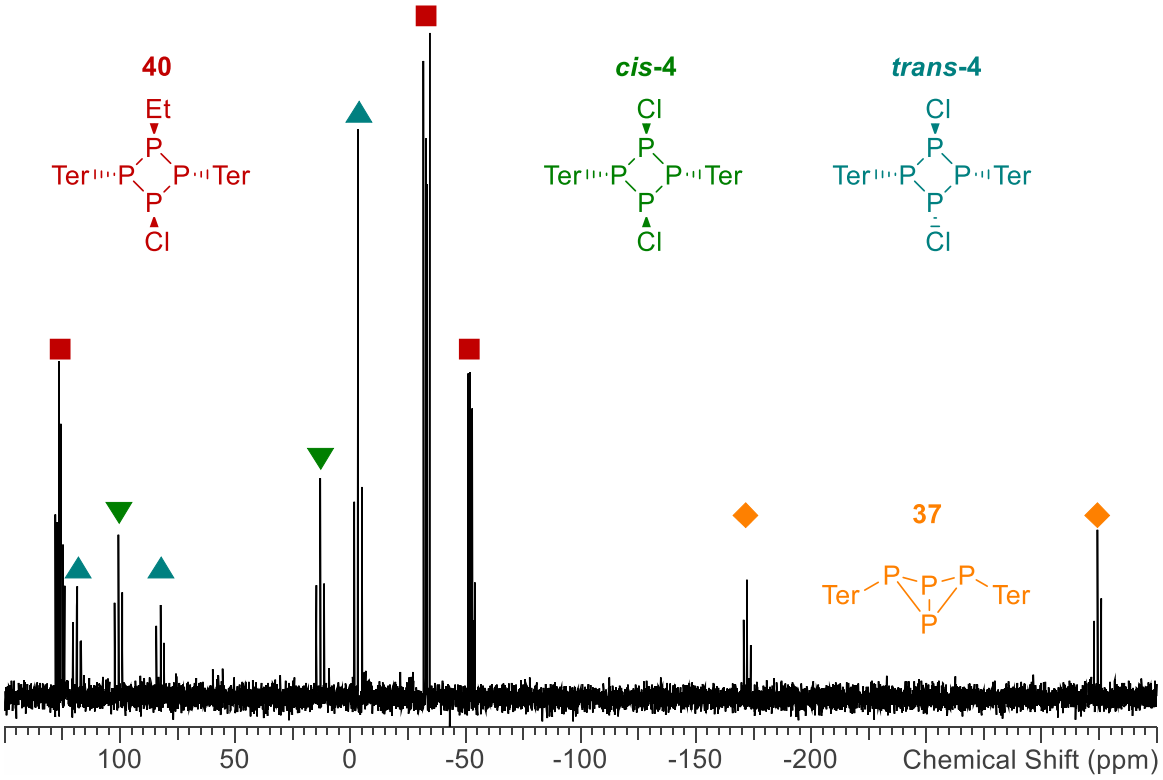

Figure 20: ^{31}P NMR spectrum of the isolated mixed crystals in CD_2Cl_2.

Furthermore, a new set of signals was observed at −52.6 ppm, −33.1 ppm and 126.1 ppm (red blocks in Figure 20), which belong to the major product (62.3 %) of this reaction. Its identity was determined unambiguously by comparison with calculated ^{31}P NMR data (Figure 21 and Table 11) and by its crystal structure (Figure 22).

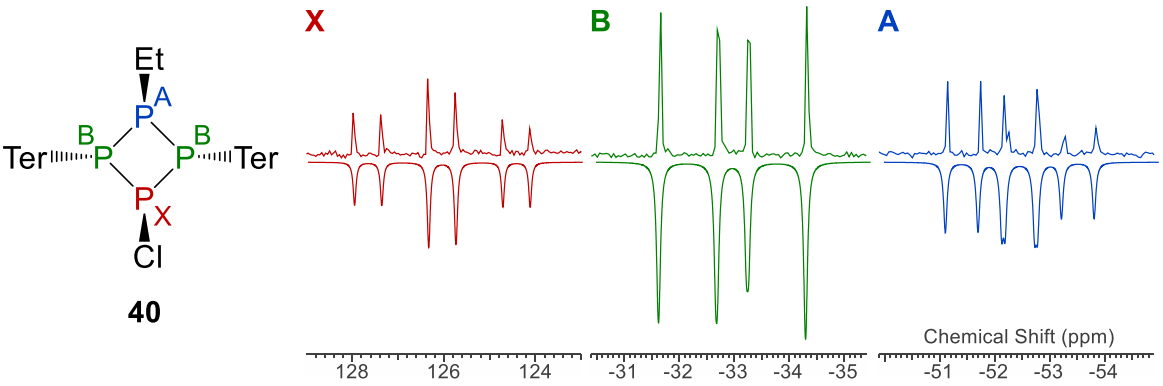

Figure 21: Experimental (upwards) and simulated (downwards) ^{31}P NMR resonances of **40** in CD_2Cl_2.

In its ^{31}P NMR spectrum, 1-chloro-3-ethyl-*cyclo*-tetraphosphane **40** is characterized by an AB_2X spin system. The resonances of P_A and P_X (Figure 22) are split into triplets of doublets with a mutual ^2J coupling constant of 72.8 Hz, which causes the doublet splitting.

The ^{1}J coupling constants of P_A with P_B and P_X with P_B are 124.8 Hz and 197.7 Hz, respectively, and are accountable for the triplet splitting. Thus, the resonance of the Ter-substituted phosphorus centers P_B is split into a doublet of doublets. The experimentally observed chemical shifts and coupling constants are in best agreement with calculated values for a *cyclo*-tetraphosphane with *cis*-arranged ethyl and chloride substituents, which is also the arrangement observed in the solid state.

Table 11: Experimental ^{31}P NMR chemical shifts and ^{31}P-^{31}P coupling constants of **40** in CD_2Cl_2. Calculated values in parentheses (PBE1PBE/6-31G(d,p)).

X	***δ* [ppm]**	***J* [Hz]**	
		P_A-X	P_B-X
P_A	−52.6 (−71.3)	–	–
P_B	−33.1 (−54.6)	−124.8 (−99.1)	–
P_X	126.1 (126.9)	72.8 (41.2)	−197.7 (−162.1)

X-ray single crystal analyses provided more insight into the composition of the isolated mixed crystals. The mixture of ***cis*-4**, ***trans*-4**, and **40** crystallized in the orthorhombic space group $Pna2_1$ as a benzene solvate with four molecules per unit cell. For the measured crystal, the crystal structure was separated into three layers, which are shown separately for reasons of clarity. The A-layer (Figure 22, Figure 23) comprised the *cis*-1,3-dichloro-*cyclo*-tetraphosphane ***cis*-4** with an occupancy of 27.0 % as well as the 1-chloro-3-ethyl-*cyclo*-tetraphosphane **40** with an occupancy of 60.9 %. The only difference between both molecules in the A-layer were the ethyl substituent and chloride substituent at P2A, respectively, while all other atoms shared the exact same position. The B- and C-layer both comprised the *trans*-1,3-dichloro-*cyclo*-tetraphosphane ***trans*-4** with a combined occupancy of 11.4 %. They differed only in the spatial arrangement of the central P_4Cl_2 unit. The B-layer is shown in Figure 23 (right). While the occupancy of **40** in the crystal is consistent with the relative content of **40** observed in the ^{31}P NMR spectrum, the opposite is the case for ***trans*-4** and ***cis*-4**, which were observed in a ratio of roughly 1 : 2.4 in the solid state, which could possibly hint at an dynamic equilibrium in solution.

Due to impaired accuracy of the geometric parameters because of considerable disorders within the crystal, only averaged values over all layers will be discussed.

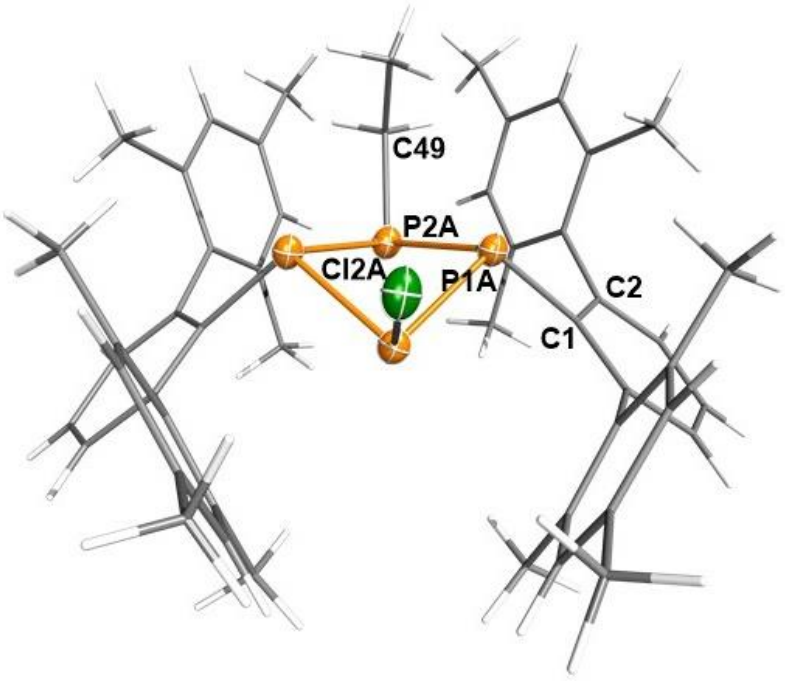

Figure 22: Molecular structure of **40** in the crystal (*Pna*2$_1$) as part of the A-layer with 60.9 % occupancy. Thermal ellipsoids drawn at the 50 % probability level and −150 °C. Carbon and hydrogen atoms rendered as wireframe for clarity. The solvent molecule is not shown. Averaged selected bond lengths (Å), angles (°) and dihedral angles (°) for all layers: P−C 1.839, P−Cl 2.083, P−P 2.234; P−P−P 84.05; P−P−P−P 129.1.

The average P−P bonds lengths (2.234 Å) are only marginally longer than the sum of covalent radii for typical P−P single bonds (cf. Σr_{cov}(P–P) = 2.22 Å).[11] The average P–C bond lengths (1.839 Å) are within the range of typical P−C single bonds whereas the averaged P−Cl bond lengths (2.083 Å) over all layers are slightly shorter than the sum of covalent radii for P−Cl single bonds (cf. Σr_{cov}(P–C) = 1.84 Å, Σr_{cov}(P–Cl) = 2.10 Å).[11] The mean P−P−P angles are 84.05°. Furthermore, a puckering of the P_4 ring system can be observed with an average fold angle of 129.1°. These values are actually in relatively good agreement with previously reported crystallographic data on the *cis*-1,3-dichloro-*cyclo*-tetraphosphane ***cis*-4**.[5] The crystal structure of the *cis*-1,3-dichloro-*cyclo*-tetraphosphane ***cis*-4** within the measured mixed crystal resembles that of **40**, with the exception of the chloride substituent in place of the ethyl substituent at P2A (Figure 23, left). The *trans*-1,3-dichloro-*cyclo*-tetraphosphane ***trans*-4** (Figure 23, right) comprises one chloride substituent in equatorial position and one in axial position. The P_4 ring appears to be slightly tilted

towards the side of the axially substituted phosphorus atom. This effect was observed for the optimized structure of ***trans*-4** as well. This tilting can most likely be attributed to the reduction of steric strain due to the chloride substituent in axial position.

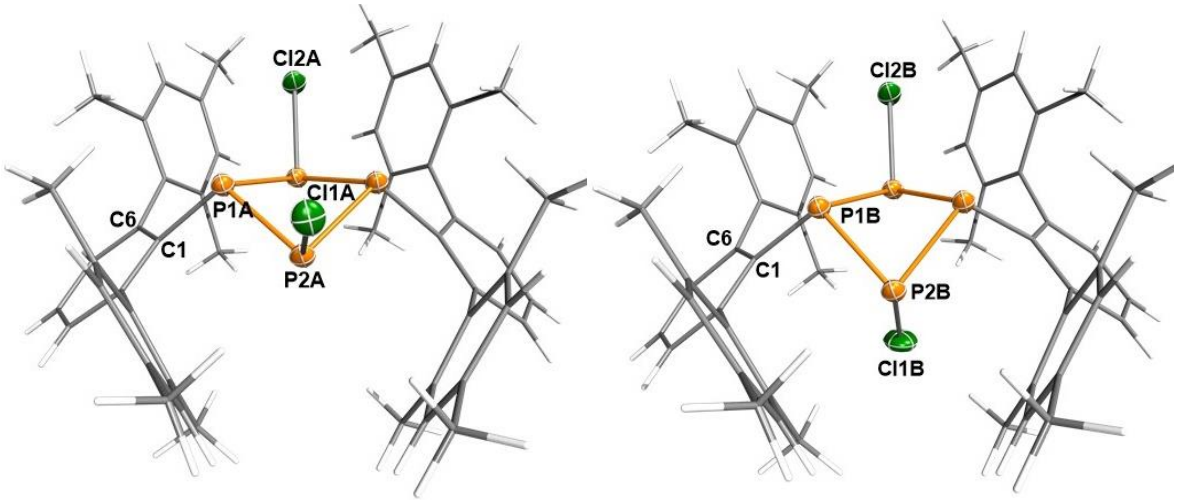

Figure 23: Molecular structure of ***cis*-4** (left) and ***trans*-4** (right) in the crystal (*Pna*2_1) Thermal ellipsoids drawn at the 50 % probability level and −150 °C. Carbon and hydrogen atoms rendered as wireframe for clarity. The solvent molecule is not shown.

The observation of ethyl substituted phosphorus atoms within the cyclic tetraphosphanes was not too surprising, since organometallic dialkylzinc reagents are indeed used to alkylate electrophilic phosphorus atoms in nucleophilic substitution reactions.[43] Still, another approach for the treatment of zinc phosphadiide **35** was attempted in order to investigate the influence of the reaction conditions on the product distribution.

Following *Method B* (cf. Chapter 5.3.6), the reaction was not carried out at −80 °C but instead at 0 °C to increase the reaction rate. Furthermore, instead of directly adding neat PCl_3 to a solution of **35**, the solution of **35** in THF was added dropwise to a cooled solution of PCl_3 in *n*-pentane, which contained an almost twentyfold excess of PCl_3 with respect to **35**. Upon addition of the zinc phosphadiide, the solution took on a yellow color, which deepened over the course of the addition. After the addition had been completed and the solution had warmed to ambient temperature, the volatile components were removed *in vacuo* and the yellow residue was extracted with benzene. A ^{31}P NMR spectrum at this stage of workup showed that, again, a mixture of *cyclo*-tetraphosphanes was formed. The attempt to isolate any product by crystallization from a concentrated solution in THF yielded colorless crystals, which were not of sufficient quality for X-ray crystal structure determination but were,

however, characterized by means of ^{31}P NMR spectroscopy. They were found to be mixed crystals of the 1-chloro-3-ethyl-*cyclo*-tetraphosphane **40** (Figure 22) and the 1,3-diethyl-*cyclo*-tetraphosphane **41** (Figure 24). This means that not only was this second attempt of treating [TerP(ZnEt)$_2$]$_2$ (**35**) with PCl$_3$ unsuccessful in yielding the desired 1,3-dichloro-*cyclo*-tetraphosphanes ***cis*-4** and ***trans*-4** more selectively, but it actually yielded a doubly ethyl-substituted *cyclo*-tetraphosphane in addition to **40**.

1,3-Diethyl-*cyclo*-tetraphosphane **41** was identified by comparison of its experimental ^{31}P NMR spectrum with calculated ^{31}P NMR data. The experimentally observed chemical shifts and coupling constants are in best agreement with calculated values for a *cyclo*-tetraphosphane with *cis*-arranged ethyl substituents (Table 12). In its ^{31}P NMR spectrum, **41** is characterized by two triplet resonances of an A_2X_2 spin system at −83.0 ppm and −26.4 ppm with a ^1J coupling constant of 124.8 Hz. Both resonances were assigned to the respective phosphorus centers. The ethyl substituted phosphorus atoms resonate in the lower field at −83.0 ppm while the terphenyl substituted phosphorus centers resonate at −26.4 ppm.

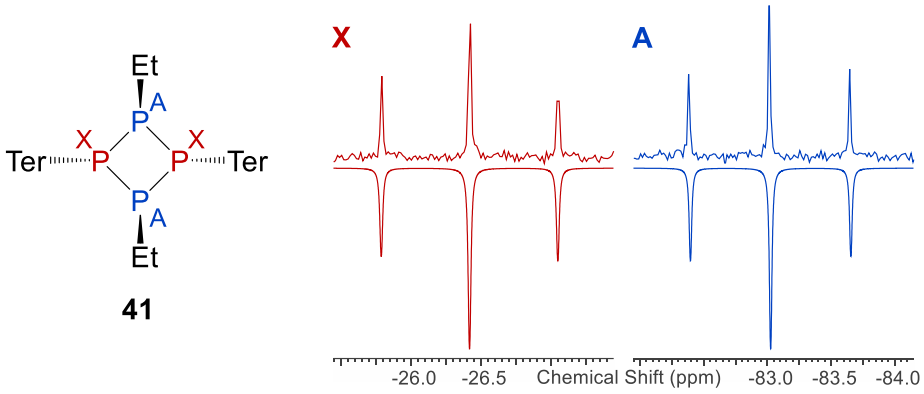

Figure 24: Experimental (upwards) and simulated (downwards) ^{31}P NMR resonances of **41** in C_6D_6.

Table 12: Experimental ^{31}P NMR chemical shifts and ^{31}P-^{31}P coupling constants of **41** in C_6D_6. Calculated values in parentheses (PBE1PBE/6-31G(d,p)).

X	***δ* [ppm]**	***J* [Hz]**
		P_A-X
P_A	−83.0 (−108.6)	–
P_X	−26.4 (−44.3)	−124.8 (−96.9)

In lieu of a crystal structure, the optimized molecular structure at the PBE1PBE/6-31G(d,p) level theory is shown in Figure 25. According to computational studies, the molecular structure of **41** resembles that of **40** in the crystal with similar P−P−P angles within the P_4 ring and a marginally larger fold angle.

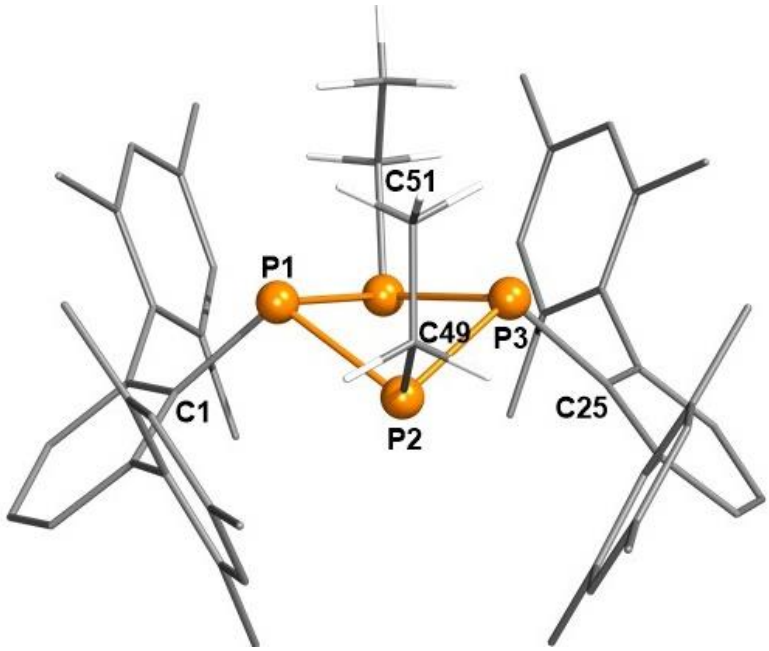

Figure 25: Optimized molecular structure of **41** at the PBE1PBE/6-31G(d,p) level of theory. Hydrogen atoms at the terphenyl substituents were omitted for clarity.

4 Conclusions and Perspectives

In conclusion, the reactions of terphenylphosphane with equimolar amounts of organometallic ethylzinc reagents gave rise to the two novel zinc phosphides $[TerPH(ZnEt)]_2$ and TerPH(ZnCl). Both compounds were fully characterized in the solid state and in solution by means of X-ray crystal structure determination, NMR and Raman spectroscopy, and, in case of the former, by elemental analysis, mass spectrometry and differential scanning calorimetry. Intriguingly, $[TerPH(ZnEt)]_2$ was found to form a dimer in the crystal and in solution while TerPH(ZnCl) apparently exists exclusively as a monomeric compound.

Furthermore, the reaction of terphenyl phosphane with two equivalents of diethylzinc gave rise to a novel zinc phosphadiide $[TerP(ZnEt)_2]_2$ which resembled the structural motif of $[TerPH(ZnEt)]_2$ in the solid state with the exception of exocyclic ethylzinc moieties instead of hydrogen atoms at the negatively charged phosphorus center. This compound was characterized by means of X-ray crystal structure determination, NMR spectroscopic investigations at variable temperatures, Raman spectroscopy, elemental analysis, and mass spectrometry. Although existing exclusively as a dimer in the solid state, data obtained from variable temperature $^{31}P\{^1H\}$ NMR experiments and computational studies hint at an underlying monomer-dimer equilibrium in solution.

Additionally, zinc phosphide $[TerPH(ZnEt)]_2$ and zinc phosphadiide $[TerP(ZnEt)_2]_2$ were tested for their applicability in P−P coupling reactions with PCl_3 with the aim of synthesizing 1,3-dichloro-*cyclo*-tetraphosphanes $[ClP(\mu\text{-}PTer)]_2$. While, in fact, the previously reported *cis*- and *trans*-isomer of said compound were formed during these reactions, it became apparent that zinc phosphides that still bear ethyl substituents at the zinc atom are only limitedly suitable precursors for the selective synthesis of 1,3-dichloro-*cyclo*-tetraphosphanes. Chlorozinc phosphides like TerPH(ZnCl) might pose a better precursor for that purpose, however, due to time limitations no P−P coupling reactions were tested for the latter compound.

5 Experimental

5.1 Working Technique

Unless denoted otherwise, all manipulations were carried out under oxygen- and moisture-free conditions under argon using standard Schlenk or drybox techniques. For that purpose, all glassware was baked out thrice with a heat gun in high vacuum and allowed to cool to ambient temperature under argon. Substances sensitive to hydrolysis were handled under argon atmosphere inside a drybox. Solvents were dried and distilled under argon atmosphere and handled via syringes which were purged with argon thrice prior to use.

Solvents and reactants were obtained from commercial sources or were synthesized. Dichloromethane (CH_2Cl_2) was purified according to a literature procedure,[44] dried over P_4O_{10}, stored over CaH_2 and freshly distilled prior to use. Diethyl ether (Et_2O), tetrahydrofuran (THF), dimethoxyethane, benzene and toluene were dried over Na/benzophenone and freshly distilled prior to use. *n*-Pentane and *n*-hexane were dried over Na/benzophenone/tetraglyme (tetraglyme = $Me(OCH_2CH_2)_3OMe$) and freshly distilled prior to use. Fluorobenzene (PhF) and dimethylsulfoxide (DMSO) were dried over CaH_2 and freshly distilled prior to use and then stored over molecular sieves. Deuterated dichloromethane (CD_2Cl_2) was purified the same way as regular dichloromethane.[44] PCl_3 (Merck, for synthesis) was dried over P_4O_{10}, freshly distilled and degassed. Deuterated benzene (C_6D_6), deuterated toluene (toluene-d_8), deuterated tetrahydrofuran (THF-d_8) and triethylamine (NEt_3, Sigma Aldrich, 99 %) were dried over Na and freshly distilled prior to use. 2-Bromomesitylene (abcr, 98 %), 1,3-dichlorobenzene (abcr, 98 %), magnesium turnings (abcr, 99.8 %), lithium aluminum hydride ($LiAlH_4$, abcr, 97 %), *n*-butyllithium (*n*-BuLi, Acros, 2.5 mol/L in hexanes), and diethylzinc ($ZnEt_2$, Fluka, 1.0 mol/L in hexanes) were used without further purification. $TerPH_2$ and EtZnCl were prepared according to literature procedures.[4,37,38] $ZnCl_2$ was a gift from the group of Prof. Dr. Martin Köckerling at the university of Rostock and was used as received.

The following table gives an overview of the commercial sources of reactants that were used as well as their methods of purification, if applicable.

Table 13: Utilized reactants, their source and purification.

Reactant	**Source**	**Purification**
1,3-dichlorobenzene	abcr (98 %)	–
n-BuLi	Acros (2.5 mol/L in hexanes)	–
$LiAlH_4$	abcr (97 %)	–
MesBr	abcr (98 %)	–
Mg turnings	abcr (99.8 %)	–
NEt_3	Sigma-Aldrich (99 %)	Drying over Na, Distillation
PCl_3	Merck (zur Synthese)	Drying over P_4O_{10}, Distillation, Degassing
$ZnCl_2$	Gift	–
$ZnEt_2$	Fluka (1 mol/L in hexanes)	–

5.2 Analytical Methods

5.2.1 X-ray Crystal Structure Determination

X-ray quality crystals were selected in Fomblin YR-1800 perfluoroether (Alfa Aesar) at ambient temperature unless denoted otherwise. The samples were cooled to 173(2) K or 123(2) K during measurement. The data were collected on a *Bruker* ***Kappa Apex II CCD*** diffractometer or a *Bruker* ***D8 Quest CMOS*** diffractometer using graphite monochromated Mo K_α radiation (λ = 0.71073 Å). The structures were solved by direct methods (SHELXS-2013)[45] and refined by full matrix least squares procedures (SHELXL-2013).[46] Semi-empirical absorption corrections were applied (SADABS).[47] All non-hydrogen atoms were refined anisotropically. Hydrogen atoms bound to phosphorus atoms were refined freely, while all other hydrogen atoms were included in the refinement at calculated positions using a riding model.

Disordered groups or molecules were split in parts. The occupancy of each part was refined freely. Detailed crystallographic data as well as bond lengths (Å), angles and torsion angles (°) of all data sets are summarized in Chapter 6.1 of the appendix.

5.2.2 NMR Spectroscopy

^{1}H-, ^{13}C{^{1}H}- and ^{31}P{^{1}H} NMR spectra were obtained on *Bruker AVANCE 250* (250 MHz), *300* (300 MHz) or *500* (500 MHz) spectrometers and were referenced internally to the deuterated solvent (^{13}C: CD_2Cl_2, δ_{ref} = 54.00 ppm; C_6D_6, δ_{ref} = 128.39 ppm, THF-d_8, δ_{ref} = 67.57 ppm), to protic impurities in the deuterated solvent (^{1}H: $CHDCl_2$, δ_{ref} = 5.31 ppm, C_6HD_5, δ_{ref} = 7.16 ppm, THF-d_7, δ_{ref} = 3.58 ppm, toluene-d_7, δ_{ref} = 2.09 ppm) or externally (^{31}P: 85 % H_3PO_4, δ_{ref} = 0 ppm). All measurements were carried out at room temperature unless denoted otherwise. For NMR spectra simulation, the calculated and experimental ^{31}P NMR spectra were transferred to gNMR.[48] The full lineshape iteration procedure of gNMR was applied to match the calculated to the experimental spectrum. The signs of $^{1}J(^{31}P,^{31}P)$ coupling constants are negative,[49,50] the signs of all other $^{n}J(^{31}P,^{31}P)$ coupling constants were derived from calculated spectra (cf. Chapter 5.4.1) or given as absolute values. Relative concentration ratios in product mixtures

were determined based on integrated ^{31}P NMR spectra, however, the accuracy for species with similar coordination environments is estimated with approx. ±10 % and with approx. ±20 % for different coordination environments.[51]

5.2.3 Vibrational Spectroscopy

IR spectra of crystalline samples were recorded on a ***Nicolet 380 FT-IR*** spectrometer (*Thermo Scientific*) equipped with a *Smart Orbit* ATR unit at ambient temperature.

Raman spectra of crystalline samples were recorded using a ***LabRAM HR 800 Horiba Jobin YVON*** Raman spectrometer equipped with an *Olympus BX41* microscope with variable lenses (*Olympus MPlan* 10x/0.25, 50x/0.75, 100x/0.90 and *LMPlanFL N* 50x/0.50). The samples were excited by an infrared laser (785 nm, 100 mW) or a red laser (633 nm, 17 mW). All measurements were carried out at ambient temperature unless stated otherwise.

5.2.4 Elemental Analysis, Melting Point Determination and DSC

Elemental analyses were obtained using a ***vario MICRO cube*** (*Elementar*) or a ***TruSpec CHNS Micro*** (*Leco*).

Melting points (uncorrected) were determined using a *Stanford Research Systems* ***EZ Melt*** at a heating rate of 20 °C/min. DSC analyses were carried out at a heating rate of 5 °C/min using a *Mettler Toledo* ***DSC 823e***.

5.2.5 Mass Spectrometry

Mass spectra were acquired on a **Finnigan MAT 95-XP** (Thermo Electron) using crystalline samples.

5.3 Syntheses and Analytical Data

5.3.1 *P*-(2,6-bis-(2,4,6-trimethylphenyl)phenyl)-*P*,*P*-dihalophosphane

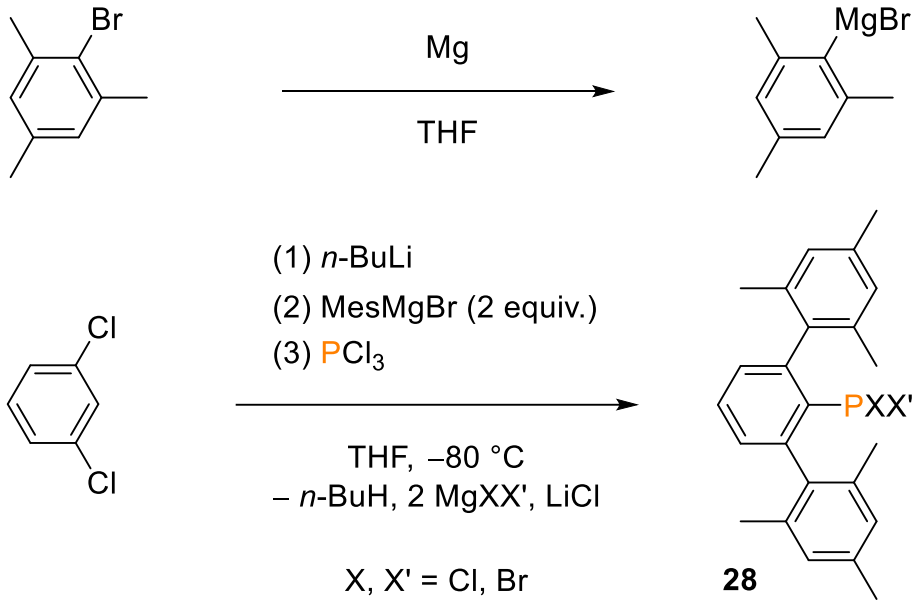

59.85 g (0.30 mol) of MesBr were added dropwise to a stirred suspension of 8.045 g (0.33 mol) Mg turnings in 200 mL THF over a period of 25 minutes during which the mixture started to heat noticeably, whereupon it was cooled to 0 °C. After the addition was complete, the reaction mixture was stirred at room temperature until no further heat development was observed, then refluxed for 2.5 hours, and cooled to ambient temperature afterwards.

In the meantime, a solution of *n*-butyllithium (2.5 M in hexanes, 51 mL, 0.1275 mol) was added dropwise to a stirred solution of 1,3-dichlorobenzene (17.8 g, 0.121 mol) in 250 mL THF at −80 °C over a period of 35 minutes. This mixture was stirred at −80 °C for 1 hour, whereupon the MesMgBr solution was added dropwise at −80 °C over a period of 1 hour. The stirred mixture was allowed to warm to ambient temperature overnight.

The next day, after refluxing the mixture for 2 hours, a dark brown solution was obtained which was re-cooled to −80 °C. PCl_3 (33.5 g, 0.244 mol) was added over a period of 15 minutes, giving a golden-brown solution which was warmed to ambient temperature and stirred for another 15 minutes. Afterwards, the solvent was removed *in vacuo*, high-boiling impurities were distilled off at 120 °C over a period of 75 minutes using a cold trap and the

yellowish residue was extracted thrice with benzene (150 mL) by repeated filtration and back-distillation of the solvent.

The red-orange filtrate was filtered once more, concentrated to incipient crystallization, and kept at ambient temperature overnight, giving a first crop of pale yellow, block-shaped crystals. The supernatant was concentrated again, yielding further crops of product. With the first two crops, 28.0 g (61.2 mmol, 50.6 %) of a yellow solid were obtained.

^{1}H NMR (CD_2Cl_2, 300.1 MHz): δ = 2.01 (s, *o*-Me), 2.05 (s, *o*-Me), 2.05 (s, *o*-Me), 2.33 (superimposed s, *p*-Me), 6.94 (superimposed m, Mes-*m*-H), 7.10 (superimposed m, *m*-H), 7.62 (superimposed m, *p*-H). **^{31}P{^{1}H} NMR** (CD_2Cl_2, 121.5 MHz): δ = 148.1 (s, $TerPBr_2$, 25 %), 155.9 (s, TerPClBr, 46 %), 160.9 (s, $TerPCl_2$, 29 %). **Raman** (633 nm, 4 scans, 60 s, cm^{-1}): $\tilde{\nu}$ = 3117 (1), 3044 (2), 3010 (1), 2983 (1), 2917 (4), 2854 (1), 2729 (1), 1612 (8), 1578 (1), 1569 (1), 1559 (1), 1477 (2), 1441 (1), 1433 (1), 1380 (3), 1302 (10), 1281 (1), 1261 (1), 1238 (1), 1181 (1), 1163 (1), 1088 (1), 1037 (6), 1022 (1), 1003 (1), 942 (1), 909 (1), 851 (1), 811 (1), 734 (5), 720 (1), 596 (1), 576 (8), 559 (1), 548 (1), 525 (1), 501 (7), 489 (1), 468 (5), 432 (6), 403 (10), 377 (1), 340 (2), 326 (1), 300 (1), 280 (1), 246 (1), 207 (1), 180 (1).

5.3.2 2,6-Bis-(2,4,6-trimethylphenyl)phenylphosphane (3)

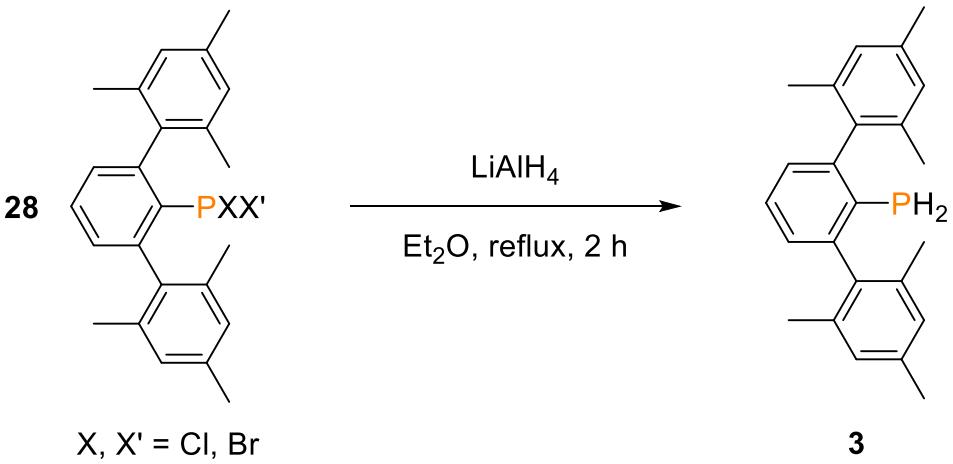

A solution of TerPXX' (X, X' = Cl, Br; 14.0 g, 30.6 mmol) in approx. 400 mL of diethyl ether was added to a stirred suspension of $LiAlH_4$ (2.36 g, 62.2 mmol, 2.0 equiv.) in 20 mL diethyl ether at 0 °C. The mixture was then refluxed for 2 hours and left stirring at ambient temperature overnight. All volatile components were removed *in vacuo*, whereupon the flask

containing the off-white residue was placed in a warm water bath and dried *in vacuo* for 2 hours. The dried residue was extracted twice with benzene (150 mL) by repeated back-distillation of the solvent. The yellowish solution was concentrated to incipient crystallization at approx. 80 °C, placed into a hot water bath (80 °C), and allowed to cool to ambient temperature overnight to facilitate crystallization. In total, 6.9 g (19.9 mmol, 65 %) of $TerPH_2$ in the form of colorless, block-shaped crystals were obtained.

Mp.: 212 °C. **CHN** calc. (found) in %: C 83.20 (82.80), H 7.86 (7.89). **^{1}H NMR** (CD_2Cl_2, 300.1 MHz): δ = 1.97 (s, 12 H, *o*-Me), 2.31 (s, 6 H, *p*-Me), 3.01 (d, $^{1}J(^{1}H,^{31}P)$ = 211 Hz, 2 H, P*H*$_2$), 6.95 (s, 4 H, Mes-*m*-H), 7.02 (dd, $^{3}J(^{1}H,^{1}H)$ = 7.6 Hz, $^{4}J(^{1}H,^{31}P)$ = 2.3 Hz, 2 H, *m*-H), 7.39 (t, $^{3}J(^{1}H,^{1}H)$ = 7.6 Hz, 1 H, *p*-H). **^{13}C{^{1}H} NMR** (CD_2Cl_2, 75.5 MHz): δ = 20.5 (s, *o*-Me), 21.4 (s, *p*-Me), 128.4 (d, $^{3}J(^{13}C,^{31}P)$ = 1.8 Hz, *m*-C), 128.8 (s, Mes-*m*-C), 128.8 (s, *p*-C), 130.4 (d, $^{2}J(^{13}C,^{31}P)$ = 7.7 Hz, *o*-C), 136.1 (s, Mes-C), 137.6 (s, Mes-C), 139.7 (d, $^{3}J(^{13}C,^{31}P)$ = 2.2 Hz, Mes-*i*-C), 145.9 (d, $^{1}J(^{13}C,^{31}P)$ = 11.0 Hz, *i*-C). **^{31}P{^{1}H} NMR** (CD_2Cl_2, 121.5 MHz): δ = −147.9 (s). **IR** (ATR, 32 scans, cm^{-1}): $\tilde{\nu}$ = 3042 (w), 2967 (w), 2940 (w), 2912 (m), 2852 (w), 2729 (w), 2317 (w), 2299 (m), 1611 (w), 1564 (m), 1481 (w), 1446 (s), 1436 (m), 1394 (m), 1375 (m), 1284 (w), 1265 (w), 1242 (w), 1180 (w), 1165 (w), 1114 (w), 1097 (w), 1068 (m), 1044 (w), 1032 (m), 1011 (m), 888 (w), 850 (s), 834 (m), 798 (s), 764 (m), 740 (m), 730 (s), 720 (s), 702 (m), 677 (m), 619 (w), 605 (w), 588 (m), 575 (m), 561 (m), 548 (m). **Raman** (633 nm, 4 scans, 60 s, cm^{-1}): $\tilde{\nu}$ = 3127 (1), 3046 (3), 3020 (3), 2972 (2), 2938 (2), 2913 (6), 2854 (2), 2731 (1), 2313 (3), 2303 (7), 1613 (7), 1579 (3), 1566 (2), 1485 (2), 1435 (1), 1396 (1), 1381 (4), 1304 (10), 1285 (1), 1266 (1), 1244 (1), 1181 (1), 1166 (2), 1068 (2), 1044 (6), 1032 (2), 1006 (3), 992 (1), 944 (2), 859 (1), 854 (1), 836 (1), 799 (1), 741 (2), 732 (1), 721 (1), 577 (10), 562 (8), 520 (4), 507 (1), 476 (1), 463 (1), 444 (3), 369 (4), 347 (1), 323 (3), 306 (1), 277 (2), 263 (3), 243 (4), 197 (2), 148 (7).

5.3.3 Synthesis of [TerPH(ZnEt)]$_2$ (34)

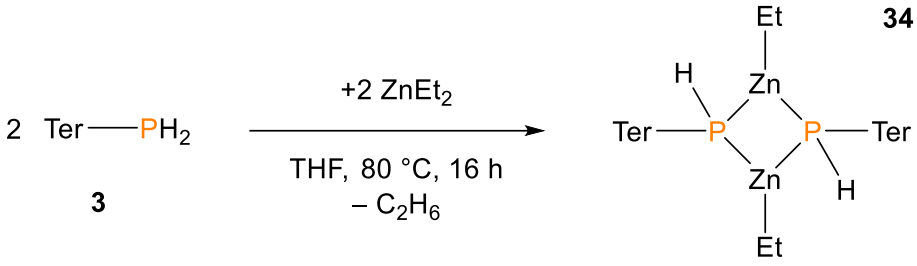

To a stirred solution of TerPH$_2$ (1.041 g, 3.0 mmol, 1 equiv.) in 25 mL of THF, 3 mL of a 1 M ZnEt$_2$ solution in *n*-hexane was added at ambient temperature. The solution was then degassed, stirred, heated to 80 °C in an oil bath, and left stirring at 80 °C overnight. During the night, the previously colorless solution took on a yellow hue. The solution was concentrated to incipient crystallization, placed into a hot water bath (70 °C), and allowed to slowly cool to ambient temperature overnight to facilitate crystallization. A few days later, 1.015 g (76 % yield) of a crystalline, off-white solid was obtained in three crops, which still contained a certain amount of the starting material and were recrystallized from THF.

Mp. 195 °C (decomposition). **CHN** calc. (found) in %: C 70.99 (70.32), H 7.10 (7.08). **^{1}H NMR** (THF-d$_8$, 300.1 MHz): δ = 0.02 (q, $^3J(^1H,^1H)$ = 8.12 Hz, 4 H, Zn−C*H*$_2$−CH$_3$), 1.04 (t, $^3J(^1H,^1H)$ = 8.12 Hz, 6 H, Zn−CH$_2$−*CH*$_3$), 2.03 (s, 24 H, *o*-CH$_3$), 2.25 (s, 12 H, *p*-CH$_3$), 3.02 (d, $^1J(^1H,^{31}P)$ = 208.5 Hz, 2 H, P*H*), 6.77 (d, $^3J(^1H,^1H)$ = 7.55 Hz, 4 H, *m*-H), 6.86 (s, 8 H, Mes-*m*-H), 7.05 (t, $^3J(^1H,^1H)$ = 7.55 Hz, 2 H, *p*-H). **^{13}C{^{1}H} NMR** (THF-d$_8$, 75.5 MHz): δ = 5.7 (s, Zn−*C*H$_2$−CH$_3$), 12.9 (s, Zn−CH$_2$−*C*H$_3$), 21.2 (s, *o*-CH$_3$), 21.4 (s, *p*-CH$_3$), 124.9 (s, *p*-C), 128.0 (s, *m*-C), 129.0 (s, Mes-*m*-C), 136.5 (s, Mes-*p*-C), 136.7 (s, Mes-*o*-C), 142.6 (s, Mes-*i*-C), 144.8 (d, $^2J(^{13}C,^{31}P)$ = 9.5 Hz, *o*-C), *i*-C not observed. **^{31}P{^{1}H} NMR** (THF-d$_8$, 121.5 MHz): δ = −166.2 (broad). **Raman** (633 nm, 5 s, 20 scans, cm^{-1}): $\tilde{\nu}$ = 3062 (1), 3047 (1), 3029 (1), 3014 (1), 2977 (1), 2916 (3), 2885 (2), 2848 (2), 2801 (1), 2359 (2), 1612 (3), 1579 (3), 1566 (1), 1492 (1), 1481 (1), 1453 (1), 1438 (1), 1412 (1), 1393 (3), 1382 (2), 1378 (2), 1306 (5), 1285 (1), 1266 (1), 1242 (2), 1183 (1), 1159 (3), 1119 (1), 1095 (1), 1046 (4), 1005 (1), 977 (1), 959 (1), 946 (1), 909 (1), 885 (1), 850 (1), 839 (2), 801 (1), 764 (1), 746 (1), 738 (1), 725 (2), 658 (1), 590 (1), 576 (3), 562 (2), 540 (1), 523 (2), 499 (2), 487 (1), 457 (2), 388 (4), 366 (1), 349 (1), 331 (2), 302 (1), 283 (1), 257 (2), 252 (2), 236 (3), 224 (2), 192 (1), 121 (9), 89 (10). **MS** (CI positive, *iso*-butane, m/z): 851 [M –Et]$^+$, 755 [M –ZnEt −Et]$^+$, 439 [TerPZnEt +H]$^+$, 347 [TerPH$_3$]$^+$.

5.3.4 Synthesis of [TerP(ZnEt)$_2$]$_2$ (35)

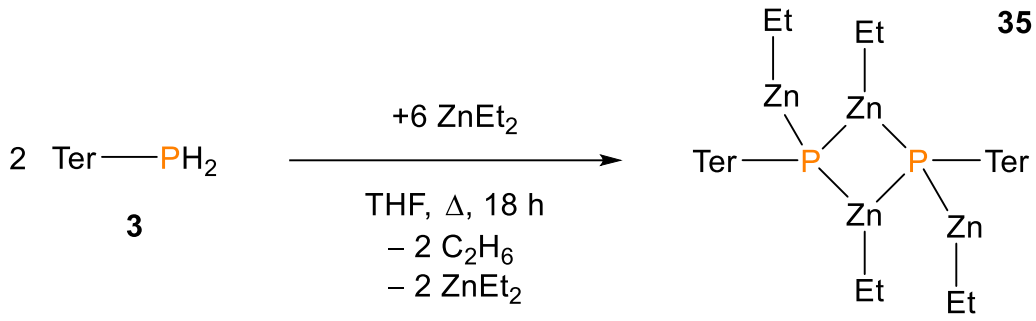

To a stirred solution of TerPH$_2$ (1.042 g, 3.02 mmol, 1 equiv.) in 10 mL of THF, 9 mL of a 1 M ZnEt$_2$ solution in *n*-hexane was added at ambient temperature. The solution was then degassed, stirred, and heated to 100 °C for 2 hours using an oil bath. During that time, the previously colorless solution took on a yellow hue and the formation of a white precipitate was observed. The mixture was then degassed one more time and left stirring overnight (16 hours) at 80 °C. The next day, the precipitate was dissolved by adding 20 mL of THF and heating the degassed solution. The hot, yellow solution was allowed to cool to ambient temperature overnight to facilitate crystallization. This way, a total of 1.23 g (1.15 mmol, 77 %) of pure, crystalline [TerP(ZnEt)$_2$]$_2$ was obtained.

Mp. 230 °C (decomposition). **CHN** calc. (found) in %: C 63.06 (62.81), H 6.61 (6.68). **^{1}H NMR** (THF-d$_8$, 300.1 MHz): δ = −0.03 (q, ^{3}J(^{1}H,^{1}H) = 7.93 Hz, 8 H, Zn−C*H*$_2$−CH$_3$), 1.02 (t, ^{3}J(^{1}H,^{1}H) = 7.93 Hz, 12 H, Zn−CH$_2$−C*H*$_3$), 1.99 (s, 24 H, *o*-CH$_3$), 2.33 (s, 12 H, *p*-CH$_3$), 6.73 (d, ^{3}J(^{1}H,^{1}H) = 7.55 Hz, 4 H, *m*-H), 6.99 (s, 8 H, Mes-*m*-H), 7.04 (t, ^{3}J(^{1}H,^{1}H) = 7.55 Hz, 2 H, *p*-H). **^{13}C{^{1}H} NMR** (THF-d$_8$, 75.5 MHz): δ = 8.5 (s, Zn−*C*H$_2$−CH$_3$), 12.6 (s, Zn−CH$_2$−*C*H$_3$), 21.3 (s, *o*-CH$_3$), 21.5 (s, *p*-CH$_3$), 125.7 (s, *p*-C), 128.5 (s, *m*-C), 129.2 (s, arom. *C*H), 130.6 (s, Mes-*m*-C), 130.9 (s, arom. *C*H), 136.2 (s, arom. *C*), 136.6 (s, arom. *C*), 137.9 (s, arom. *C*), 139.3 (s, arom. *C*), 143.7 (s, arom. *C*), 146.1 (s, arom. *C*). **^{31}P{^{1}H} NMR** (THF-d$_8$, 121.5 MHz): δ = −161.7 (broad). **Raman** (633 nm, 5 s, 20 scans, cm^{-1}): $\tilde{\nu}$ = 3038 (1), 3018 (1), 2971 (1), 2943 (1), 2915 (3), 2882 (2), 2853 (2), 2802 (1), 1613 (2), 1576 (1), 1566 (1), 1484 (1), 1461 (1), 1435 (1), 1415 (1), 1385 (2), 1377 (1), 1305 (4), 1286 (1), 1264 (1), 1235 (1), 1182 (1), 1175 (2), 1166 (1), 1151 (4), 1090 (1), 1040 (2), 1025 (1), 1007 (1), 963 (1), 947 (1), 925 (1), 911 (1), 886 (1), 860 (1), 803 (1), 741 (3), 723 (1), 661 (1), 593 (1), 580 (7), 563 (2), 527 (2),

506 (2), 494 (5), 473 (1), 459 (2), 387 (4), 363 (1), 348 (1), 333 (1), 304 (1), 283 (0), 264 (1), 244 (2), 213 (3), 137 (5), 85 (10). **MS** (CI positive, *iso*-butane, m/z): 1037 $[M - Et]^+$, 942 $[M - ZnEt - Et]^+$, 848 $[M - 2\ ZnEt - Et + H]^+$, 819 $[M - 2\ ZnEt_2 + H]^+$, 755 $[M - Ter + 2\ H]^+$, 689 $[M - 4\ ZnEt + H]^+$, 534 $[TerP(ZnEt)_2]^+$, 438 $[TerPZnEt + H]^+$, 375 $[TerPEt + 2\ H]^+$, 347 $[TerPH_3]^+$, 345 $[TerPH]^+$, 93 $[ZnEt]^+$.

5.3.5 Treating $[TerPH(ZnEt)]_2$ (34) with PCl_3 and NEt_3

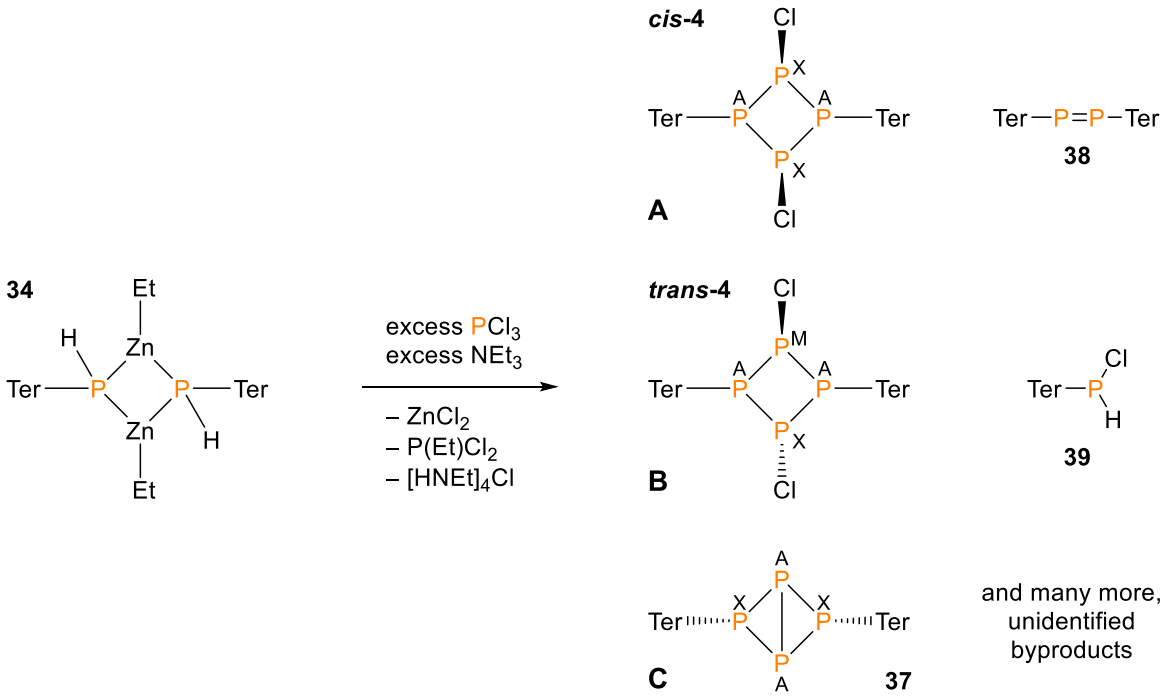

To a vigorously stirred solution of 0.176 g (0.2 mmol) $[TerPH(ZnEt)]_2$ and 0.4 g (4.0 mmol, 20 equiv.) of NEt_3 in 10 mL of THF 0.55 g (4.0 mmol, 20 equiv.) of PCl_3 were added dropwise at −80 °C causing the previously colorless solution to turn yellow. After the addition was complete, the solution was allowed to warm to ambient temperature while the flask was covered with aluminum foil to exclude light. While warming, the solution took on a light-orange color, which turned back to yellow once the solution reached ambient temperature. Stirring at ambient temperature was continued for 18 hours (overnight). The volatile components were removed *in vacuo* and to the remaining foamy, yellow oil 10 mL of benzene were added. The yellow solution was filtered through a glass sintered frit to filter off precipitated $ZnCl_2 \cdot THF$ which, however, proved challenging since inorganic salts

kept crystallizing. A ^{31}P NMR spectrum of the solution at this stage of workup showed that a mixture of many products was formed.

^{31}P{^{1}H} NMR of the reaction mixture (C_6D_6, 121.5 MHz): δ = −117.8 (m), −91.0 (m), −50.9 (d, $J(^{31}P,^{31}P)$ = 302 Hz), 22.7 (m), 26.5 (t, $J(^{31}P,^{31}P)$ = 302 Hz), 94.0 (d, $J(^{31}P,^{31}P)$ = 239 Hz), 107.5 (m), 160.8 (s), 176.2 (d, $J(^{31}P,^{31}P)$ = 239 Hz), 187.7 (d, $J(^{31}P,^{31}P)$ = 302 Hz), 492.6 (s).

Some other signal groups were assigned to the desired *cyclo*-tetraphosphanes **A** and **B** as well as bicyclo[1.1.0]tetraphosphane **C**, none of which could be isolated.

^{31}P{^{1}H} NMR (C_6D_6, 121.5 MHz): δ = −323.9 (t, $^{1}J(^{31}P_A,^{31}P_X)$ = 182 Hz, **C**, P_A), −171.1 (t, $^{1}J(^{31}P_X,^{31}P_A)$ = 182 Hz, **C**, P_X); −3.3 (superimposed t, $^{1}J(^{31}P_A,^{31}P_B)$ = 213 Hz, $^{1}J(^{31}P_A,^{31}P_X)$ = 213 Hz, **B**, P_A), 82.5 (td, $^{1}J(^{31}P_M,^{31}P_A)$ = 213 Hz, $^{2}J(^{31}P_M,^{31}P_X)$ = 16 Hz, **B**, P_M), 118.8 (td, $^{1}J(^{31}P_X,^{31}P_B)$ = 213 Hz, $^{2}J(^{31}P_X,^{31}P_A)$ = 16 Hz, **B**, P_X); 13.0 (t, $^{1}J(^{31}P_A,^{31}P_X)$ = 203 Hz, **A**, P_A), 100.6 (t, $^{1}J(^{31}P_X,^{31}P_A)$ = 203 Hz, **A**, P_X).

After several attempts to isolate any of the desired products, TerP(H)Cl was isolated as colorless, block-shaped crystals from PhF.

^{1}H NMR (C_6D_6, 300.1 MHz): δ = 2.00 (s, 6 H), 2.14 (s, 6 H), 2.19 (s, 6 H), 6.04 (d, $^{1}J(^{1}H,^{31}P)$ = 205 Hz, 1 H, P*H*), 6.84 (broad, 1 H, *p*-H), 6.85 (broad, Mes-*m*-H, 2 H), 6.88 (broad, Mes-*m*-H, 2 H), 6.92 (dd, $^{3}J(^{1}H,^{1}H)$ = 7.6 Hz, $^{4}J(^{1}H,^{31}P)$ = 2.5 Hz, *m*-H, 2 H). **^{31}P NMR** (C_6D_6, 121.5 MHz): δ = 24.5 (d, $^{1}J(^{31}P,^{1}H)$ = 205 Hz). **Raman** (633 nm, 20 scans, 10 s, cm^{-1}): $\tilde{\nu}$ = 3121 (1), 3063 (1), 3040 (1), 2916 (2), 2856 (1), 2733 (1), 2327 (1), 1613 (1), 1573 (1), 1482 (1), 1440 (1), 1382 (1), 1304 (3), 1284 (1), 1264 (1), 1244 (1), 1180 (1), 1167 (1), 1112 (1), 1047 (2), 1007 (1), 948 (1), 907 (1), 831 (1), 806 (1), 768 (1), 757 (1), 739 (1), 721 (1), 594 (1), 578 (5), 562 (2), 550 (1), 526 (1), 518 (1), 512 (1), 501 (1), 473 (1), 443 (1), 436 (1), 419 (1), 390 (1), 352 (2), 325 (1), 301 (1), 280 (1), 259 (1), 243 (1), 230 (1), 207 (1), 161 (1), 96 (10), 88 (9), 80 (10). **MS** (CI positive, *iso*-butane, m/z): 381 $[M+H]^+$, 365 $[M-CH_3]^+$, 345 $[TerPH]^+$, 329 $[M-CH_3-HCl]^+$.

5.3.6 Treating $[TerP(ZnEt)_2]_2$ (35) with PCl_3

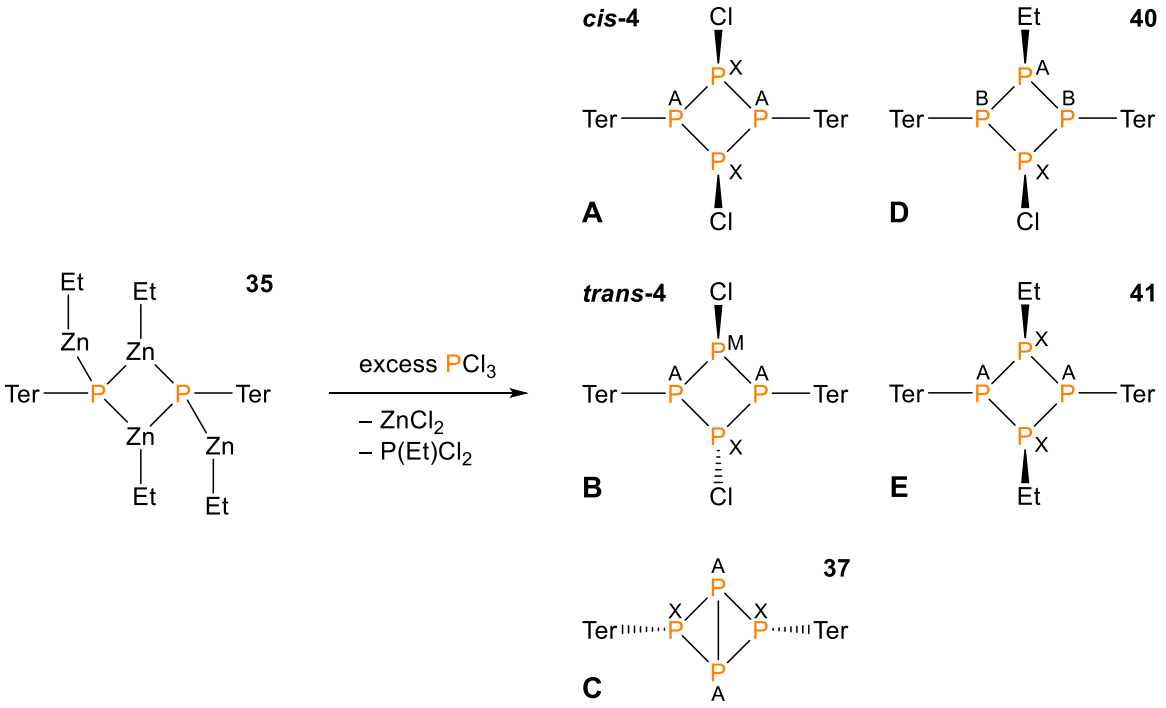

Method A:

0.47 g (3.43 mmol, 36 equiv.) of PCl_3 were added to a solution of 0.100 g (0.094 mmol) $[TerP(ZnEt)_2]_2$ in 5 mL of THF at −80 °C. The solution was allowed to warm to ambient temperature over the course of 1 hour, whereupon the solvent was removed *in vacuo* and the residue was extracted with benzene. The suspension was filtered through a glass sintered frit, the clear filtrate was concentrated to incipient crystallization in hot benzene, placed into a warm water bath (40 °C), and allowed to slowly cool to ambient temperature overnight. The next day, small colorless platelets ($ZnCl_2$·THF) as well as larger colorless, block-shaped crystals were isolated. The latter were suitable for X-ray crystal structure determination and were thus found to be mixed crystals of **A**, **B**, **C** and **D**.

$^{31}P\{^1H\}$ NMR of the isolated mixed crystals following *Method A* (CD_2Cl_2, 121.5 MHz): δ = −52.6 (td, $^1J(^{31}P_A,^{31}P_B)$ = 125 Hz, $^2J(^{31}P_A,^{31}P_X)$ = 73 Hz, **D**, P_A), −33.1 (dd, $^1J(^{31}P_B,^{31}P_A)$ = 125 Hz, $^1J(^{31}P_B,^{31}P_X)$ = 198 Hz, **D**, P_B), 126.1 (td, $^1J(^{31}P_X,^{31}P_B)$ = 198 Hz, $^2J(^{31}P_X,^{31}P_A)$ = 73 Hz, **D**, P_X); −323.9 (t, $^1J(^{31}P_A,^{31}P_X)$ = 182 Hz, **C**, P_A), −171.1 (t, $^1J(^{31}P_X,^{31}P_A)$ = 182 Hz, **C**, P_X); −3.3 (superimposed t, $^1J(^{31}P_A,^{31}P_B)$ = 213 Hz, $^1J(^{31}P_A,^{31}P_X)$ = 213 Hz, **B**, P_A), 82.5 (td, $^1J(^{31}P_M,^{31}P_A)$ = 213 Hz, $^2J(^{31}P_M,^{31}P_X)$ = 16 Hz, **B**, P_M), 118.8 (td, $^1J(^{31}P_X,^{31}P_B)$

= 213 Hz, $^{2}J(^{31}P_X,^{31}P_A)$ = 16 Hz, **B**, P_X); 13.0 (t, $^{1}J(^{31}P_A,^{31}P_X)$ = 203 Hz, **A**, P_A), 100.6 (t, $^{1}J(^{31}P_X,^{31}P_A)$ = 203 Hz, **A**, P_X).

Method B:

A solution of 0.213 g (0.2 mmol) $[TerP(ZnEt)_2]_2$ in 12.5 mL of THF was added dropwise to a vigorously stirred solution of 0.52 g (3.8 mmol, 19 equiv.) PCl_3 in 25 mL of *n*-pentane at 0 °C over the course of 15 minutes. After adding a few drops, the previously colorless solution took on a yellow color which gradually deepened over orange to red-orange as more $[TerP(ZnEt)_2]_2$ was added. After the addition was complete, the bright, red-orange solution was allowed to warm to ambient temperature while the color lightened again to orange. All volatile components were removed *in vacuo* whereupon the flask was placed in a warm water bath (50 °C) and dried *in vacuo* for 30 minutes. The dried, orange residue was extracted twice with benzene (10 mL) by repeated back-distillation of the solvent, dried again *in vacuo*, and dissolved in 5 mL of THF. A ^{31}P NMR spectrum of the solution at this stage of workup showed that a mixture of products was formed. After concentrating the solution to incipient crystallization, mixed crystals of *cyclo*-tetraphosphanes **D** and **E** grew which were not suitable for X-ray crystal structure determination and were therefore only characterized by $^{31}P\{^{1}H\}$ NMR spectroscopy.

$^{31}P\{^{1}H\}$ NMR of the isolated mixed crystals following *Method B* (C_6D_6, 202.5 MHz): δ = −83.0 (t, $^{1}J(^{31}P_A,^{31}P_X)$ = 125 Hz, **E**, P_A), −26.4 (t, $^{1}J(^{31}P_X,^{31}P_A)$ = 125 Hz, **E**, P_X); −52.4 (td, $^{1}J(^{31}P_A,^{31}P_B)$ = 125 Hz, $^{2}J(^{31}P_A,^{31}P_X)$ = 73 Hz, **D**, P_A), −32.9 (dd, $^{1}J(^{31}P_B,^{31}P_A)$ = 125 Hz, $^{1}J(^{31}P_B,^{31}P_X)$ = 198 Hz, **D**, P_B), 123.3 (td, $^{1}J(^{31}P_X,^{31}P_B)$ = 198 Hz, $^{2}J(^{31}P_X,^{31}P_A)$ = 73 Hz, **D**, P_X).

The remaining supernatant was dried *in vacuo* and, after crystallization from PhF, afforded rather pure, needle-shaped crystals of *exo*-*exo*-bicyclotetraphosphane **C**, however, they were not of sufficient quality for X-ray crystal structure determination.

^{1}H NMR: (C_6D_6, 300.1 MHz): δ = 2.05 (s, Mes-*o*-CH_3, 24 H), 2.36 (s, Mes-*p*-CH_3, 12 H), 6.70 (s, *p*-H, 2 H), 6.72 (s, *m*-H, 4 H), 6.90 (s, Mes-*m*-H, 8 H). **$^{31}P\{^{1}H\}$ NMR**: (C_6D_6, 121.5 MHz): δ = −323.9 (t, $^{1}J(^{31}P_A,^{31}P_X)$ = 182 Hz, P_A), −171.1 (t, $^{1}J(^{31}P_X,^{31}P_A)$ = 182 Hz, P_X). **Raman** (633 nm, 20 scans, 20 s, cm^{-1}): $\tilde{\nu}$ = 3041 (1), 2985 (1), 2940 (2), 2918 (3), 2885 (2), 2861 (1), 2730 (1), 1611 (3), 1570 (1), 1483 (1), 1449 (1), 1383 (2), 1301 (4), 1282 (1), 1262 (1), 1244 (1), 1227 (1), 1181 (1), 1165 (1), 1115 (1), 1038 (3), 1002 (1),

991 (1), 946 (1), 916 (3), 848 (1), 808 (1), 740 (2), 718 (1), 652 (1), 620 (1), 588 (1), 578 (5), 560 (2), 523 (2), 511 (1), 494 (1), 470 (2), 440 (2), 430 (3), 400 (3), 363 (1), 342 (1), 303 (2), 283 (1), 261 (1), 224 (2), 79 (10). **MS** (CI positive, *iso*-butane, m/z): 751 $[M+H]^+$, 750 $[M]^+$, 401 $[TerP+C_4H_9]^+$, 391 $[TerP_3-CH_3]^+$,$]^+$, 375 $[TerP_2]^+$, 347 $[TerPH_3]^+$, 345 $[TerPH]^+$.

5.3.7 Treating $[TerP(ZnEt)_2]_2$ (35) with CH_2Cl_2

To 213 mg (0.2 mmol) of $[TerP(ZnEt)_2]_2$ 10 mL of dichloromethane were added. Due to the low solubility of the starting material the solution was thoroughly degassed and heated to 60 °C for 1 hour using an ultrasonic bath. After that, the flask was placed into a drying oven, which was preheated to 60 °C, and kept there overnight. The next day, a ^{31}P NMR spectrum showed that various products were formed, none of which could be isolated.

$^{31}P\{^1H\}$ NMR of the reaction mixture (C_6D_6, 121.5 MHz): δ = −169.9 (s), −159.2 (s), −147.7 (s), −82.8 (d, $J(^{31}P,^{31}P)$ = 85 Hz), −75.0 (s), −71.5 (s), −63.2 (s), −28.0 (s), −7.6 (d, $J(^{31}P,^{31}P)$ = 85 Hz).

5.3.8 Treating $[TerP(ZnEt)_2]_2$ with DMSO

To 213 mg (0.2 mmol) of $[TerP(ZnEt)_2]_2$ 1 mL of DMSO was added. The mixture was degassed and heated to 60 °C while being treated with ultrasound for about 40 minutes. During that time the solution already took on a yellow color, however, solvation of the phosphane was still incomplete. Afterwards, the flask was placed into a preheated drying oven (70 °C) and kept there overnight. The next day, the mixture displayed a dark orange or rather brown color. A ^{31}P NMR spectrum showed that a number of products were formed, none of which could be isolated.

$^{31}P\{^1H\}$ NMR of the reaction mixture (C_6D_6, 121.5 MHz, absolute intensity > 3 %): δ = −180.9 (s), −101.4 (s), −76.8 (s), −75.2 (s), −73.4 (s), −63.2 (s), 24.9 (s), 492.3 (s).

5.3.9 Synthesis of TerPH(ZnCl)·2THF (36)

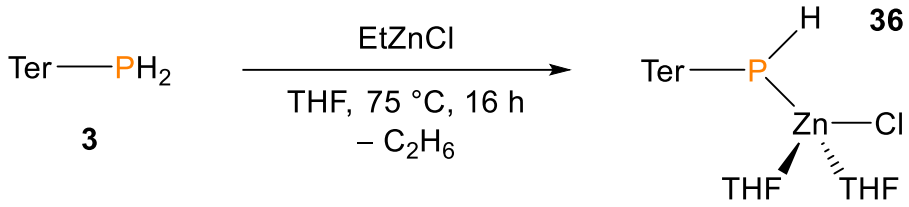

In order to synthesize EtZnCl *in situ*, a modified literature procedure was followed.[37,38] To 136 mg of $ZnCl_2$ (1 mmol) 5 mL of THF were added along with 1 mL of a 1 M $ZnEt_2$ solution in hexanes. This mixture was placed into a preheated ultrasonic bath (60 °C) and treated with ultrasound for 25 minutes until a clear solution was obtained. The hot solution was transferred into another flask containing 346 mg (1 mmol) of $TerPH_2$ in 5 mL of THF and a stir bar. The mixture was thoroughly degassed and placed into a preheated oil bath (75 °C) while stirring was continued overnight. During that time, the solution took on a light-orange color. A ^{31}P NMR spectrum of the reaction mixture showed that the conversion of the starting material was incomplete, however, after concentrating the solution to approx. 1 mL, a copious amount of colorless, block-shaped crystals grew over the course of a few days which contained impurities to an extent of approx. 10 % according to ^{31}P NMR spectroscopy. Still, they were of sufficient quality for X-ray crystal structure determination. Recrystallization could not be attempted yet.

Mp. 223 °C (decomposition). **CHN** calc. (found) in %: C 65.09 (53.24), H 7.17 (4.72). **^{1}H NMR** (THF-d_8, 250.1 MHz): δ = 2.07 (s, 12 H, *o*-CH_3), 2.27 (s, 6 H, *p*-CH_3), 6.80 (dd, $^{3}J(^{1}H,^{1}H)$ = 7.48 Hz, $^{4}J(^{1}H,^{31}P)$ = 1.8 Hz, 2 H, *m*-H), 6.86 (s, 4 H, Mes-*m*-H), 7.09 (t, $^{3}J(^{1}H,^{1}H)$ = 7.48 Hz, 1 H, *p*-H), P*H* could not be assigned yet. **^{13}C{^{1}H} NMR** (THF-d_8, 62.9 MHz): δ = 21.4 (s, *o*-CH_3), 21.5 (s, *p*-CH_3), 125.4 (s, *p*-C), 128.2 (d, $^{3}J(^{13}C,^{31}P)$ = 2.3 Hz, *m*-C), 128.9 (s, Mes-*m*-C), 136.3 (s, Mes-*p*-C), 137.1 (s, Mes-*o*-C), 142.3 (d, $^{3}J(^{13}C,^{31}P)$ = 2.2 Hz, Mes-*i*-C), 145.4 (d, $^{2}J(^{13}C,^{31}P)$ = 11.6 Hz, *o*-C), *i*-C not observed. **^{31}P NMR** (THF-d_8, 101.3 MHz): δ = −182.9 (broad d, $^{1}J(^{31}P,^{1}H)$ = 198 Hz). **Raman** (633 nm, 20 s, 20 scans, cm^{-1}): $\tilde{\nu}$ = 3046 (1), 3032 (1), 3010 (1), 2990 (1), 2970 (1), 2939 (1), 2915 (1), 2880 (1), 2856 (1), 2735 (1), 2316 (1), 1613 (2), 1576 (2), 1565 (1), 1487 (1), 1448 (1), 1384 (2), 1304 (4), 1282 (1), 1259 (1), 1247 (1), 1243 (1), 1182 (1), 1168 (1), 1160 (1), 1110 (1), 1046 (3), 1004 (1), 946 (1), 924 (1), 880 (2), 803 (1), 773 (1),

742 (1), 722 (2), 594 (1), 579 (5), 564 (2), 551 (1), 525 (2), 515 (1), 462 (1), 450 (2), 386 (3), 373 (1), 343 (1), 326 (2), 303 (1), 280 (3), 264 (1), 247 (1), 205 (2), 79 (10).

5.3.10 Synthesis of TerP(H)Li·3THF (29)

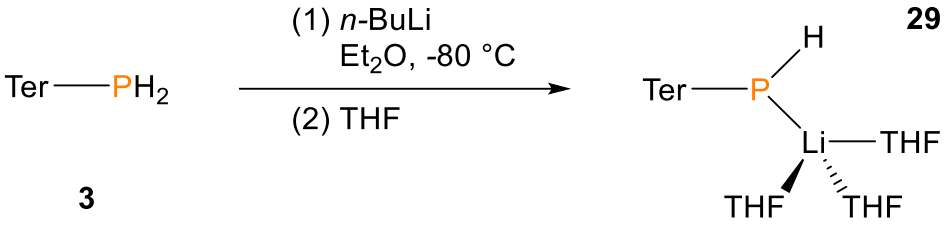

A solution of 693 mg (2.0 mmol) of $TerPH_2$ in 80 mL of diethyl ether was cooled to −80 °C, whereupon 0.86 mL (2.15 mmol, 1.1 equiv.) of a 2.5 M *n*-BuLi solution in hexanes were added dropwise, affording a yellow suspension. The solvent was removed *in vacuo* and the yellow residue was dissolved in THF. The yellow solution was concentrated to incipient crystallization and kept at ambient temperature overnight to facilitate crystallization of analytically pure, yellow, block-shaped crystals of TerP(H)Li·3THF.

^{1}H NMR (CD_2Cl_2, 300.1 MHz): δ = 2.11 (s, 12 H, *o*-Me), 2.23 (s, 6 H, *p*-Me), 6.38 (m, 2 H, *m*-H), 6.48 (dd, $^{3}J(^{1}H,^{1}H)$ = 8.12 Hz, $^{3}J(^{1}H,^{1}H)$ = 6.23 Hz, 1 H, *p*-H), P*H* not observed. **^{13}C{^{1}H} NMR** (CD_2Cl_2, 75.5 MHz): δ = 21.0 (d, $^{5}J(^{13}C,^{31}P)$ = 2.2 Hz, *o*-Me), 21.4 (s, *p*-Me), 117.0 (d, $^{4}J(^{13}C,^{31}P)$ = 1.6 Hz, *p*-C), 126.5 (d, $^{3}J(^{13}C,^{31}P)$ = 2.5 Hz, *m*-C), 128.3 (s, Mes-*m*-C), 134.3 (s, Mes-*p*-C), 137.3 (s, Mes-*o*-C), 140.8 (d, $^{2}J(^{13}C,^{31}P)$ = 11.6 Hz, *o*-C), 145.0 (d, $^{3}J(^{13}C,^{31}P)$ = 2.2 Hz, Mes-*i*-C), 157.9 (d, $^{1}J(^{13}C,^{31}P)$ = 42.4 Hz, *i*-C). **^{31}P{^{1}H} NMR** (CD_2Cl_2, 121.5 MHz): δ = −138.3 (s).

5.4 Software

5.4.1 Computational Details

All computations were carried out using the Gaussian09 program package[52] and the standalone version of NBO 6.0.[53–56] For all calculations, the hybrid DFT functional PBE1PBE[57–59] and a 6-31G(d,p) basis[60–69] (NMR, NBO data) or a cc-pVDZ basis at H and C, an aug-cc-pVDZ basis at P and Cl,[70–75] as well as an energy consistent pseudopotential of the Stuttgart/Cologne group for Zn (ECP10MDF)[76] in combination with a suitable aug-cc-pVDZ basis[77] (thermodynamic data) was used. All structures were fully optimized and confirmed as minima by frequency analyses. Calculated frequencies were scaled by 0.9512, which was found to be a suitable value for the hybrid DFT functional PBE1PBE1 and the 6-31G(d,p) basis set.[36] Partial charges were determined by a Natural Population Analysis using the NBO program. Chemical shifts and coupling constants were derived by the GIAO method.[78–82] The calculated absolute shifts ($\sigma_{calc,X}$) were referenced to the experimental absolute shift of 85 % H_3PO_4 in the gas phase ($\sigma_{ref,1}$ = 328.35 ppm),[83] using PH_3 ($\sigma_{ref,2}$ = 594.45 ppm) as a secondary standard:[84]

$$\delta_{calc,X} = (\sigma_{ref,1} - \sigma_{ref,2}) - (\sigma_{calc,X} - \sigma_{calc,PH_3})$$

$$= \sigma_{calc,PH_3} - \sigma_{calc,X} - 266.1 \text{ ppm}$$

At the PBE1PBE/6-31G(d,p) level of theory, $\sigma_{calc,PH3}$ amounts to +605.13 ppm whereas at the PBE1PBE/aug-cc-pVDZ level of theory it amounts to +636.75 ppm. It should be emphasized that all computations were carried out for single, isolated gas phase molecules. There may well be significant differences between gas phase, solution and solid state data.

5.4.2 Simulation of NMR spectra

NMR spectra were simulated and fitted to experimental ^{31}P NMR data using the full line-shape iteration procedure of the gNMR program package.[48]

5.4.3 Figures, Graphs and Schemes

Figures which, for example, show the molecular structures obtained via X-ray crystal structure determination were created with *Ortep3v2*[85] and *Diamond 3*[86] for Windows. Three-dimensionally rendered graphics were created with *Povray 3.6*[87] for Windows. A postprocessing of those figures (Labeling, etc.) and the creation of schemes was performed with *ChemDraw Professional 15.0*.[88] NMR and Raman spectra were edited and presented using the *ACD/Spectrus Processor 2015.2.5*.[89]

5.4.4 Calculation of thermodynamic data based on VT NMR analyses

The $^{31}P\{^{1}H\}$ NMR spectra were evaluated using the *ACD/Spectrus Processor 2015.2.5*.[89] Concentrations were obtained by integration relative to an internal standard (PPh_3) and used to calculate the equilibrium constants at each temperature. The logarithmized equilibrium constants were plotted against the reciprocal temperatures using *Microsoft Office Excel 2013*.[90] The gradient and its deviation were obtained by linear regression using the software's RGP function and used to calculate the Gibbs energy. The standard deviation of the calculated Gibbs energy was obtained by linear error propagation using the gradient's deviation.

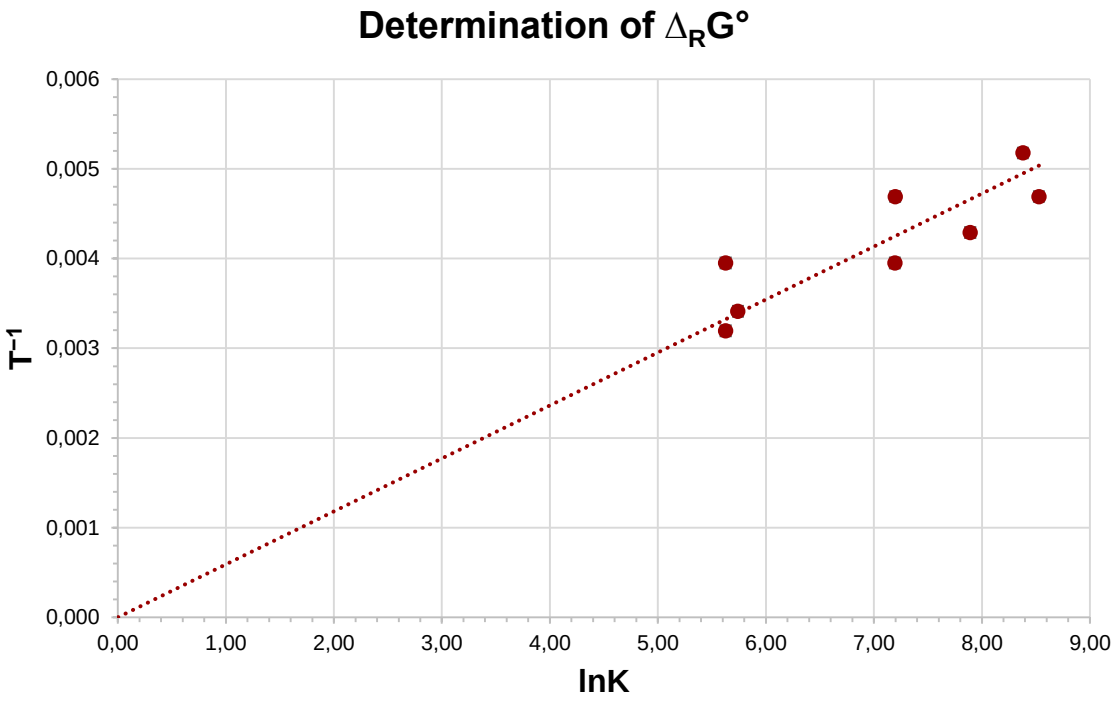

6 Appendix

6.1 Structural Data

Table A1: Crystallographic details of **34**, **35**, and **[40,*cis*-4,*trans*-4]**·C_6H_6.

Compound	**34**	**35**	**[40,*cis*-4,*trans*-4]**·C_6H_6
Chem. formula	$C_{52}H_{62}P_2Zn_2$	$C_{56}H_{70}P_2Zn_4$	0.61($C_{50}H_{55}P_4Cl$) 0.39($C_{48}H_{50}P_4Cl_2$)·C_6H_6
Formula weight [g/mol]	879.69	1066.54	895.62
Color	colorless	colorless	colorless
Crystal system	triclinic	triclinic	orthorhombic
Space group	$P\bar{1}$	$P\bar{1}$	$Pna2_1$
a [Å]	10.8093(6)	10.2057(4)	32.261(3)
b [Å]	10.8260(6)	11.3816(4)	7.8955(8)
c [Å]	23.1428(13)	12.4429(4)	19.2583(18)
α [°]	93.521(3)	84.574(2)	90
β [°]	100.576(3)	83.672(2)	90
γ [°]	118.168(3)	65.168(2)	90
V [Å^3]	2312.4(2)	1301.84(8)	4905.5(8)
Z	2	1	4
$\rho_{calc.}$ [g/cm^3]	1.263	1.360	1.213
μ [mm^{-1}]	1.14	1.92	0.27
T [K]	173(2)	173(2)	123(2)
Measured reflections	72646	41028	37817
Independent reflections	14747	8266	13594
Reflections with $I > 2\sigma(I)$	10997	6661	8307
R_{int}	0.0451	0.0407	0.0711
F(000)	928	556	1896
$R_1(R[F^2>2\sigma(F^2)])$	0.0409	0.0398	0.0569
w$R_2(F^2)$	0.1097	0.1241	0.1271
GooF	1.033	1.042	0.996
No. of Parameters	527	296	689

Table A2: Crystallographic details of **39**, **36**·2THF, and **29**·3THF.

Compound	**39**	**36**·2THF	**29**·3THF
Chem. formula	$C_{24}H_{26}ClP$	$C_{32}H_{42}ClO_2PZn$	$C_{36}H_{50}LiO_3P$
Formula weight [g/mol]	380.87	590.44	586.67
Color	colorless	colorless	yellow
Crystal system	monoclinic	monoclinic	monoclinic
Space group	*Pc*	$P2_1/n$	$P2_1/n$
a [Å]	8.2085(5)	10.9748(8)	11.4394(7)
b [Å]	17.7645(12)	13.5999(10)	14.9418(11)
c [Å]	7.7637(4)	20.5569(15)	20.1330(14)
α [°]	90	90	90
β [°]	113.455(2)	98.466(4)	98.029(4)
γ [°]	90	90	90
V [Å^3]	1038.56(11)	3034.8(4)	3407.5(4)
Z	2	4	4
$\rho_{calc.}$ [g/cm^3]	1.218	1.292	1.108
μ [mm^{-1}]	0.27	0.976	0.11
T [K]	123(2)	123(2)	173(2)
Measured reflections	34695	41120	42671
Independent reflections	6168	9121	8213
Reflections with $I > 2\sigma(I)$	5197	5587	4563
R_{int}	0.0649	0.0669	0.0643
F(000)	404	1248	1232
$R_1(R[F^2>2\sigma(F^2)])$	0.0535	0.0476	0.0544
$wR_2(F^2)$	0.1170	0.1108	0.1380
GooF	1.039	1.007	1.001
No. of Parameters	245	390	484

Scheme A1: Numbering scheme of 1,3-bis-(2,4,6-trimethylphenyl)phenyl-hydro-2,4-diethyl-2,4-dizinca-1,3-diphosphane **34**.

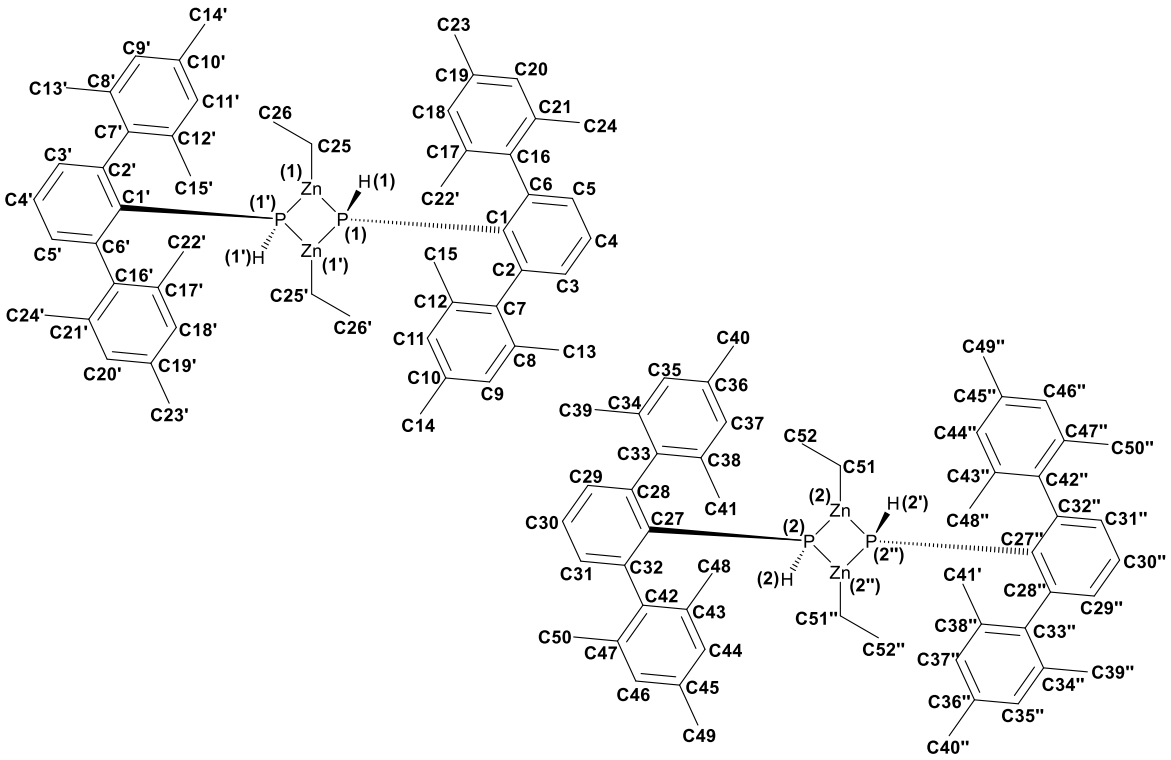

Table A3: Selected bond lengths [Å], angles [°] and torsion angles [°] of **34**.

P1−C1	1.826(2)	P2−C27	1.827(2)
P1−Zn1	2.4367(5)	P2−Zn2	2.4325(5)
P1−Zn1’	2.4428(5)	P2−Zn2’’	2.4484(5)
Zn1−C25	1.977(2)	Zn2−C51	1.982(2)
Zn1−P1’	2.4428(5)	Zn2−P2’’	2.4485(5)
C1−P1−Zn1	118.45(6)	C27−P2−Zn2	120.13(6)
C1−P1−Zn1’	122.51(6)	C27−P2−Zn2’’	122.30(6)
Zn1−P1−Zn1’	92.13(2)	Zn2−P2−Zn2’’	92.19(2)
P1−Zn1−P1’	87.87(2)	P2−Zn2−P2’’	87.81(2)
Zn1−P1−C1−C6	−63.5(2)	Zn2−P2−C27−C28	−63.6(2)
Zn1’−P1−C1−C6	49.8(2)	Zn2’’−P2−C27−C28	51.2(2)

Symmetry codes: (i) −*x*, −*y*, −*z*; (ii) −*x*+1, −*y*, −*z*+1.

Scheme A2: Numbering scheme of 1,3-bis-(2,4,6-trimethylphenyl)phenyl-1,3-ethylzinc-2,4-diethyl-2,4-dizinca-1,3-diphosphane **35**.

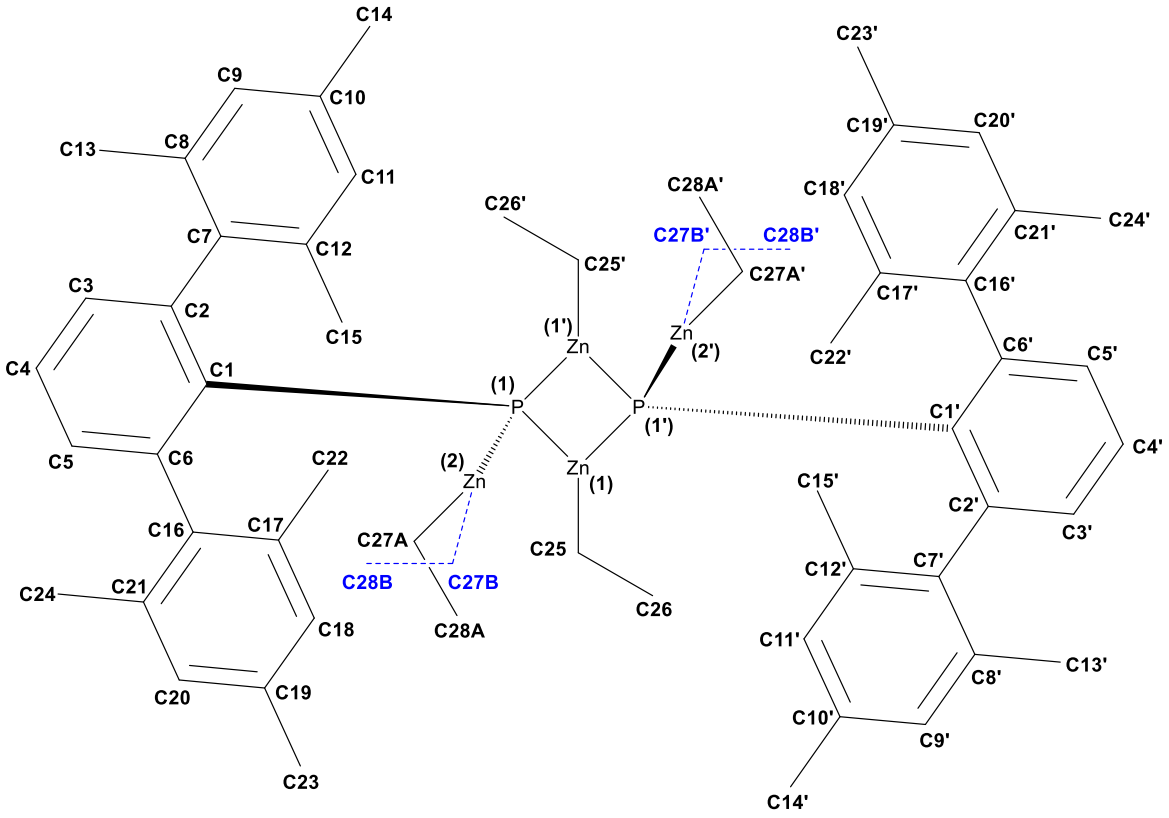

Table A4: Selected bond lengths [Å], angles [°] and torsion angles [°] of **35**.

P1−C1	1.841(2)	P1−Zn1	2.4298(6)
P1−Zn1’	2.4323(6)	P1−Zn2	2.2758(6)
Zn1−C25	1.990(2)	Zn2−C27A	1.985(6)
Zn2−C27B	1.94(3)	C1−P1−Zn1	117.78(7)
C1−P1−Zn1’	112.94(7)	C1−P1−Zn2	107.55(7)
Zn1−P1−Zn1’	86.77(2)	Zn1−P1−Zn2	124.82(3)
Zn1’−P1−Zn2	105.97(2)	P1−Zn1−P1’	93.23(2)
Zn1−C25−C26	114.6(2)	Zn2−C27A−C28A	120.0(4)
Zn2−C27B−C28B	122(2)	C1−P1−Zn1−Zn2	133.87(9)
C1−P1−Zn1’−Zn2	−120.34(8)	P1−C1−C2−C6	−177.86(3)
P1−Zn1−C25−C26	−143.13(2)	C2−C1−P1−Zn2	−143.68(2)
C2−C1−P1−Zn1	74.69(2)	C6−C1−P1−Zn1	−103.089(2)

Symmetry code: (i) –*x*+1, −*y*+2, −*z*+1.

Scheme A3: Numbering scheme of 1,3-bis-(2,4,6-trimethylphenyl)phenyl-*cyclo*-tetraphosphanes **[40,*cis*-4,*trans*-4]**·C_6H_6.

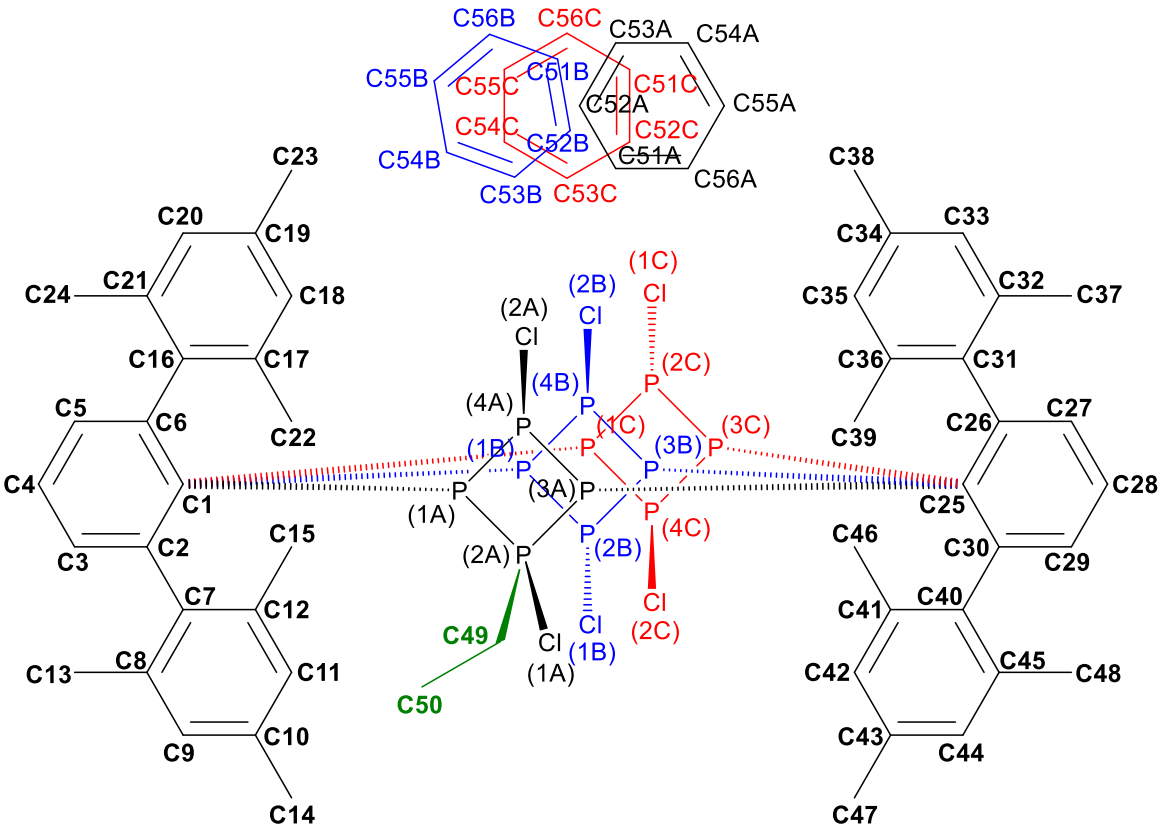

Table A5: Selected bond lengths [Å], angles [°] and torsion angles [°] of **[40,*cis*-4,*trans*-4]**·C_6H_6.

P1A–C1	1.849(5)	P1A–P4A	2.227(2)
P1A–P2A	2.229(2)	P2A–P3A	2.237(2)
P3A–P4A	2.230(2)	P3A–C25	1.864(5)
P2A–Cl1A	2.092(7)	P4A–Cl2A	2.082(2)
P2A–C49	1.83(2)	C49–C50	1.50(2)
P1B–C1	1.83(1)	P1B–P4B	2.23(1)
P1B–P2B	2.24(1)	P2B–P3B	2.23(1)
P3B–P4B	2.24(1)	P3B–C25	1.83(1)
P2B–Cl1B	2.08(1)	P4B–Cl2B	2.08(1)
P1C–C1	1.83(1)	P1C–P4C	2.23(1)
P1C–P2C	2.24(1)	P2C–P3C	2.23(1)
P3C–P4C	2.24(1)	P3C–C25	1.84(1)
P2C–Cl1C	2.09(1)	P4C–Cl2C	2.08(1)

Table A5: Continuation.

C1−P1A−P4A	106.4(2)	C1−P1A−P2A	106.6(2)
C25−P3A−P4A	105.5(2)	C25−P3A−P2A	106.7(2)
P4A−P1A−P2A	84.4(1)	P4A−P3A−P2A	84.1(1)
P1A−P2A−P3A	84.75(8)	P1A−P4A−P3A	84.97(8)
Cl1A−P2A−P1A	101.1(4)	Cl1A−P2A−P3A	99.6(4)
Cl2A−P4A−P1A	99.3(1)	Cl2A−P4A−P3A	100.1(1)
C49−P2A−P1A	100.4(8)	C49−P2A−P3A	100.0(9)
C1−P1B−P4B	111(2)	C25−P3B−P4B	102(2)
P4B−P1B−P2B	82.9(8)	P4B−P3B−P2B	83.0(8)
P1B−P2B−P3B	79.2(6)	P1B−P4B−P3B	79.2(7)
Cl1B−P2B−P1B	105(1)	Cl2B−P4B−P1B	101(1)
C1−P1C−P4C	105(2)	C25−P3C−P4C	107(2)
P4C−P1C−P2C	82.3(8)	P4C−P3C−P2C	82.3(8)
P1C−P2C−P3C	79.1(6)	P1C−P4C−P3C	79.2(7)
Cl1C−P2C−P1C	103(1)	Cl2C−P4C−P1C	101(1)
C1−P1A−P2A−P4A	105.504(2)	C25−P3A−P2A−P4A	−104.43(2)
C49−P2A−P4A−Cl2A	−1.14(1)	Cl1A−P2A−P4A−Cl2A	−2.260(5)
C2−C1−P1A−P4A	141.441(4)	C6−C1−P1A−P2A	−137.649(4)
Cl1A−P2A−P1A−P3A	−99.44(2)	Cl2A−P4A−P1A−P3A	−99.44(2)
P1A−P2A−P4A−P3A	130.91(2)	P1B−P2B−P4B−P3B	116.61(2)
C1−P1B−P2B−P4B	110.24(2)	C25−P3B−P2B−P4B	−100.96(2)
Cl1B−P2B−P4B−Cl2B	−178.64(3)	Cl1B−P2B−P1B−P3B	−101.334(1)
Cl2B−P4B−P1B−P3B	−99.28(2)	C2−C1−P1B−P2B	58.01(1)
C1−P1C−P2C−P4C	−103.85(2)	C25−P3C−P2C−P4C	105.30(2)
P1C−P2C−P4C−P3C	−115.61(2)	Cl1C−P2C−P4C−Cl2C	178.56(3)
Cl1C−P2C−P1C−P3C	100.34(1)	Cl2C−P4C−P1C−P3C	99.00(2)

Scheme A4: Numbering scheme of 2,6-bis-(2,4,6-trimethylphenyl)phenyl-chlorophosphane **39**.

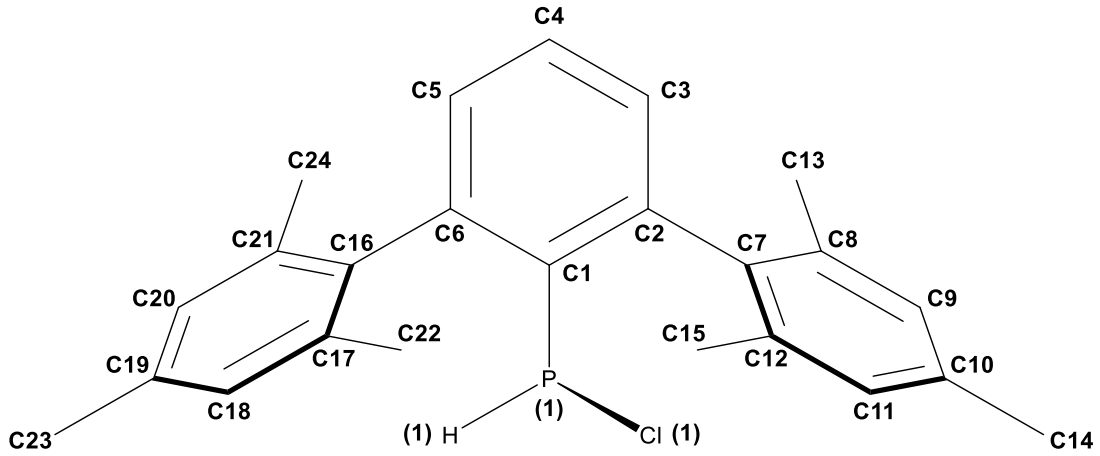

Table A6: Selected bond lengths [Å], angles [°] and torsion angles [°] of **39**.

P1−Cl1	2.0732(2)	C1−C2	1.4120(5)
P1−C1	1.830(3)	C2−C7	1.5048(4)
H1−P1−Cl1	109.(3)	P1−C1−C2	118.3(2)
H1−P1−C1	106.(3)	P1−C1−C6	121.1(2)
Cl1−P1−C1	103.07(1)	C1−C2−C7	121.4(2)
C1−C6−C16	122.3(3)	H1−P1−C1−C6	21.318(3)
H1−P1−C1−C2	−155.197(3)	Cl1−P1−C1−C2	89.923(3)
Cl1−P1−C1−C6	−93.562(3)	H1−P1−C1−Cl1	114.880(3)

Scheme A5: Numbering scheme of chloro-bis-tetrahydrofurano-2,6-bis-(2,4,6-trimethylphenyl)-phenylphosphidyl zinc **36**·2THF.

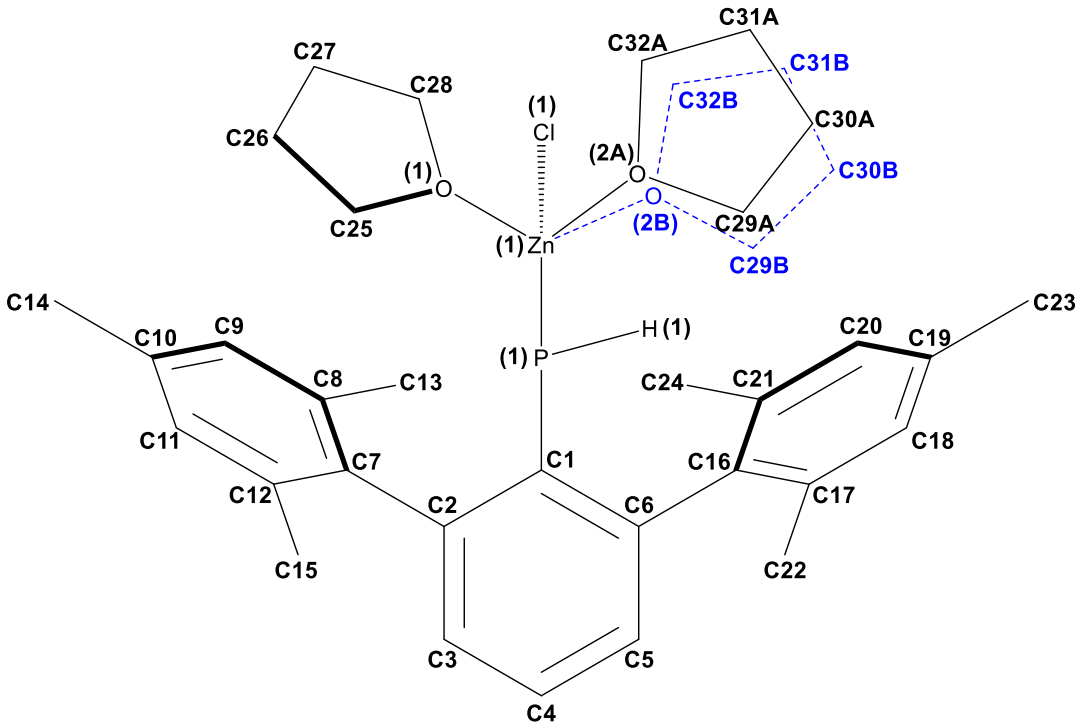

Table A7: Selected bond lengths [Å], angles [°] and torsion angles [°] of **36**·2THF.

P1−C1	1.836(2)	Zn1−O1	2.0705(2)
Zn1−Cl1	2.2057(7)	Zn1−O2A	2.097(2)
P1−Zn1	2.3092(7)	Zn1−O2B	2.15(3)
Cl1−Zn1−P1	143.10(3)	C1−P1−Zn1	105.87(7)
C1−P1−H1	100.0(2)	O1−Zn1−Cl1	100.16(5)
Zn1−P1−H1	92.2(2)	O1−Zn1−O2A	92.3(3)
O1−Zn1−P1	108.29(5)	O1−Zn1−O2B	94.3(7)
O2A−Zn1−P1	100.3(5)	O2B−Zn1−P1	101.2(2)
P1−C1−C2−C7	2.720(3)	Zn1−P1−C1−C2	−90.44(2)
Zn1−P1−C1−C6	93.57(2)	Cl1−Zn1−P1−H1	83.214(2)
H1−P1−C1−C6	−1.647(2)	O1−Zn1−P1−O2A	−95.844(5)

Scheme A6: Numbering scheme of lithium 2,6-bis-(2,4,6-trimethylphenyl)phenylphosphide **29**·3THF.

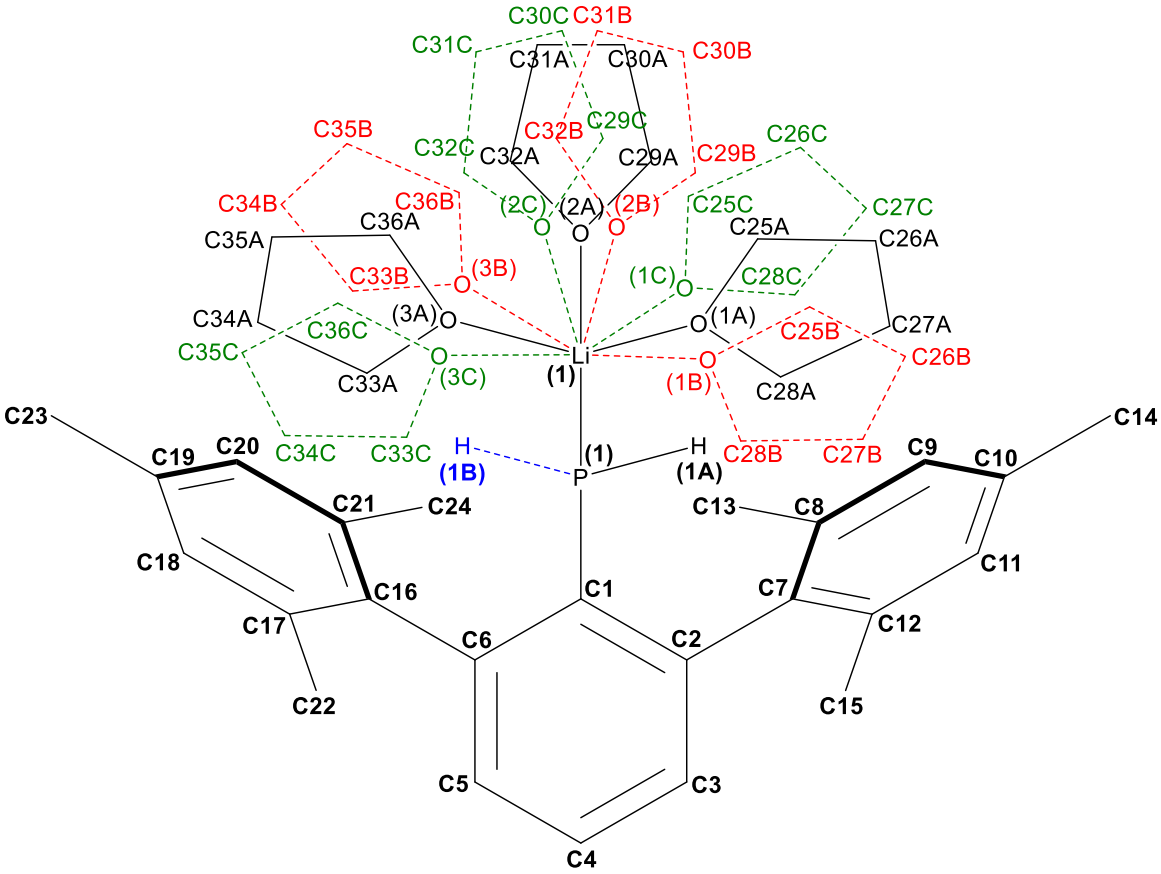

Table A8: Selected bond lengths [Å], angles [°] and torsion angles [°] of **29**·3THF.

P1−C1	1.806(2)	P1−Li1	2.536(4)
Li1−O1A	1.931(9)	Li1−O1B	2.00(1)
Li1−O1C	2.23(3)	Li1−O2A	1.938(6)
Li1−O2B	2.08(2)	Li1−O2C	2.07(7)
Li1−O3A	1.946(8)	Li1−O3B	2.01(5)
Li1−O3C	1.87(2)	C1−P1−Li1	125.4(1)
P1−Li1−O1A	104.1(3)	P1−Li1−O2A	127.3(2)
P1−Li1−O3A	106.4(3)	P1−Li1−O1B	107.9(4)
P1−Li1−O2B	118.2(7)	P1−Li1−O3B	112(2)
P1−Li1−O1C	92.0(7)	P1−Li1−O2C	120(2)
P1−Li1−O3C	114.7(5)	Li1−P1−C1−C6	−82.3(2)
Li1−P1−C1−C2	99.8(2)	Li1−O1A−C25A−C26A	−151(1)

Table A8: Continuation.

Li1−O2A−C29A−C30A	156.0(4)	Li1−O3A−C33A−C34A	−128.8(7)
Li1−O1B−C25B−C26B	−104(2)	Li1−O2B−C29B−C30B	−147(2)
Li1−O3B−C33B−C34B	−145(8)	Li1−O1C−C25C−C26C	−133(3)
Li1−O2C−C29C−C30C	116(1)	Li1−O3C−C33C−C34C	174(2)

6.2 List of Figures

6.3 List of Schemes

6.4 List of Tables

6.5 List of References

[1] H. Köhler, A. Michaelis, *Ber. Dtsch. Chem. Ges.* **1877**, *10*, 807–814.

[2] A. Michaelis, G. Schroeter, *Ber. Dtsch. Chem. Ges.* **1894**, *27*, 490–497.

[3] G. He, O. Shynkaruk, M. W. Lui, E. Rivard, *Chem. Rev.* **2014**, *114*, 7815–7880.

[4] J. Bresien, C. Hering, A. Schulz, A. Villinger, *Chem. Eur. J.* **2014**, *20*, 12607–12615.

[5] A. Hinz, A. Schulz, A. Villinger, *Inorg. Chem.* **2016**, *55*, 3692–3699.

[6] J. Bresien, A. Schulz, A. Villinger, *Phosphorus, Sulfur Silicon Relat. Elem.* **2016**, *191*, 601–604.

[7] W. A. Merrill, R. J. Wright, C. S. Stanciu, M. M. Olmstead, J. C. Fettinger, P. P. Power, *Inorg. Chem.* **2010**, *49*, 7097–7105.

[8] M. Lehmann, A. Schulz, A. Villinger, *Angew. Chemie, Int. Ed.* **2012**, *51*, 8087–8091.

[9] W. Kuchen, H. Buchwald, *Angew. Chem.* **1956**, *68*, 791.

[10] K. Karaghiosoff, H.-W. Lerner, A. Wörner, N. Wiberg, *Z. Naturforsch., B: J. Chem. Sci.* **2002**, *57b*, 1027–1035.

[11] P. Pyykkö, M. Atsumi, *Chem. Eur. J.* **2009**, *15*, 12770–12779.

[12] J. Bresien, A. Schulz, A. Villinger, *Chem. Eur. J.* **2015**, *21*, 18543–18546.

[13] J. Bresien, K. Faust, A. Schulz, A. Villinger, *Angew. Chemie, Int. Ed.* **2015**, *54*, 6926–6930.

[14] I. Krossing, A. Reisinger, *Coord. Chem. Rev.* **2006**, *250*, 2721–2744.

[15] J. Bresien, A. Schulz, A. Villinger, *Dalton Trans.* **2016**, *45*, 498–501.

[16] R. Riedel, H.-D. Hausen, E. Fluck, *Angew. Chem.* **1985**, *97*, 1050–1050.

[17] J. Bresien, K. Faust, C. Hering-Junghans, J. Rothe, A. Schulz, A. Villinger, *Dalton Trans.* **2016**, *45*, 1998–2007.

[18] M. Westerhausen, M. Wieneke, K. Doderer, W. Schwarz, *Z. Naturforsch., B: J. Chem. Sci.* **1996**, *51*, 1439–1442.

[19] A. Bashall, J. M. Cole, F. García, A. Primo, A. Rothenberger, M. McPartlin, D. S.

Wright, *Inorg. Chim. Acta* **2003**, *354*, 41–48.

[20] G. Sapelza, P. Mayer, M. Westerhausen, *Z. Anorg. Allg. Chem.* **2005**, *631*, 3087–3091.

[21] M. Westerhausen, G. Sapelza, P. Mayer, *Angew. Chemie, Int. Ed.* **2005**, *44*, 6234–6237.

[22] M. Westerhausen, G. Sapelza, M. Zabel, A. Pfitzner, *Z. Naturforsch., B: J. Chem. Sci.* **2004**, *59*, 1548–1550.

[23] K. Hansen, T. Szilvási, B. Blom, E. Irran, M. Driess, *Chem. Eur. J.* **2014**, *20*, 1947–1956.

[24] H. Schmidbaur, S. Schnatterer, *Chem. Ber.* **1983**, *116*, 1947–1954.

[25] P. W. Dyer, J. Fawcett, M. J. Hanton, *Organometallics* **2008**, *27*, 5082–5087.

[26] R. A. Bartlett, M. M. Olmstead, P. P. Power, G. A. Sigel, *Inorg. Chem.* **1987**, *26*, 1941–1946.

[27] E. Urnezius, J. D. Protasiewicz, *Main Group Chem.* **1996**, *1*, 369–372.

[28] E. Urnezius, S. J. Klippenstein, J. D. Protasiewicz, *Inorg. Chim. Acta* **2000**, *297*, 181–190.

[29] R. Melenkivitz, D. J. Mindiola, G. L. Hillhouse, *J. Am. Chem. Soc.* **2002**, *124*, 3846–3847.

[30] B. F. Wicker, J. Scott, J. G. Andino, X. Gao, H. Park, M. Pink, D. J. Mindiola, *J. Am. Chem. Soc.* **2010**, *132*, 3691–3693.

[31] R. Waterman, T. D. Tilley, *Chem. Sci.* **2011**, *2*, 1320.

[32] J. Bresien, A. Schulz, A. Villinger, Unpublished Results.

[33] M. Mantina, A. C. Chamberlin, R. Valero, C. J. Cramer, D. G. Truhlar, *J. Phys. Chem. A* **2009**, *113*, 5806–5812.

[34] G. W. Rabe, I. A. Guzei, A. L. Rheingold, *Inorg. Chim. Acta* **2001**, *315*, 254–257.

[35] E. E. Zvereva, A. R. Shagidullin, S. A. Katsyuba, *J. Phys. Chem. A* **2011**, *115*, 63–69.

[36] J. P. Merrick, D. Moran, L. Radom, *J. Phys. Chem. A* **2007**, *111*, 11683–11700.

[37] J. Boersma, J. G. Noltes, *Tetrahedron Lett.* **1966**, *7*, 1521–1525.

[38] A. Guerrero, D. L. Hughes, M. Bochmann, *Organometallics* **2006**, *25*, 1525–1527.

[39] B. M. Cossairt, C. C. Cummins, *New J. Chem.* **2010**, *34*, 1533–1536.

[40] A. R. Fox, R. J. Wright, E. Rivard, P. P. Power, *Angew. Chemie, Int. Ed.* **2005**, *44*, 7729–7733.

[41] S. Shah, G. P. A. Yap, J. D. Protasiewicz, *J. Organomet. Chem.* **2000**, *608*, 12–20.

[42] C. Overländer, J. J. Tirrée, M. Nieger, E. Niecke, C. Moser, S. Spirk, R. Pietschnig, *Appl. Organomet. Chem.* **2007**, *21*, 46–48.

[43] P. J. Murphy, H. Böckemeier, in *Science of Synthesis* (Ed.: C. Ramsden), Georg Thieme Verlag, **2007**, pp. 2057–2081.

[44] C. B. Fischer, S. Xu, H. Zipse, *Chem. Eur. J.* **2006**, *12*, 5779–5784.

[45] G. M. Sheldrick, *SHELXS-2013: Program for the Solution of Crystal Structures*, University of Göttingen, Germany, **2013**.

[46] G. M. Sheldrick, *SHELXL-2013: Program for the Refinement of Crystal Structures*, University of Göttingen, Germany, **2013**.

[47] G. M. Sheldrick, *SADABS Version 2*, University of Göttingen, Germany, **2004**.

[48] P. H. M. Budzelaar, *gNMR for Windows*, NMR Simulation Program, IvorySoft **2006**.

[49] E. G. Finer, R. K. Harris, *Mol. Phys.* **1967**, *13*, 65–75.

[50] E. G. Finer, R. K. Harris, *Prog. Nucl. Magn. Reson. Spectrosc.* **1970**, *6*, 61–118.

[51] K. Huynh, E. Rivard, W. LeBlanc, V. Blackstone, A. J. Lough, I. Manners, *Inorg. Chem.* **2006**, *45*, 7922–7928.

[52] *Gaussian 09, Revision C.01*, M. J. Frisch, G. W. Trucks, H. B. Schlegel, G. E. Scuseria, M. A. Robb, J. R. Cheeseman, G. Scalmani, V. Barone, B. Mennucci, G. A. Petersson, H. Nakatsuji, M. Caricato, X. Li, H. P. Hratchian, A. F. Izmaylov, J. Bloino, G. Zheng, J. L. Sonnenberg, M. Hada, M. Ehara, K. Toyota, R. Fukuda, J. Hasegawa, M. Ishida, T. Nakajima, Y. Honda, O. Kitao, H. Nakai, T. Vreven, J. A. Montgomery, Jr., J. E. Peralta, F. Ogliaro, M. Bearpark, J. J. Heyd, E. Brothers, K. N.

Kudin, V. N. Staroverov, T. Keith, R. Kobayashi, J. Normand, K. Raghavachari, A. Rendell, J. C. Burant, S. S. Iyengar, J. Tomasi, M. Cossi, N. Rega, J. M. Millam, M. Klene, J. E. Knox, J. B. Cross, V. Bakken, C. Adamo, J. Jaramillo, R. Gomperts, R. E. Stratmann, O. Yazyev, A. J. Austin, R. Cammi, C. Pomelli, J. W. Ochterski, R. L. Martin, K. Morokuma, V. G. Zakrzewski, G. A. Voth, P. Salvador, J. J. Dannenberg, S. Dapprich, A. D. Daniels, O. Farkas, J. B. Foresman, J. V. Ortiz, J. Cioslowski, D. J. Fox, Gaussian, Inc., Wallingford CT, **2010**.

[53] E. D. Glendening, J. K. Badenhoop, A. E. Reed, J. E. Carpenter, J. A. Bohmann, C. M. Morales, C. R. Landis, F. Weinhold, **2013**.

[54] J. E. Carpenter, F. Weinhold, *J. Mol. Struct.: Theochem* **1988**, *169*, 41–62.

[55] F. Weinhold, J. E. Carpenter, *The Structure of Small Molecules and Ions*, Plenum Press, **1988**.

[56] F. Weinhold, C. R. Landis, *Valency and Bonding. A Natural Bond Orbital Donor-Acceptor Perspective*, Cambridge University Press, **2005**.

[57] J. P. Perdew, K. Burke, M. Ernzerhof, *Phys. Rev. Lett.* **1996**, *77*, 3865–3868.

[58] J. P. Perdew, K. Burke, M. Ernzerhof, *Phys. Rev. Lett.* **1997**, *78*, 1396–1396.

[59] C. Adamo, V. Barone, *J. Chem. Phys.* **1999**, *110*, 6158–6170.

[60] R. Ditchfield, W. J. Hehre, J. A. Pople, *J. Chem. Phys.* **1971**, *54*, 724–728.

[61] W. J. Hehre, R. Ditchfield, J. A. Pople, *J. Chem. Phys.* **1972**, *56*, 2257–2261.

[62] P. C. Hariharan, J. A. Pople, *Theor. Chim. Acta* **1973**, *28*, 213–222.

[63] P. C. Hariharan, J. A. Pople, *Mol. Phys.* **1974**, *27*, 209–214.

[64] M. S. Gordon, *Chem. Phys. Lett.* **1980**, *76*, 163–168.

[65] M. M. Francl, W. J. Pietro, W. J. Hehre, J. S. Binkley, M. S. Gordon, D. J. DeFrees, J. A. Pople, *J. Chem. Phys.* **1982**, *77*, 3654–3665.

[66] R. C. J. Binning, L. A. Curtiss, *J. Comp. Chem.* **1990**, *11*, 1206–1216.

[67] J.-P. Blaudeau, M. P. McGrath, L. A. Curtiss, L. Radom, *J. Chem. Phys.* **1997**, *107*, 5016–5021.

[68] V. A. Rassolov, J. A. Pople, M. A. Ratner, T. L. Windus, *J. Chem. Phys.* **1998**, *109*,

1223–1229.

[69] V. A. Rassolov, M. A. Ratner, J. A. Pople, P. C. Redfern, L. A. Curtiss, *J. Comp. Chem.* **2001**, *22*, 976–984.

[70] T. H. J. Dunning, *J. Chem. Phys.* **1989**, *90*, 1007–1023.

[71] R. A. Kendall, T. H. J. Dunning, R. J. Harrison, *J. Chem. Phys.* **1992**, *96*, 6796–6806.

[72] D. E. Woon, T. H. J. Dunning, *J. Chem. Phys.* **1993**, *98*, 1358–1371.

[73] K. A. Peterson, D. E. Woon, T. H. J. Dunning, *J. Chem. Phys.* **1994**, *100*, 7410–7415.

[74] T. Hashimoto, K. Hirao, H. Tatewaki, *Chem. Phys. Lett.* **1995**, *243*, 190–192.

[75] A. K. Wilson, T. van Mourik, T. H. J. Dunning, *J. Mol. Struct.: Theochem* **1996**, *388*, 339–349.

[76] B. Metz, H. Stoll, M. Dolg, *J. Chem. Phys.* **2000**, *113*, 2563–2569.

[77] K. A. Peterson, *J. Chem. Phys.* **2003**, *119*, 11099–11112.

[78] F. London, *J. Phys. Radium* **1937**, *8*, 397–409.

[79] R. McWeeny, *Phys. Rev.* **1962**, *126*, 1028–1034.

[80] R. Ditchfield, *Mol. Phys.* **1974**, *27*, 789–807.

[81] K. Wolinski, J. F. Hinton, P. Pulay, *J. Am. Chem. Soc.* **1990**, *112*, 8251–8260.

[82] J. R. Cheeseman, G. W. Trucks, T. A. Keith, M. J. Frisch, *J. Chem. Phys.* **1996**, *104*, 5497–5509.

[83] C. J. Jameson, A. De Dios, A. K. Jameson, *Chem. Phys. Lett.* **1990**, *167*, 575–582.

[84] C. van Wüllen, *Phys. Chem. Chem. Phys.* **2000**, *2*, 2137–2144.

[85] L. J. Farrugia, *J. Appl. Crystallogr.* **1997**, *30*, 565.

[86] *Diamond: Crystal and Molecular Structure Visualization*, Crystal Impact, Dr. H. Putz & Dr. K. Brandenburg GbR, Kreuzherrenstr. 102, 53227 Bonn, Germany, http://www.crystalimpact.com/diamond

[87] *Persistence of Vision™ Raytracer, Version 3.6*, Persistence of Vision Pty. Ltd. **2004**, http://www.povray.org/download/

[88] *ChemDraw Professional, Version 15.0*, PerkinElmer, Inc., Waltham, MA, USA, **2015**, www.cambridgesoft.com

[89] *ACD/Spectrus Processor, Version 2015.2.5*, Advanced Chemistry Development, Inc., Toronto, Ontario, Kanada, **2015**, www.acdlabs.com

[90] *Microsoft Office Excel Professional, Version 2013*, Microsft Corporation, Redmond, WA, USA, **2013**, www.microsoft.com